Unsteady Pool Fires- Experiments and Modeling

Thesis submitted in partial fulfillment of the award of the

Degree of Doctor of Philosophy
in Fire Engineering

By

Shivakumar A
Register No/USN: 18PHREN037

Fire and Combustion Research Center

August 2021

JGI JAIN
DEEMED-TO-BE UNIVERSITY

Declaration

I hereby declare that this thesis titled **Unsteady pool fires - experiments and modeling**, submitted by **Shivakumar. A** in partial fulfillment of the requirements of the **Degree of Doctor of Philosophy in Fire Engineering** of JAIN (Deemed-to-be- University), is based on the results of the research work carried out by me and written by me under the guidance and supervision of **Dr. C. S. Bhaskar Dixit, Director of Fire and Combustion Research Center and Prof. H. S. Mukunda, Fire and Combustion Research Center** . The manuscript has been subjected to plagiarism check by TURNITIN software. This Thesis or any part thereof has not been submitted for any purpose to any other University or Institute.

Shivakumar A

Bengaluru
Date: 27/08/2021

C. S. Bhaskar

Endorsement of Guide

FIRE & COMBUSTION RESEARCH CENTRE
Signature
JAIN UNIVERSITY

JGI JAIN
DEEMED-TO-BE UNIVERSITY

Certificate

This is to certify that this thesis titled **Unsteady pool fires - experiments and modeling**, submitted by **Shivakumar. A** in partial fulfillment of the requirements of the **Degree of Doctor of Philosophy in Fire Engineering** of JAIN (Deemed-to-be- University), is based on the results of the research work carried out under my guidance and supervision. The manuscript has been subjected to plagiarism check by TURNITIN software. This Thesis or any part thereof has not been submitted for any purpose to any other University or Institute

Prof. H. S. Mukunda

Dr. C. S. Bhaskar Dixit

Bangalore
Date: 27/08/2021

FIRE & COMBUSTION RESEARCH CENTRE
Signature
JAIN UNIVERSITY

JGI JAIN
DEEMED-TO-BE UNIVERSITY

DATE: 26.08.2021

PLAGIARISM VERIFICATION

Title of the Thesis: **Unsteady Pool Fires- Experiments & Modeling**

Total Pages: **147**

Name of the Researcher: **Shivakumar A**

Department: **Fire and Combustion Research Center**

Name of the Guide: **Dr. C.S. Bhaskar Dixit and Prof. H.S. Mukunda**

This is to certify that the above thesis was scanned for similarity detection. Process and outcome is given below

Software Used: TURNITIN

Date: 26.08.2021

Similarity Index: 20%

Total word count: 31492

Checked By
Name & Signature
Dr.Mythili P Rao

Exclusion of Self-Published Work:

The content of the chapters and the publications which have been excluded from the software check:

1. Review of Literature
2. Bibliography / References
3. Appendices / Publications

The published work has been included in the Thesis and has not been submitted for any degree to any other University / Institute.

The complete report of the above thesis has been reviewed by the Undersigned (Please tick the box)

☐ The similarity index is below the accepted norms.

☑ The Similarity index is above accepted norms, because of the following reasons:

1. Experiments on unsteady pool fires—effects of fuel depth, pan size and wall material. Sadhana 46:53.(2021) https://doi.org/10.1007/s12046-021-01571-x **12%**

2. Effects of Fuel Depth and Pan Wall Material for Unsteady Pool Fires with Different Fuels. Fire Technology https://doi.org/10.1007/s10694-021-01159-1(2021) **4%**

The thesis may be processed for Evaluation.

Student	Guide
Shivakumar A	Dr. C.S. Bhaskar Dixit

FIRE & COMBUSTION RESEARCH CENTRE * JAIN UNIVERSITY * Signature

Unsteady pool fires- experiments and modeling

ORIGINALITY REPORT

20%	4%	19%	%
SIMILARITY INDEX	INTERNET SOURCES	PUBLICATIONS	STUDENT PAPERS

PRIMARY SOURCES

1	A Shiva Kumar, A V E Sowriraajan, C S Bhaskar Dixit, H S Mukunda. "Experiments on unsteady pool fires – effects of fuel depth, pan size and wall material", Sādhanā, 2021 Publication	12%
2	A. Shiva Kumar, H. S. Mukunda, C. S. Bhaskar Dixit. "Effects of Fuel Depth and Pan Wall Material for Unsteady Pool Fires with Different Fuels", Fire Technology, 2021 Publication	4%
3	baadalsg.inflibnet.ac.in Internet Source	1%
4	hdl.handle.net Internet Source	<1%
5	"Fire", Lees Loss Prevention in the Process Industries, 2012. Publication	<1%
6	www.iitp.ac.in Internet Source	<1%

Acknowledgments

My heartfelt thanks to Prof. H. S. Mukunda and Dr. C. S. Bhaskar Dixit for giving me an opportunity to work in Fire and Combustion Research Center and for their continuous teaching and guidance throughout this journey. This thesis would not have been possible without their guidance and persistent help. I take this opportunity to thank Dr. A.Ve. Sowriraajan for his support extended in performing the experiments. I am also thankful to Mr. Basavaraj and Mr. Ravi for helping me to carryout the experiments successfully as planned. Thanks to my family members for their continuous encouragement and support and I finally thank the management of Jain (deemed to be) University for providing me with the facilities and resources to carry out the work on time.

Abstract

This thesis constitutes an investigation of the behavior of unsteady pool fires and the development of an unsteady model to capture the temporal behavior of open pool fires taking into account the effect of various control parameters such as fuel depth, pan material, pan diameter, initial fuel temperature, thermochemical and transport properties of fuels and ambient pressure,

The motivation for this study arose from an examination of the literature on pool fires from 1958 (Hottel) till recent times. It was uncovered that the studies on unsteady pool fires did not always provide complete details of the geometry and the properties of the wall material while the results on burn rate presented showed unexplainable differences and attempts to harmonize the results proved very difficult because of the absence of the crucial input data. Also, earlier researchers who attempted to fix the unknown extinction coefficient in the models on radiation to explain the burn rate results for large pans have obtained very different values pointing to serious questions on the validity of the currently accepted model. Therefore, the present work is a combination of specifically designed experiments to explore the effects of a range of parameters in pool fires and to (a) construct a predictive model for the mean burn rate as a function of various parameters and (b) develop an unsteady predictive model to capture the time-varying behavior of pan fires.

The experimental studies have been conducted on pool fires with 0.1 to 2 m diameter pans with depths of 40, 50, 60, and 90 mm with n-heptane fuel depths of 10, 20, and 30 mm without water, some experiments on n-heptane fuel floated on water and also experiments in 0.2 m diameter pan with kerosene, diesel, ethanol, and methanol fuel depths of 10 and 20 mm without water in a large indoor fire laboratory. Pans of 0.2 m diameter are made of glass, stainless steel, mild steel, and aluminum and larger diameter pans only of mild steel. More

than seventy experiments have been conducted with n-heptane include some with initial fuel temperatures of 290, 319, and 343 K as also experiments with kerosene, diesel, ethanol, and methanol at ambient temperature. Data on the temporal evolution of mass burn, pan wall temperatures, temperatures inside the liquid at some depths, and gas phase temperatures at select heights from the pool surface have been obtained from the experiments. These experiments were extended to fuels like diesel, kerosene, methyl, and ethyl alcohols.

One general result of significance from the experiments on pans with diameters up to 0.2 m is that the mass flux at the initial burning phase which is largely controlled by convection remains the same irrespective of the type of fuel, pan material, and fuel depth. Such a feature is valid for larger pan sizes as well, except that the burn flux transitions to larger values much earlier.

With regard to the pan material effect with n-heptane, glass pans show mildly increasing low flux values (10 to 15 g/m^2s) and mild steel and aluminum pans show an initial low flux value ($\sim$ 10 g/m^2s) and then a sharp change to large flux values depending on the depth. At larger depths, the flux values go up to 65 g/m^2s. With stainless steel pans, the mass flux variation occurs smoothly all through towards increasing values. Whereas the burn flux of diesel in stainless steel and mild steel pans does not vary much with time, the burn flux in the case of kerosene is the same in both SS and MS for nearly 50 % of the time and then, for MS pans becomes much larger than for SS pans. The fact that large burn fluxes are observed in the small pans is due to the combined role of conduction and radiation. Specific experiments conducted by keeping the side walls cooled with water at ambient temperature showed that the burn flux dropped to the values close to convectively controlled levels ($\sim$ 10 g/m^2s), but the relative roles of conduction and radiation would be obtained with the full mathematical model.

In respect of fuel depth effect, the data on burn behavior for n-heptane fuel shows an interesting result that the mass flux reaches 60 to 65 g/m^2s even with

pan diameters of 0.2 m at larger fuel depths ($\sim$ 30 mm), the mass flux values normally expected at large pan diameters and the mass flux for kerosene fuel increases from 27 g/m^2s to 50 g/m^2s when fuel depth is increased from 10 to 20 mm respectively. In the case of diesel, ethanol, and methanol fuels, an increase in the mass flux values is $\sim$ 10 to 20 % when fuel depth is increased from 10 to 20 mm.

In so far as the pan diameter effect is concerned, the results are similar to those in the literature. As diameter exceeds 0.5 m, other geometric features like pan wall thickness and material have a smaller role.

In respect of the water depth below the n-heptane fuel, the decrease in the average burn rate is about 1 % per mm water depth up to 20 mm for all pans below 0.5 m diameter. Larger size pans with burn rates controlled largely by radiation show a much reduced effect of the water depth.

Explaining the observed features of burn needed more careful modeling of the conduction and radiation fluxes. Accounting for wall conduction demanded the estimation of the heat flowing along the wall and being transferred to the liquid inside both from the sides as well as the pan bottom. Wall temperatures at several locations along the vertical side and bottom of the pan using thermocouples for the number of cases were measured and these were subject to analysis.

In order to account for various effects in a holistic manner, a dimensionless number, M_{pc} based on the geometric parameters, fuel, and pan material properties that affect the pan burn behavior has been constructed as

$$M_{pc} = P_1 P_3 [1.5 + 8.5 P_2] \text{ with} \quad (1)$$

$$P_1 = \left[\frac{k_w}{h_{pan} h_{g,conv}} \frac{h_{fu}}{h_{fb}} \right]^{1/4} \quad (2)$$

$$P_2 = \left[1 - \exp(-0.25 (d_{pan}/0.21)^{1.5} / P_1) \right] \left[1 + 0.1 (h_{wr}/h_{pan})^{2.3} \right] \quad (3)$$

$$P_3 = \left[\frac{(T_{bfu} - T_0)}{(T_{bfu} - 300)} \frac{300}{T_{bfu}} \right]^{-0.35} \quad (4)$$

Where k_w is the pan wall conductivity, $d_{pan},\ h_{pan},\ h_{fu},\ h_{fb}$ are the pan diameter

and depth, fuel depth and the free board (the space between the pan tip and the fuel surface), $h_{g,conv}$ is the convective heat transfer coefficient, T_0 and T_{bfu} are the fuel initial temperature and the boiling point. The latent heat of fuel, L_{fu} enters the prediction of the burn flux as follows.

$$\bar{\dot{m}}''_{fu}(g/m^2 s) = M_{pc}\frac{h_{g,conv}(T_f - T_{bfu})}{4L_{fu}} \tag{5}$$

In the earlier equations, the parameter P_1 accounts for conductive flux in addition to fuel depth and associated free-board effects, P_2 accounts for the effect of pan diameter and water on the mass burn rate, and P_3 for initial temperature effects. The above correlation has been tested for a wide range of parameters. The wide range of parameters includes the pan diameter from 0.05 to 2 m or more, pan materials from highly conducting variety like aluminum and practically relevant materials like mild steel and stainless steel, pan depths of about 60 mm for smaller size pans and 100 mm for large pans and fuel thicknesses up to 40 mm or more, free board of more than 5 mm, initial fuel temperatures from very low values up to a near boiling point for n-heptane, kerosene, diesel, gasoline, methyl, and ethyl alcohol. The correlation has been found to be correct to less than a mean of 5% for both unsteady and steady experiments over this range of parameters.

The second part of this work consists in evolving a code to describe the unsteady behavior of the pool burn. Accounting for conduction heat transfer into the liquid pool involved invoking nucleate-film boiling effects in a simple way by enhancing the wall-to-liquid heat transfer coefficient. This was considered adequate in view of the complexity of dealing with these effects that depend on the material of the pan and the nature of the surface. The traditional expression for radiation flux dependence on the pan diameter with extinction coefficient needed to be altered in favor of a different strategy involving a view factor that invokes mass flux based Reynolds number to account for fuel depth related effects with the characteristic dimension being the pan diameter. Combining select observations of earlier work and the present experiments, a MATLAB

code has been developed for tracking the time-dependent behavior of pool fire as influenced by wall conduction, convection, and radiation as well as liquid phase conduction. Some constants of the model are obtained by calibration against a few experiments. Predictions against earlier as well as the current experimental data are set out. The outstanding-to-good quality of predictions in most cases is attributed to the detailed physics taken into account in the model.

Thus, the major contributions of the work are:

(a) A correlation that allows the prediction of mean burn flux for unsteady and steady burning pool fires over a wide range of parameters,

(b) A detailed consideration of the model for conduction heat transfer along the pan wall into the fuel (for the first time in the literature),

(c) A modified radiation heat transfer model that takes note of fuel depth effects on burn flux, and

(d) Incorporating the new elements into a MATLAB code that makes predictions of the temporal variation of the mass burn with the inputs, namely, the geometric parameters and material properties of the pan and the fuel.

The code does have some key constants fixed by the requirement to match the observed behavior in select experiments. Finally, the code operates with no free constants. It has been tested against a much wider range of experiments and found to lead to reliable results. It is also used to elucidate the role of conduction, convection, and radiant heat transfer fluxes in each of the cases. In the view of the author, this code is a novel and new contribution to the field of pan fires and can be used with confidence by any prospective researcher or practitioner.

Symbols

A_1	Cross sectional area (m)
AL	Aluminum
B	Spalding transfer number
C_{pw}	Specific heat (kJ/kgK)
d_{pan}	Diameter of Pan (m)
F	Flame shape factor
GL	Glass
H_s	Heat of phase change (kj/kg)
h_{pan}	Height of pan (m)
h_{fu}	Depth of fuel (m)
h_{wr}	Depth of water below the fuel (m)
h_{fb}	Height of free board (m)
$h_{g,conv}$	Convective heat transfer coefficient in gas phase (kW/m^2K)
L_{fu}	Latent heat of vaporization of the fuel (kJ/kg)
k_w	Thermal Conductivity of pan(kW/mK)
k_2	Convective heat transfer coefficient (kW/m^2K)
$\bar{\dot{m}}''_{fu}$	Mean burn flux (kg/m^2s)

$\bar{\dot{m}}''_{\infty}$	Mean burn flux (kg/m^2s)
M_{pc}	Dimensionless pan burn number
MS	Mild Steel
SS	Stainless Steel
T_p	Pan tip temperature (K)
T_{wb}	Bottom outer wall temperature (K)
T_f	Flame Temperature (K)
T_{bot}	Fuel bottom temperature (K)
T_s	Fuel surface temperature (K)
W	Dimensionless number to capture behavior of T_p
$W1$	Dimensionless number to calculate C_3
Y_s	Smoke Yield

Greek Symbols

ρ_{fu}	Density of fuel (kg/m^3)
α_{fu}	Thermal diffusivity of fuel (m^2/s)
ϵ	Emissivity
κ_{ex}	Extinction coefficient ($1/m$)
η_{fu}	Dimensionless distance-into-fuel coordinate (eqn. 5.30)

σ	Stefan-Boltzmann constant (W/m^2K^4)
	Subscripts
conv, cond	Convection, Conduction
rad, tot	Radiation, Total
p, pm	Pan tip, Steady pan tip
s, f	Surface, Flame
wb, wbc	Pan bottom outer wall, pan bottom central zone

Contents

List of Tables

,

List of Figures

,

Chapter 1

Introduction and Review of Literature

This chapter describes the introduction to pool fires and the earlier work carried out by researchers to characterize the behavior of pool fires with various fuels over a range of pan diameters under different experimental conditions. The methods used to measure the mass loss, temperatures of pan, fuel, and gas phase temperatures are presented. The effect of various control parameters on the burn behavior and the role of different heat feedback mechanisms to the pool surface are also described. Further, models available in the literature to predict the mass burn rate of pool fires, gaps in the literature, and the motivation to carryout this study are discussed. Finally, the motivation for the present study in attempting to seek to improve the understanding in terms of model behavior and predictability of pool fires is set out.

1.1 Pool Fires

A pool fire is a fire that results from the heat released by the chemical reaction between the fuel vapor and air with the air drawn by natural convection by the fire over a liquid fuel pool or a horizontal solid surface. Hence, it is a coupled process. As the air entrainment into the fire changes, so does the chemical heat release and the flame behavior (this is unlike the classical combustion process that is driven by a controlled air supply). The liquid fuel pool generally may be fuel stored in a container, fuel on a horizontal substrate, or fuel floated on the water. Pool fires are classified into open or enclosure pool fires, based on the

presence or absence of enclosure around them. In open pool fires, the oxidizer is not limited by the surrounding conditions, whereas in the case of enclosure pool fires the amount of oxidizer available for combustion can get limited by the nature of the enclosure. Further, the heat required for fuel vaporization is received from the flame by conduction, convection, and radiation heat transfer modes whose individual contribution depends on the various controlling parameters like pan geometry, pan material, type of fuel, wind velocity, and enclosure. Variation of these parameters alters the heat feedback to the pool surface which in turn changes the behavior of pool fire.

The earliest reported research and data are from Bilnov and Khudiakov who performed the experimental studies and collated the work of other researchers from 1946 onward into a book in Russian in 1957 and was available in English translation in 1961 (Bilnov and Khudiakov, 1961). Its initial inspiration seems to have been because of the combustion behavior of gases, liquids, and solids. Combustion of liquid fuels has been reported on 3.7 mm to 50 m. The fuels investigated are benzene, kerosene, and several alcohols including the higher ones. While benzene and kerosene appear related to the fact that these fuels were extensively used in missiles and also for propulsion systems of space vehicles during that period, it is unclear why the higher-order alcohols are considered important in the fire studies. The work is also interesting because they have put together various scaling laws to explain some of the dependences. This work has led to the inspiration of similar work in the USA. Burgess et al (1961) have performed experiments on a variety of fuels: methanol, liquefied natural gas, liquid hydrogen, xylene, butane, and hexane in pan diameters of 75 mm to 2.4 m. The purpose of these investigations has been related to safety in handling and transportation of these gases and liquids. Hottel (1958) having had access to the work of Blinov and Khudiakov, conducted an analysis of the Russian data and this work is the most cited in this area. He set out the data on a plot to indicate the effect of diameter on mass burning rate of several fuels as in Fig. 1.1. The most important inference from his study is that for pans of

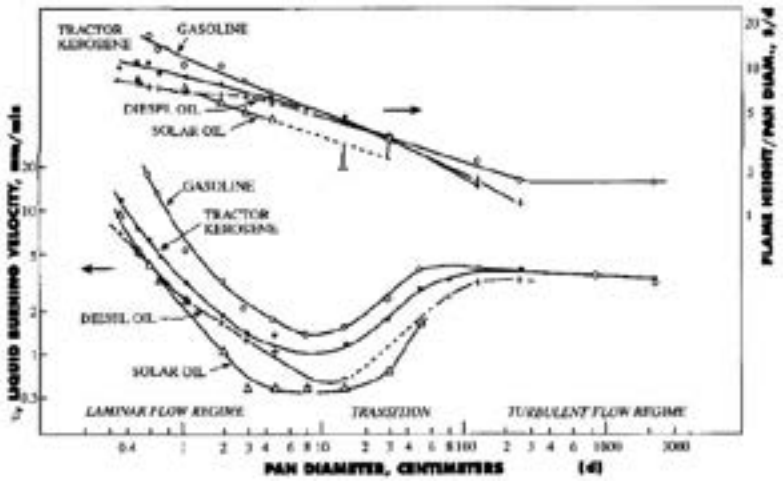

Figure 1.1: Burning rate and flame height from pool fires as a function of pan diameter (from Hottel, 1958)

less than 0.1 m diameters the fuel regression rate decreases with an increase in pool diameter, flattens out before increasing with diameter up to 1 m, and settles down to an asymptotic value at larger diameters of the pools. Following tradition, Hottel (1958) set out the data in Fig. 1.1 in terms of linear regression rate (mm/min). As can be noticed, the plot contains data on gasoline, kerosene, and diesel whose density varies from about 750 to 850 kg/m^3. Since the burn rate is heat flux controlled and what is relevant is to examine fuel mass flux (called burn flux here), it would have been more appropriate to set out the data on this basis. He also wrote the heat balance equation as

$$\dot{q}''_s = k_1 \frac{T_f - T_s}{d} + k_2(T_f - T_s) + \sigma T_f^4 F \left[1 - \exp\left(-k d_{pan}\right)\right] \tag{1.1}$$

which when expressed in words will be:

Heat flux to the surface = Heat flux due to conduction + convection + radiation

Where k_1 is a constant related to thermal conductivity, T_f and T_s are the flame and liquid surface temperatures, k_2 is the convective heat transfer coefficient, F is the flame shape factor, k is termed the opacity coefficient, also termed as extinction coefficient in later literature. The dimension d in the first term is a characteristic dimension at this stage and it must really be related to the

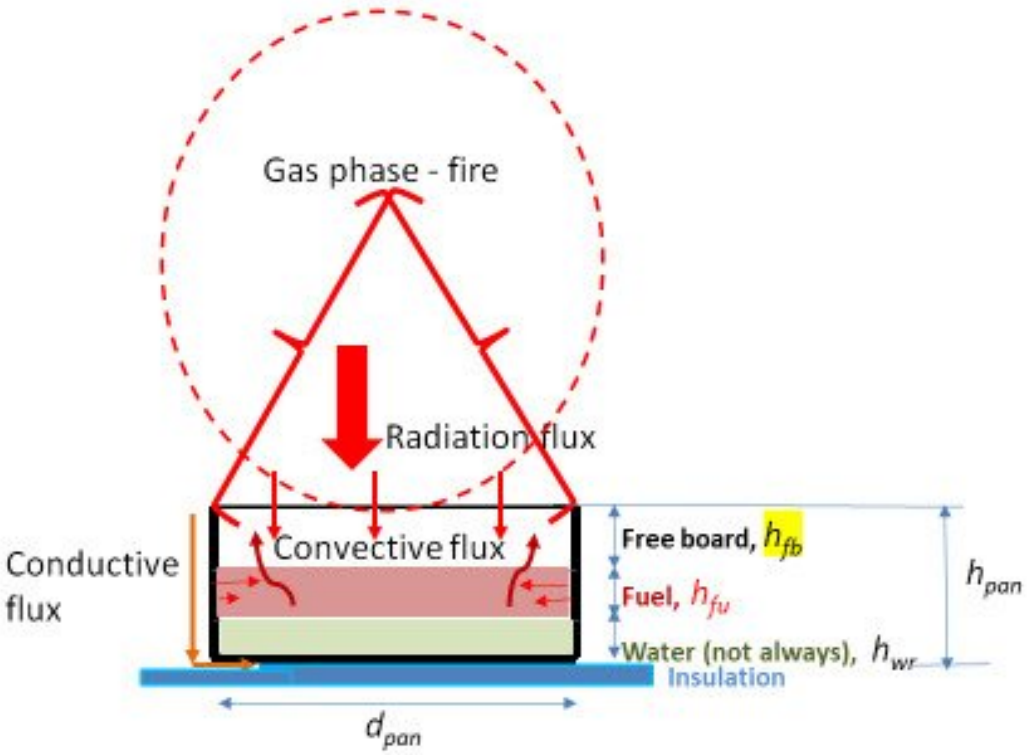

Figure 1.2: Pan geometry and heat transfer modes

distance between the pan tip and the fuel surface and modeling the conduction process is needed for this. Since no later effort in modeling this term till now has accounted for this term systematically, it has remained unexplored.

It is perhaps appropriate to introduce the geometry and the thermal nature of the problem. Figure 1.2 shows the schematic diagram of the pan with the most important dimensions - pan diameter, pan depth, fuel depth, free board, and the depth of water if it is also present. The three heat transfer modes indicated in the figure are the same as those set out in equation 1.1. Liquid phase conduction is a mode of heat transfer inside the liquid that has to be accounted for in unsteady pool fires. Two other modes whose magnitudes are small and have opposite behavior are the heat radiated back from the pool surface and in-depth heat absorbed by radiation. These are ignored from consideration here both because they are small and their models are still to be developed.

Burgess et al (1961) also put down the expression for burn flux as the ratio of this flux to the heat absorbed by the regressing fuel. They set down the expression for the mass flux, $\dot{m}''$ for large pans in the limit of zero conduction and convection as

$$\dot{m}'' = \sigma T_f^4 F[1 - \exp(-kd_{pan})]/H_s = \dot{m}''_\infty[1 - \exp(-kd_{pan})] \tag{1.2}$$

where $\dot{m}''_\infty = \sigma T_f^4 F/H_s$, H_s is the heat of phase change at the surface. While truly, conduction term tends to zero in the limit of large pans, convection even if it is a small fraction compared to radiation, is always present. The radiation term has two factors, namely the flame shape factor F, and the extinction coefficient, k. These two parameters have been subjected to more detailed consideration in the studies in the seventies and early eighties [de Ris and Orloff, 1972; de Ris et al, 1972; Orloff and de Ris, 1982]. The study of de Ris and Orloff (1972) is an attempt to explain the experimental data on heat transfer to the fuel surface for small pans using experimental data on simulated gaseous flames by Corlett (1970). They conclude that the mass flux is a function of the Spalding transfer number, B. The data that they present shows that for a range of B's between 1.5 and 3 for many liquid fuels considered here it varies as $\dot{m}'' \sim B$. This will be shown to be incorrect since the burn flux is shown to vary with fuel depth (later), a feature that is not accounted for in getting the above result. They also indicate that radiation heat transfer needs to be modeled and Orloff (1982) undertook to do this. Using photographs of the flames and approximating them into an axisymmetric flame shape for the case of polymethyl methacrylate (PMMA) and evolving an average absorption-emission coefficient from flame transmittance measurements and an averaged flame temperature, he formulated a simple radiation model. Measured flame temperature (T_f) was about 1260 K, but recommended value for calculation was set at 1200 K. The convective flux was estimated from the stagnant film hypothesis as 8.5 kW/m^2 for 0 size lip and 3.8 kW/m^2 for a lip size of 76 mm. Subsequently, Orloff and de Ris (1982) have presented a model for estimating

Table 1.1: Liquid pool fire burning mode based on diameter

d_{pan} (m)	Burning mode
< 0.05	convective, laminar
0.05-0.2	convective, turbulent
0.2-1	radiative, optically thin
>1	radiative, optically thick

the burn flux of moderate pool fires (0.1 to 0.7 m dia) using a procedure that invokes approximations to flame structure similar to the one adopted by Orloff (1981). They estimate the radiation flux with an extinction coefficient based on a curve fit that is expected to be very accurate (in fact, the coefficients have five to six significant digits). However, they choose a fixed value of 1200 K as the flame temperature as recommended in Orloff (1982). If we recognize that T_f appears in terms of the fourth power, any small errors in the choice can result in gross errors in the prediction of the heat fluxes and so, burn flux as well.

In 1983, Babrauskas provided an important and valuable review of the status of the research on pan fires (Babrauskas, 1983). Putting together the ideas from Blinov and Khudiakov (1961), and Hottel (1958), he has set out the classification based on the mode of heat transfer controlling the pool fire burn as in Table 1.1. The mode for very small pans is not different from those of gases through tubes studies in combustion science. For pans with d_{pan} between 0.05 and 0.2 m, the process is convectively dominated. The term turbulent needs to be interpreted in terms of pulsations that control the air entrainment due to free convection. With the increase in pan diameter, this process becomes more chaotic even though the pulsation is a dominant mode of air entrainment. Of course, radiation heat transfer gains a greater role in the heat transfer process. And, when the pan diameter goes beyond a meter or so, the radiation heat

transfer is the most dominant mode. The role of conduction in the heat transfer process has remained unstated here because the visible gas phase combustion has remained the focus. For pans below 0.2 m dia (some limited effects even up to 0.5 m dia), conduction heat transfer will play a role depending on the pan material.

Babrauskas was also the first to identify the differences between steady mode and unsteady mode operations. He has expanded on the various transient effects in the latter mode - (a) conduction effects changing with time, (b) lip effects on convective and radiative effects also changing, and (c) the bottom of the vessel being heated progressively with thin fuel layer. He goes on to state that short burning fires may not achieve steady state at all and in fact, the time required to establish a steady burn profile may take as long as 600 s. These aspects are important because while most standards that use pan fires for qualifying foams (to be brought out subsequently) use unsteady mode with a typical time from ignition to start of extinguishment is 60 s. However, most experimental studies have concentrated on the steady mode of operation, and not many on the unsteady mode where conduction effects cannot be excluded. He has brought up the effects of pan material and wind. While wind effects are a function of both pan diameter and the free board, it is outside the purview of this thesis and not discussed here. However, the work on pan materials that have remained very weakly explored (a brief study on methanol is performed by Vali, 2014) is a subject of serious study here.

Further, Babrauskas (1983) has performed an interesting analysis to extract radiation parameters. Invoking the eqn. 1.2, using the experimental data on large burn fluxes and a non-linear curve fitting procedure, he estimated the burn flux at infinite pan diameter, $\dot{m}''_{\infty}$, and k for about 20 fuels, and these values (of k) have become the basis in many later studies. What has turned out is that for the same fuels, the values obtained by others are widely different (for gasoline and diesel in Chatris et al, 2001; Munoz et al, 2004) and hence

serious questions have arisen on the approach to dealing with radiational flux in this manner. This will be discussed in more detail subsequently.

At this stage, it is considered important to list the fuels and the parameters set out in the standards for qualifying foam based fire extinguishing systems using pan fire. Table 1.2 sets out the details of major fire standards developed in Europe and the USA. The pan sizes used are large - typically upwards of 2 m making radiation heat transfer the primary mode controlling the burn rate of the fuel. NFPA-11 test uses a very huge pan and gasoline as the fuel while other standards use n-heptane as the fuel. Using a pure fuel has the advantage of known phase transformation behavior in comparison to the use of a mix of hydrocarbons that may allow some fragments to evaporate leaving behind components that have a higher boiling point and so, changing the composition of the fuel. ISO and NFPA tests use about 290 liters, and the others use about 150 to 200 liters with the NFPA test having the smallest thickness $\sim$ 30 mm and others with different thicknesses. The lip height (or free-board as the term used in this thesis) is also different, the smallest being 48 mm for ISO and largest, at 600 mm for NFPA. Fuel temperature is set at specific values around 20 °C in the case of ISO, NFPA, and BS procedures, and FM and UL specify a range as more than 10 °C. It is unclear why such variability exists in the standards and the general implication is that these parameters do not affect the extinguishment test significantly. All the standards invoke a pre-burn time of 60 s implying that by this time, the burn rate would have reached steady conditions. One key parameter that is sure to be significant is the fuel temperature. Given a choice, the manufacturers who want their foam to get cleared will try to seek tests at 12 °C instead of 25 °C because the chances of thermal penetration and storage of heat that might lead to fuel burn will be much less severe even with the foam layer above . Another important parameter is the wind speed. The suggested upper limit of 3 m/s seems too large and normally, it is expected that the tests are performed under in-door conditions, the surroundings being quiescent - typical random wind movements would be less than 0.5

Table 1.2: Parameters considered in the standards in fire test, ISO = ISO 7203-1, NFPA = NFPA-11, BS-EN = BS-EN 1568-3, FM = FM 5130, UL = UL - 162

Parameters	ISO	NFPA	BS-EN	FM	UL
Pan area, m^2	4.46	9.29	4.46	4.65	4.65
Pan depth, mm	203.2	914.0	203.2	304.8	304.8
T_{amb}, C	10 to 20	15 to 25	10 to 20	-	-
T_w, C	15 to 20	15 to 25	15 to 20	22 to 29	-
T_{fu}, C	15 to 20	>21	15 to 20	>10	
$T_{foam\ soln}$, C	15 to 20	15 to 20	15 to 20	-	-
Wind speed, m/s	≤ 3	≤ 3	≤ 3	≤ 3	≤ 3
Fuel	n-heptane	Gasoline	n-heptane	n-heptane	n-heptane
Initial h_{fu}, mm	94	30.5	94	51	51
h_w, mm	45.7	274.3	45.7	51	51
h_{fb}, mm	48.3	610	48.3	203	203
Preburn time, s	60	60	60	60	60

m/s. As can be noted, all these tests are in unsteady mode.

In other tests involving fire clearance of hazardous packages, say of nuclear materials, fuels like Diesel, JP4, and JP8 have also been contemplated. For instance, 10CFR71 (Koski et al, 1992) specifies 30 min engulfing diesel or JP4 pool fire test or any other thermal test providing equivalent total heat input on exposure to fully engulfing pool-fire including radiation and convection and the packages must receive equal or greater heat in furnace testing with an averaged environment of 800 °C. Thus, the fuels of importance are n-heptane, gasoline, diesel, toluene, and JP4/JP8. In laboratory studies at many academic institutions, Factory Mutual Corporation, Sandia laboratories, and others, researchers have used ethyl and methyl alcohol as well. The tests have been conducted largely under steady conditions and a smaller number of studies under unsteady conditions at small and large pan diameters. The data from various sources are classified into large and small pans under steady and un-

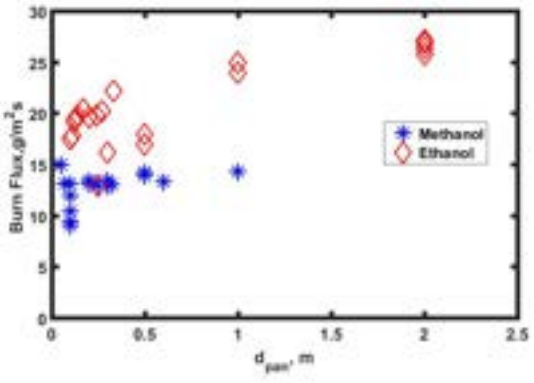

Figure 1.3: Experimental data on burn flux of Methanol and Ethanol pool fires vs. pan diameter

steady conditions. These are set out in Appendix as Tables A.1, A.2, A.3, and A.4. The data set out here include as many geometric and material details as are available in the published data. As can be noted, several early studies (like from Blinov and Khudiakov, 1958 and Koseki, 1989) have not provided all these details even if they may not be of sufficient importance for some of their results. In an overall sense, about 70 % of the experimental studies have been devoted to steady mode.

The data on methanol and ethanol are set out in Table A.5 in the Appendix as well as in Fig. 1.3. As can be seen from the figure, the burn flux values of methanol and ethanol become asymptotic with respect to the pan diameter (beyond about 0.6 m diameter). Methanol has a burn flux of about 14 g/m^2s over a range of diameters and ethanol has a 70 % higher burn flux, both features known well in the literature.

The data of hydrocarbon pool fires are set out in Fig. 1.4. It can be noted that there is considerable scatter in the data arising out of pan related parameters that are not the same in all these cases. Even so, n-heptane has the highest burn flux, followed by diesel. Kerosene and JP8 seem to have nearly the same asymptotic burn flux values, lower than diesel. The burn flux values in smaller

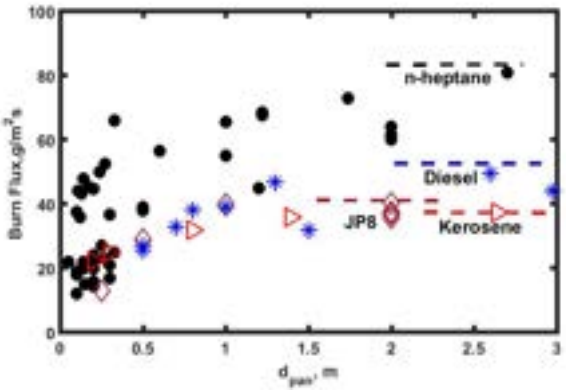

Figure 1.4: Experimental data on burn flux of hydrocarbon pool fires vs. pan diameter

diameter pans seem to indicate the influence of several parameters, particularly for n-heptane which has been studied much more than other fuels.

1.1.1 Steady Pool Fires

The data in Table A.1 show that n-heptane and toluene have a very high burn flux ($\sim$ 65 g/m^2s) even at 1 m diameter that is obtained for kerosene at a very large diameter (30 m or more). When the diameters are very large and experiments are conducted in open areas, wind effects are sure to influence these values. Diesel and JP8 have burn fluxes around 40 g/m^2s. In these experiments, a constant fuel level is maintained by continuously replenishing the fuel at a rate equal to the burn rate of the fuel. Figure 1.5 shows the different methods used to maintain a constant fuel level in the steady state experiments.

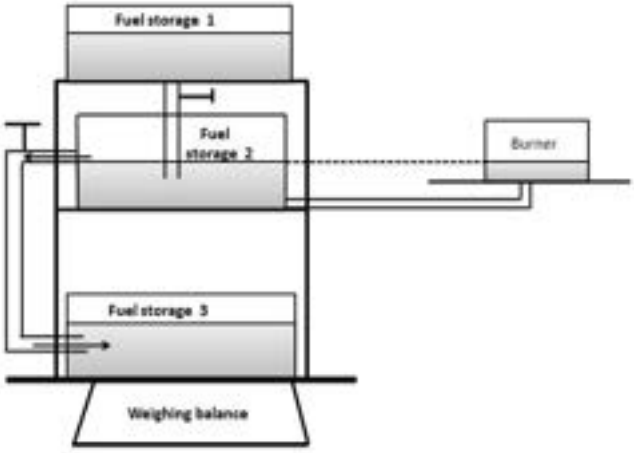

(a) Steady state experimental arrangement to maintain constant fuel level by gravity feed method, drawn from Hu et al (2014)

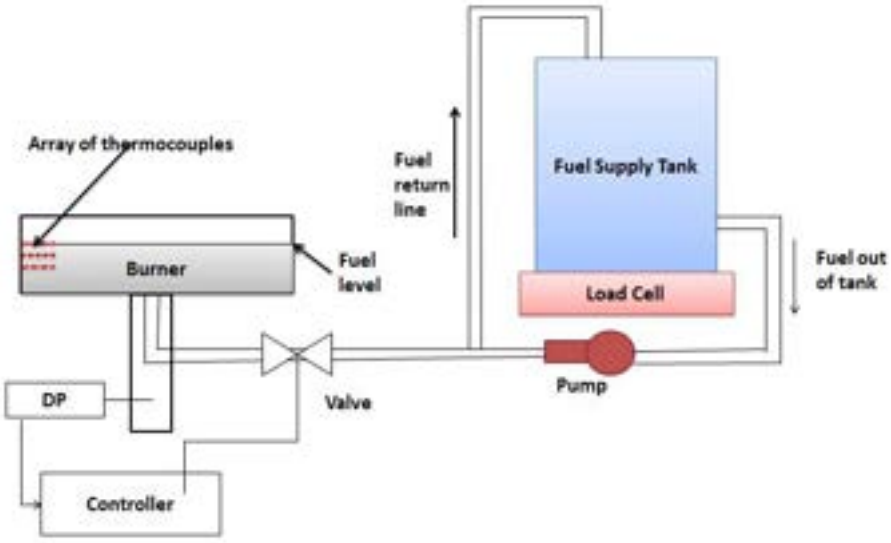

(b) Steady state experimental arrangement to maintain constant fuel level by using pressure transducer, drawn from Blanchat et al (2011)

Figure 1.5: Methods used to maintain constant fuel level in steady state experiments

Figure 1.5a shows the gravity feed method in which the liquid level in the pan will be maintained by gravity. From storage tank 1 fuel enters storage tank 2 and the fuel is fed to the pan by the pipe which is connected between the bottom of the pan and tank 2. The fuel level in storage tank 2 and the pan are maintained at the same level as the excess fuel flows into the storage tank 3. Figure 1.5b shows another method of maintaining a constant fuel level. In this system, an array of thermocouples is located immediately above and below the fuel surface to measure the fuel temperatures. The change in the liquid level is identified by the large variation of measured values of the fuel temperatures and that in the gas phase and the differential transducer controlling the fuel level will be adjusted to maintain the required fuel between the thermocouples. The fuel level is raised until the fuel temperature reaches a steady state. In both methods, the fuel reservoir is placed on the load cell to obtain the mass loss data during a steady burn period. Because of continuous replenishment, the pool has a certain depth towards the bottom of which, a constant temperature gets maintained, and to attain steady conditions, one needs to allow substantial time.

For instance, the experiments of Blanchat et al. (2011) on a 2 m diameter pan with JP8 fuel show that the mass loss data is obtained in the period of 18 to 24 minutes during which the fuel temperatures at various heights do not change with time as indicated in figure 1.6. Because of this feature, the fuel is not allowed to reach the bulk boiling stage and the presence of a deep temperature profile limits the burn flux even if the fuel depth is increased by using a pan of larger depth.

Table A.3 shows the data for pans with a diameter less than 0.8 m. Burn fluxes are lower than in the case of larger diameter pans as expected. The scatter in the data seems non-insignificant (for instance, see the results by Hu et al, 2014 in Table A.3 with a significant difference in burn flux for the same conditions).

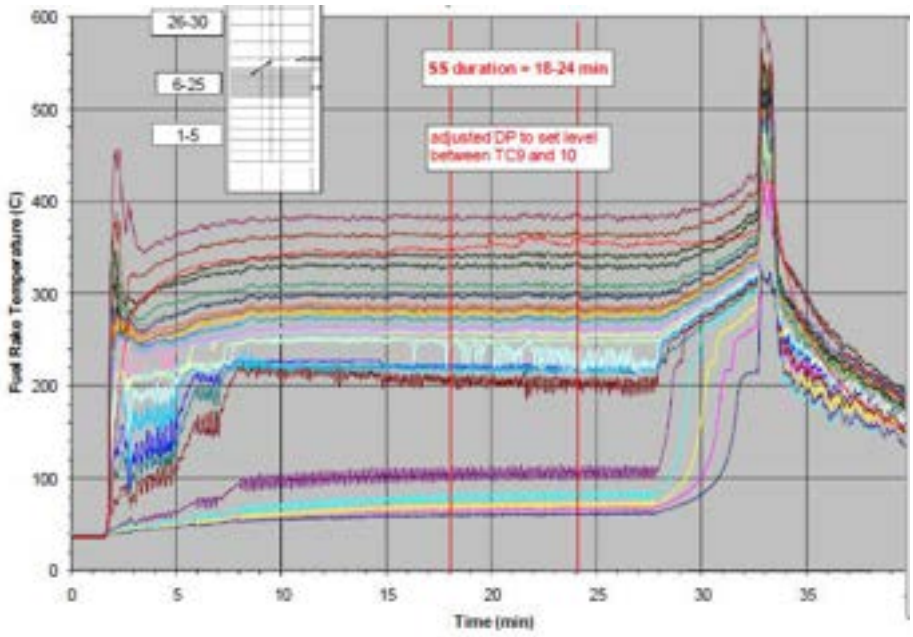

Figure 1.6: Fuel pool temperatures at various heights of 2 m pan diameter pan for JP8 [Blanchat et al (2011)]. Note the bottom line that indicates that the fuel temperature towards the bottom remains the same throughout the test between 18 and 24 mins

1.1.2 Unsteady Pool Fires

The data on large unsteady pool fires are set out in Table A.2. Figure 1.7 shows a schematic diagram of the experimental arrangement used in unsteady pool fires. It consists of a burner placed on the load cell with the required fuel depth. In this system, a constant fuel depth is not maintained but it reduces with time until the complete fuel gets burnt, while the liquid and wall temperatures keep increasing.

Among thirteen sets of data set out in Table A.2, six are on n-heptane, two on gasoline, two on kerosene, and three on diesel. The large fires of Koseki (1989) at 6 and 10 m pool diameter as well as those by Chatris et al (2001) may have been wind-affected. The influence by wind could either enhance or decrease the burn rate depending on the relative speeds between free and forced convection.

In the experiments by Koseki (1989), it is indicated that the fuel was floating over with free board of 30 to 50 mm; perhaps this may not affect the mean burn rate in view of radiation domination of the process. If we exclude the wind affected results, n-heptane and gasoline show burn fluxes of about 65 g/m^2s and kerosene and diesel about 15 % less.

The twenty two sets of data on small unsteady pool fires from 0.1 to 0.33 m diameter with n-heptane are the ones carried out by Chinese and Japanese researchers and are set out in Table A.4. The work by Chen et al (2011) at different initial temperatures is imaginative, interesting, and insightful. They show that in the unsteady state pool fires, the burning regimes can be divided into different phases: preheating, transition, bulk boiling, and decay. The preheating phase involves ignition, flame spread over the pool, and progressive growth of the fire. In the bulk boiling phase, the fuel will be at its boiling point and a large burn flux is obtained during this stage and lastly, in the decay phase, the burn flux reduces. They also measured the wall temperatures along the height of the pan wall. Though they have not consolidated the information into the model involving the conductive flux, the role of conductive heat transfer has been highlighted. The Chinese work has also some elements of novelty. They (Li et al, 2009 and Fang et al, 2011) conducted experiments at sea level as well as at high altitude in both Lhasa (altitude: 3650 m; air pressure: 65 kPa) and Hefei (altitude: 24 m, air pressure: 100.8 kPa) and have shown that the decrease in pressure at Lhasa reduces the burn flux by about 30 %.

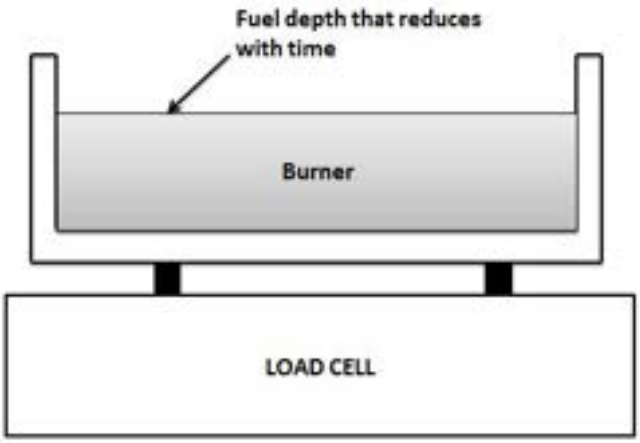

Figure 1.7: Schematic diagram of experimental arrangement for unsteady state pool fire

Figure 1.8 shows the burn fluxes for unsteady and steady pool fires. It can be noted that the unsteady pool fires have larger burn fluxes compared to the steady mode. The reason for such high mass burn rates is due to bulk boiling phenomena that is the primary feature of unsteady pan fires, a subject that will be discussed in detail in this thesis.

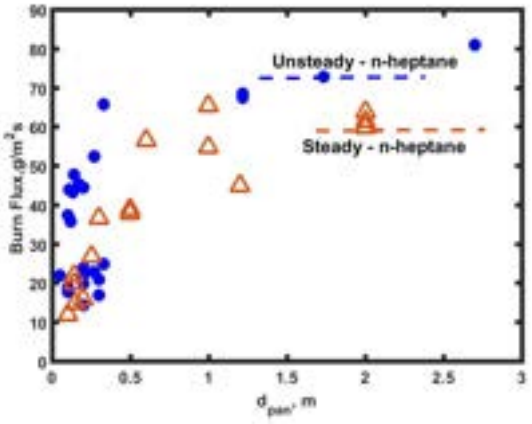

Figure 1.8: Burn flux vs pan diameter for unsteady and steady pool fires

1.1.3 Effect of fuel depth, free board, and pan material on burn flux

Fuel depth, free board (or lip height), and pan material are the other important parameters that affect the mass burn behavior of pool fires. With an increase in the fuel depth, the burn flux increases significantly. This inference can be drawn from Table A.4 only in a broad sense because precise data on this effect has not been obtained systematically. Koseki (1991) has observed the fuel thickness effect during the water boil over study in a 0.6 m diameter crude oil pool fire where it was found that the ratio of burn rate in boiling phase to burn rate in steady state increases with increase in the fuel thickness as indicated in Fig. 1.9. The experiments performed by Chen et al (2011) in a 0.2 m diameter pan for n-heptane fuel at a fuel thickness of 6.5 mm and 13 mm show that the mean burn flux increases by a factor of about 1.6 at the higher fuel depth. Even the experiments of Zhao et al (2017) in the square pans of side lengths 0.1, 0.2, and 0.3 m for n-heptane at fuel thickness varying from 2 mm to 11.5 mm show that the mass burn rates are higher at the larger fuel depths. The reason for such high mass burn rates at large fuel depths in the small and large pans is due to the transition to increased bulk boiling behavior due to conductive flux into the fuel. Even though it is perhaps reasonable to infer the role of fuel depth from these data, it is important to separate the fuel depth effect from free board since making a change in one implies the change in the other. Free board is another important parameter that influences the mass burn rate in smaller diameter pool fires. It is defined as the distance between the fuel surface to the tip of the burner. A significant free board can increase the convective heat transfer by initiating turbulence close to the pool edge altering the temperature distribution on the pan wall thus controlling the conduction heat transfer. It can also enhance the flame volume which results in increased radiation heat transfer as indicated by Babruskas (1983). The effect of free board on the burn flux in steady and unsteady state experiments is not the same. In steady state experiments, the burn flux decreases monotoni-

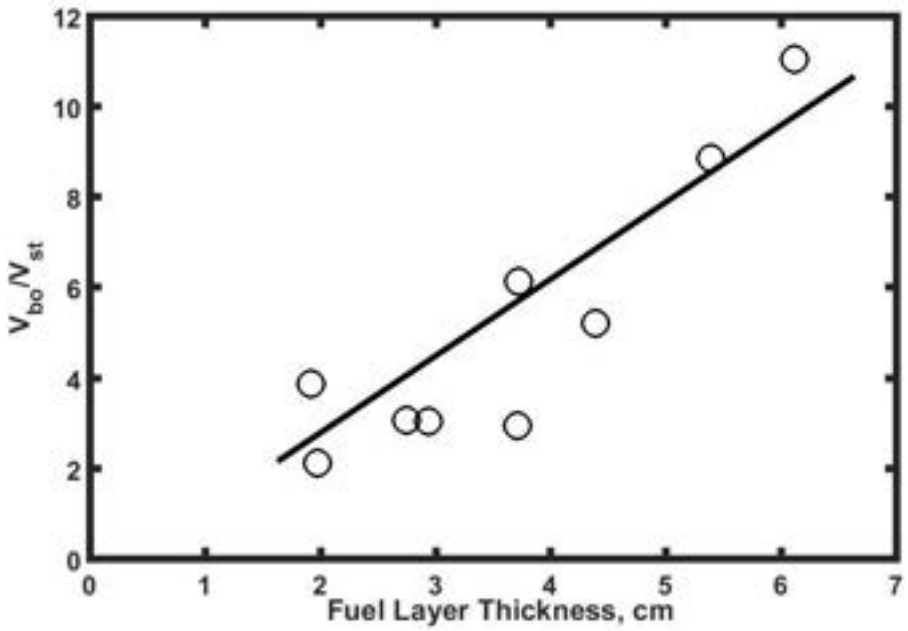

Figure 1.9: Relationship between ratio of burn rate in boiling to burn rate in steady state and fuel layer thickness in 0.6 m diameter tank crude oil fire [Koseki (1991)]

cally with an increase in free board as observed by Magnus (1961), Binov and Khudiakov (1961), Nakakuki (1994), and Dlugogorski et al. (2000). Beyond a critical free board, flame enters the pan, and the burn flux increases. In the case of unsteady pool fires, free board increases continuously with time and the burn rate can either increase or decrease. An increase is observed by Tao et al (2019) and Vinay et al (2018) in their studies. It is essentially due to heat input into the fuel for a longer time. Any possible decrease is due to reduced heat input over a longer separation distance. Which role is dominant depends on the pan diameter, pan and fuel depth, and the pan material. The unsteady pool fire experiments with the same initial fuel depth and the different free board heights can add more value to the understanding of the free board effect on the burn flux.

Besides the fuel depth and free board, the pan material affects the burn rate in small diameter pool fires. The effect of pan material on the burn flux varies de-

pending on the steady and unsteady experimental conditions. In steady state pool fire experiments, pans of high thermal conductivity show lower mass burn fluxes compared to those in pans of low thermal conductivity. In pans of higher thermal conductivity, the most of pan wall heat will be drawn away to the bottom of the pan and will be utilized to heat up the fresh fuel which is fed continuously to maintain the constant fuel depth. Due to this the conduction heat feedback at the fuel surface from the adjacent wall will be limited and hence, the lower mass burn flux. Whereas in the pans of low conductivity the heat drawn away to the bottom of the pan will be less resulting in the higher wall heat feed back to the fuel surface which further leads to higher burn fluxes as observed by Nakakuki (1994) and Vali et al (2014). Contrary to this, in unsteady pool fire experiments, an increase in thermal conductivity of pan material leads to enhanced pan wall conduction heat feedback, which further leads to the bulk boiling phenomenon, and hence, higher burn fluxes are obtained. In summary, it is important to emphasize that fuel depth, free board and pan material alter the heat transfer rate to the pool and have coupled effects on the burn flux.

1.2 Heat transfer mechanisms in pool fires

The heat transfer mechanisms are already illustrated in Fig. 1.2. Just to restate the current understanding, the diffusion flame above the pool surface generates the heat, the total heat released from the flame is transferred as positive heat feed back to the pool surface through conduction, convection, and radiation, and the rest is convected and radiated into the atmosphere.

1.2.1 Radiation Heat to Pool Surface

The radiation is the dominant mode of heat transfer in large pool fires and the experiments of Modak and Croce (1977) in square PMMA beds of sizes 0.025 to

1.22 m and heat feed back calculations at fuel surface show that for large pan diameters the radiation heat feed back is more than 80 percent of net energy transfer. Regarding the variation in intensity across the pool, there have been differing observations. The inference of Modak and Croce (1977) was that high local burn rates at the pool center imply that the pool center receives more heat feed back than the outer regions. This inference was simple to obtain because the fuel was a solid. In the case of liquids, the level is maintained the same, no matter which part of the pan receives the heat and so it is not simple to determine where the heat flux is larger. In order to get at the heat flux distribution, one needs to mount flux gauges near a fixed fuel surface to obtain the magnitude of radiation flux received locally. Such measurements have been made. Fischer et al (1987) performed experiments in 0.5 m diameter ethanol pool fire and the measurements of the radiation intensity show that at the center of the pool radiation fluxes are large and it reduces in both axial and radial directions. Contrary to this, Adiga et al (1989) have observed that in kerosene pool fires with an increase in diameter from 0.15 m to 0.5 m the radiation flux is smaller in the middle region and increases up to about midway along the radius. Kalssen and Gore (1992) measured the radiation feed back to fuel surface at 8 radial locations in the 0.3, 0.6, and 1 m pan with methyl alcohol, n-heptane, and toluene fuels, their results show that the radiation heat flux does not vary along the fuel surface for toluene and n-heptane but reduces towards the pan edge in case of methanol fuel. Hamins et al (1994) performed experiments to measure the radiation characteristics as a function of radius and azimuth in 0.3 m diameter simple burner, 0.3 m, and 0.38 m diameter ring burners for methanol, MMA, n-heptane, and toluene fuels. Their measurements show that the radial heat flux along the pool surface is flat for luminous fires but decreases towards the pool edge in non-luminous fires and the variation of total heat flux is flat for both luminous and non luminous fires. It is worth emphasizing that in most of the studies the variation of the measured radiation flux along the pool surface is not significant in luminous fires,

even though the flame temperature is not the same along the radial direction.

1.2.2 Liquid phase and pan wall heat transfer

In the literature, many more studies have been carried out on heat transfer by gas phase to the fuel and only limited information can be found on the heat transfer in the liquid phase. Several authors have measured the liquid temperatures at several locations to understand the heat transfer mechanism. The measurements on the liquid phase temperatures by Blinov and Khudiakov (1958) and Hasegawa (1989) show that there exists a hot zone below the boiling fuel surface, followed by the steep thermal gradient region and cold zone, the temperatures in the hot zone are nearly constant and equal to the fuel surface temperatures. The calculations performed by Blinov and Khudiakov (1958) show that the convection in the liquid phase is strong in the upper layers compared to that in the lower layers. Similar results were obtained by Vali et al (2014) for the experiments performed in quartz, copper, aluminum, and stainless steel pans for methanol fuel. The velocity fields observed in the quartz pan indicate that maximum fluid motion occurs in a zone 3 to 4 mm from the liquid surface and the heat transfer calculations performed in the liquid phase for the pan of length 18 mm show that the heat transferred from the fuel surface to underneath fuel is about 0.5 kW/m^2 indicating the weak role of convective heat transfer. The experiments of Ditch et al. (2013) in pans of 0.25 to 1 m diameter and Blanchat et al. (2011) in 2 m diameter pan for various fuels show that burn flux obtained with glass beads used to avoid convective heat transfer in condensed phase and without glass beads doesn't vary much indicating a little effect of convection heat transfer in the condensed phase. The reason for such behavior lies in the fact that the in-depth temperature of the fuel will be always lower compared to the temperature of the fuel surface and the buoyancy doesn't allow significant liquid phase convection to occur.

In the steady-state experiments researchers have justifiably ignored the pan

wall conduction by cooling the pan wall by water circulation at bottom of the pan (Hamins et al. 1994) and by reducing the pan wall thickness in the upper region (Ditch et al.), but in the case of unsteady pan fires without wall cooling, as is usually the case, the pan wall heat conduction is important since it significantly enhances the burn flux in small and moderate sized pans. The experiments performed by Kang et al. (2010) in a 0.3 m diameter stainless steel pan show that the pan wall temperatures after the transient phase become greater than the fuel temperature enhancing pan wall heat transfer into the fuel resulting in the bulk boiling phenomena. It is important to emphasize that the pan wall conduction heat transfer in the small and moderate size pan fires affects the mass burn rate significantly and the wall conduction heat transfer is to be considered in both experiments and modeling.

1.3 Flame Temperature

Flame temperature is a crucial parameter that affects the heat flux to the pool surface and surroundings. Admittedly, the temperature achieved in the fire is a consequence of complex fuel rich chemistry coupled with turbulent flow. Flame temperature is considered an important variable that will be used in the radiant flux calculation. Measurements of the temperature have been reported by several authors. A thermocouple is a direct approach since any radiation based measurement system has to average the emission-absorption characteristics in the path. Mc-Caffrey (1961) measured the center-line temperature of natural gas at different flow rates using 1 mm diameter K type thermocouples and based on the experimental data, the flame was divided into three regions as flame, intermittent, and plume, and it was found that the measured centerline temperature is independent of pan size.

Data from several sources on the measurements of centerline flame temperature in liquid pool fires are set out in Table 1.3. Koseski et al (1991) summarized the pool fire data from the fire research institute of Japan and found that

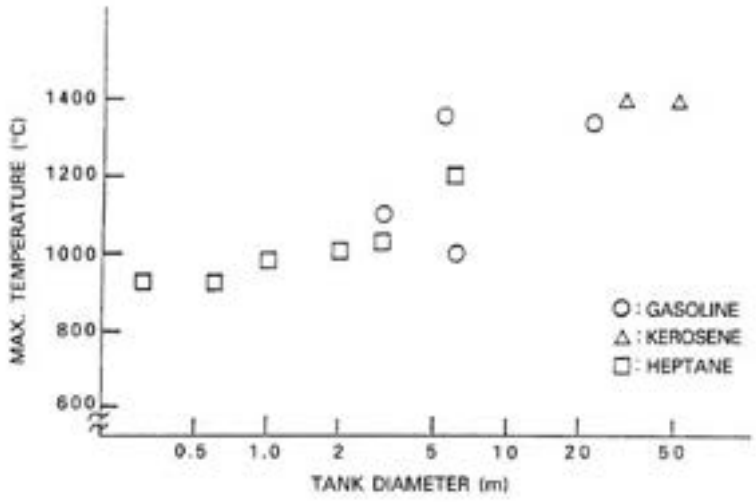

Figure 1.10: Maximum flame temperature vs. pan diameters for n-heptane, gasoline and kerosene fuel [Koseki (1991)]

the flame temperature increases with an increase in diameter for n-heptane and gasoline pool fires as indicated in Fig. 1.10, a feature which appears puzzling because it is unclear what mechanism is responsible for enhanced temperature with the increase in the pool fire size. There is not enough experimental detail set out in the paper to appreciate the possible reasons for the observation. As such these results for larger diameters are difficult to accept. The experiments of Chen et al (2012) for a 0.2 m diameter pan with n-heptane at fuel depths of 6.5 and 13 mm show that the center-line flame temperature is independent of the fuel depth and so the burn flux. These data are further discussed against the measurements made in this work in chapter 2.

Table 1.3: Flame temperature of different fuels available in the literature; * square pan

Fuel	d_{pan} (m)	T_f (K)	Reference
PMMA	0.73	1260	Orloff, 1981
n-heptane	0.2	1073	Chen et al, 2011
n-heptane	0.6	1200	Koseki, 1991
n-heptane	0.6	1200	Koseki, 1991
n-heptane	1.0	1250	Koseki, 1991
n-heptane	2.0	1279	Koseki, 1991
n-heptane	2.7*	1303	Koseki, 1990
n-heptane	3.0	1302	Koseki, 1991
n-heptane	6.0	1482	Koseki, 1991
Gasoline	3.0	1370	Koseki, 1991
Gasoline	6.0	1634	Koseki, 1991
Gasoline	24.0	1604	Koseki, 1991
Kerosene	0.15	1100	Bouhafid et al, 1988
Kerosene	30.0	1656	Koseki, 1991
Kerosene	50.0	1656	Koseki, 1991
Methanol	0.31	1440	Weckman & Strong, 1996
Methanol	0.30	1323	Hamins et al, 2016
Ethanol	0.50	1300	Fischer et al, 1987

1.4 Modeling of Pool Fires

Modeling the pool fires has been a developing field. Table 1.4 provides a consolidated statement of the burn flux models discussed above. There has been progress in the development of the models to predict the burn flux and these will be discussed now.

Blinov and Kudiakov (1958) deduced an empirical relation for the burn flux of laminar range pool fires as $v = a + b\ d^{-n}$, which explains the mass burn rate dependence on the diameter of the pan, where v is the regression rate in mm/min (the burn flux is obtained by multiplying the velocity by liquid

Table 1.4: Models available in the literature to predict burn flux

No.	Author	The Mathematical Model
1	Blinov and Kudiakov (1961)	$\dot{m}'' = \rho_{fu}\dot{r} = \rho_{fu}[a + b * d^{-n}]$
2	Hottel (1961)	$\dot{m}''H_s = (4K/d)(T_F - T_0) + h(T_F - T_0)$+ $\sigma F(T_F^4 - T_0^4)(1 - exp(-\kappa d))$
3	Burgess et al (1961)	$\dot{m}'' = \dot{m}''_\infty(1 - exp(-kD))$
4	de Ris and Orloff (1972)	$\dot{m}'' = 0.15B[ln(1 + B)/B]^{2/3}$
5	de Ris and Orloff (1982)	$\dot{m}'' = (\dot{q}''_r + \dot{q}_{conv} - \dot{q}''_{rr})/\Delta H_g$ $\dot{q}_{conv} = h/c_p[\Delta H_g(\chi_A - \chi_R/\chi_A - c_p(T_s - T_\infty)]E(y)$ $E(y) = y/(e^y - 1)$, $y = \dot{m}''c_p/h$ $\dot{q}''_r = \sigma T_f^4[1 - exp(-k_f L_m)]$ $k_f = -ln[1 - ((\chi_r L_m \dot{Q}'''_A)/3.6\sigma T_f^4 \chi_a)]/L_m$
6	Ditch et al (2013)	$\dot{m}''H_s = \left[\dot{q}''_{co} + \dot{q}''_{ro}Y_s^{1/4}[1 - exp[-(C\Delta H_g D)^p]\right]$ $\dot{m}''H_s = 12.5 + 68.3Y_s^{0.25}\left[1 - exp[-(4/3)H_s {d_{pan}}^{3/2}]\right]$
7	Sun et al (2017)	$\dot{m}'' = \dot{m}''_\infty(1 - exp(-k\beta D))(1.93(d/k)^{0.1} + 0.04)$

density), a & b are factors that depend on the fuel. Even though the equation set out by Hottel (eqn. 1.1) has brought out the heat transfer processes and the pan diameter effect on the fuel regression rate, it is not adequately detailed to account for the effect of other parameters such as fuel depth, free board, and initial temperature of fuel on the mass burn rate.

Burgess et al (1961) proposed an empirical model to predict the steady burn rate for several fuels as

$$\dot{m}'' = \dot{m}''_{\infty}(1 - exp(-kd_{pan})) \tag{1.3}$$

Where $\dot{m}''_{\infty}$ is the asymptotic mass flux, k is the extinction coefficient. As can be noticed, the model utilizes the extinction coefficient and the asymptotic mass flux values to determine the burn flux. While the values of the extinction coefficient for fuels like methanol and ethanol are much lower than for hydrocarbons, the values for various hydrocarbons, either are not available or where available, very difficult to rationalize. This is understandable since it depends on the composition of the very fuel rich reaction zone above the fuel surface and the processes of pyrolysis and reaction under rich conditions are very complex, particularly in the buoyant turbulent flow. In a more recent experimental study, Chatris et al (2001) and Munoz et al (2004) evaluate the extinction coefficients for diesel and gasoline fire tests that they have presented and come up with values that differ from earlier literature significantly. Table 1.5 that is drawn from Chatris (2001) shows the different values of k and $\dot{m}''_{\infty}$ obtained by the various researchers for the same fuels. This range of values implies that fits are dependent on specific data and any approach to resolution calls for the inclusion of all dependent parameters.

de Rris and Orloff (1972) presented a dimensionless empirical correlation based on the B number for the pool fires in convective regime as

$$\dot{m}'' = 0.15B[ln(1 + B)/B]^{2/3} \tag{1.4}$$

The expression for B number during combustion is obtained in analogous to the

Table 1.5: Asymptotic mass flux and radiation extinction coefficient from literature (from Chatris, 2001)

Author	$\dot{m}''_\infty$	k	$\dot{m}''_\infty$	k
	g/m^2s	$1/m$	g/m^2s	$1/m$
	Diesel		Gasoline	
Burgess et al (1961)	65	-	75	-
Babrauskas (1983)	34	2.8	55	2.1
Rew et al (1997)	54	1.3	67	1.48
Mangialavori and Rubino (1992)	61	-	65	-
Chatris et al (2001)	57	0.57	77	1.35
Munoz et al (2004)	62	0.63	83	1.173

Spalding mass transfer number as $B = (QY_{0\infty}/M_0 v_0 L) - (C_p(T_s - T_\infty)/L)$, which doesn't contain the sensible enthalpy term of fuel. However, this expression has very limited applicability since the other modes of heat transfer are ignored.

Orloff and de Ris (1983) presented a model for estimating the burn rate of moderate diameter pool fires (0.1 to 0.7 m dia) using a procedure that invokes approximations of flame structure and estimation of radiation flux as presented in Table 1.4 (see item 5). In these equations χ_r is the radiation fraction of the heat released, L_m is the mean beam length for radiation, $\dot{Q}'''_A$ is the chemical heat release rate per unit volume and χ_A is the completeness of combustion (a definition that is drawn from one of their earlier papers since this paper does not define it), ΔH_c is the heat of combustion, R is the radius of the pan. The expression for the length scale L_m as a polynomial in terms of η is set out below.

$$L_m/R = C_0 + C_1\eta + C_2\eta^2 + C_3\eta^3 + C_4\eta^4 + C_5\eta^5 \quad (1.5)$$

$$\eta = 3\dot{m}''\chi_A\Delta H_c/(\dot{Q}'''R) \quad (1.6)$$

The constants in the parameter η are set to values that have six significant digits. Using the extinction coefficient so obtained, radiation flux is calculated from $\dot{q}''_r = \sigma T_f^4[1-exp(-k_f L_m)]$. In this model, assuming flames of similar shape, the constant flame temperature of 1200 K and a constant $\dot{Q}'''_A$ of 1200 kW/m^3 is considered irrespective of the type of fuel burnt. This conclusion was obtained by comparing the data of methane, propane, and PMMA. Even though these results look by themselves very interesting, it is unclear if there is sufficient generality in covering various hydrocarbons since fuels like heptane, toluene, diesel, and kerosene have very different burn flux behavior. Further, it is entirely appropriate to obtain the radiation fraction of heat release (χ_r) as it influences the fire safety considerations directly. However, it seems less reasonable to make it a parameter of importance to link it to burn flux since the approach to connect it involves other approximations (like on χ_A, the completeness of combustion which is very difficult to extract).

Ndubizu et al. (1983) have proposed a model to determine the mass-burn rate of moderate diameter pool fires for the pans with fuel filled to the top, neglecting the pan wall conduction heat transfer to the fuel. The mathematical model deduced is based on the combustion zone modeling which requires assumptions of a large number of parameters whose reliable values are difficult to obtain. The temperature of the fire is related to the amount of air entrained into the fire due to buoyancy and a complex set of relations involving the air-to-fuel ratio are solved. The solution turns out to be very sensitive to the air-to-fuel ratio. The unknown in terms of flame temperature is transferred to the air-to-fuel ratio and it is not clear if this can be determined accurately either. In this model, the convective heat transfer coefficient is varied from 0.48 to 7.08 W/m^2K for the pan diameters of 0.3 m to 1.3 m. The radiation term is not different from the classical radiation term proposed by Hottel (1958). Even though the predictions obtained from this model seem to be good for the experiments performed in moderate diameter pans in steady-state mode with different fuels, the model does not consider the effect of other control parameters such as fuel depth, pan

material, and initial temperature, all of which affect the burn flux significantly.

Ditch et al. (2013) have pursued producing an empirical correlation to predict the mean mass burn rate for a large number of fuels - many of them are synthetic to create a range of fuels with different properties. The correlation is deduced as

$$\dot{m}'' H_s = 12.5 + 68.3 Y_s^{0.25} \left[1 - exp[-(4/3) H_s {d_{pan}}^{3/2}]\right] \tag{1.7}$$

where $H_s = [L_{fu} + c_{p,fu}(T_s - T_0)]$, H_s is the heat of gasification, L_{fu} is the latent heat of vaporization, Y_s is the smoke point of the fuel. The key parameters in the model are the heat of gasification and the smoke point of the fuel. In the above equation, the value 12.5 on the right-hand side refers to the convective flux from the gas phase and when added to 68.3 $Y_s^{0.25}$ the large pan size burn flux close to 80 kW/m^2 will result. While the aim of obtaining the equation has been to eliminate the lack of a procedure to determine the extinction coefficient, the fact that only dimensional quantities are used in the exponential term of the above equation indicates the fact that the physics has not been captured completely. Two plots of comparison between predictions and experiments for n-heptane and JP8 drawn from their work are set out in Fig. 1.11. If we note that the scales are logarithmic, the comparison does not look satisfactory. Surely, the exponential term of eqn. 1.7 needs reexamination. Sun et al (2017) have studied the pan fire burn flux of biodiesel and developed a correction to the curve fit of Burgess et al (1961) by invoking the fuel depth and wall thermal conductivity of pan material. Unfortunately, they do not seem to have been influenced by the progress in modeling over years.

1.5 Summary of the past work

An extensive literature review on the different aspects of the pool fires is presented in the earlier sections and the following is the summary of the above review.

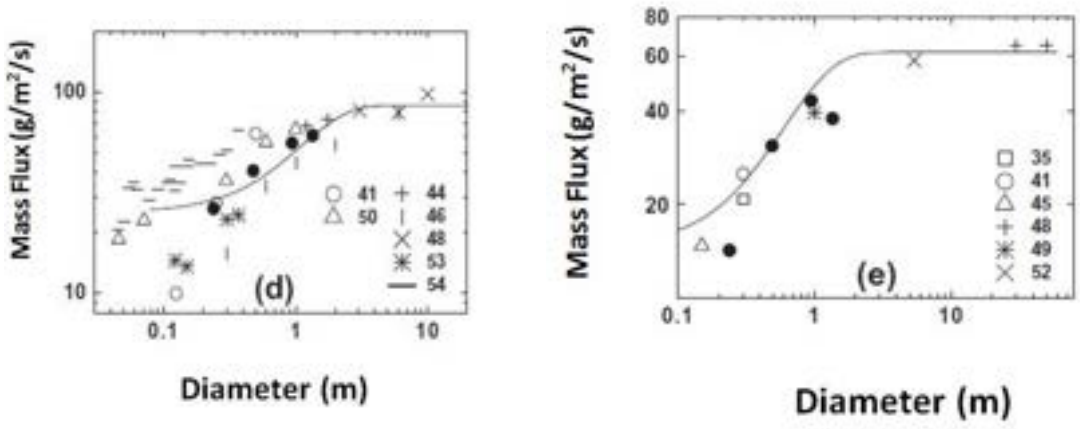

Figure 1.11: Mass burning rate experimental vs predictions from Ditch et al correlation for: (d) n-heptane; and (e) JP-8 (kerosene), drawn from Ditch et al (2013).

- The geometric data and burn flux controlling parameters such as fuel depth and free board on the pool fires that have been experimented upon are inadequate. Systematic delineation of the effects of the parameters is absent.

- The role of conduction has been highlighted and some recent studies have appeared. These have highlighted the role, but no study that incorporates the observations into a mathematical model exists.

- Most of the studies on radiation heat flux have been performed considering the extinction coefficient whose values for the same fuel and pan diameters have significant differences and hence the current models for radiation appear inadequate.

- While the fire safety standards for foam qualifications define a wide range in the fuel initial temperatures, there do not appear to be scientific data in open literature support of the fuel temperature influence.

- The best of the models available on burn flux predictions does not account for several parameters like fuel depth, free board, and initial fuel temper-

ature that can influence the burn flux significantly.

1.6 Objectives of Present Work

In view of the review of earlier literature, the present study aims at :

1. Conducting a sequence of experiments to elucidate the effects of fuel thickness (h_{fu}) and free board (h_{fb}) with

   (i) pans of diameters between 0.1 to 2 m with different depths (h_{pan}) with their own material properties, namely, density (ρ_w), specific heat (c_{pw}), and conductivity (k_w), and

   (ii) different fuels with their physical and thermal properties - density (ρ_{fu}), specific heat (c_{pfu}), boiling point (T_{bfu}), latent heat of phase transformation (L_{fu}), conductivity (k_{fu}) and stoichiometric ratio with air (S) at different initial temperatures (T_0)

2. Evolving correlations using dimensionless parameters that involve the geometric, thermodynamic, and transport properties listed above to characterize the mean burn behavior defined by the burn mass flux ($\bar{\dot{m}}''_{fu}$) and comparing them with the data from the literature as well as from this study.

3. Evolving a code for the temporal prediction of the mass burn based on heat flux balance at the surface of the fuel accounting for conductive, convective, and radiative modes of heat transfer into the liquid as also the conduction within the liquid and comparing the results from the code with data from literature and from the present study.

1.7 Organization of the Thesis

The rest of the thesis is organized as follows:

- **Chapter 2** describes the details of experimental methods used, properties of the fuels and the pan used, tools used for the measurement of mass loss, fuel, wall, and gas-phase temperatures, the experiments carried out, and the methods adopted to analyze the data.

- **Chapter 3** consists of a detailed description of the experimental study as it progressed through various stages in understanding the pool burn behavior over a range of parameters described earlier. Further, the comparison of present experimental data with the data available in the literature is also set out.

- **Chapter 4** describes the model evolution for the mean burn flux for steady and unsteady pool fires. The aim is to include all the controlling parameters through appropriate dimensionless parameters. It also presents the comparison of the predictions with the experimental data obtained here as well as from literature set out in the Appendix.

- **Chapter 5** deals with the modeling of unsteady pool fire based on the experimental results, considering all the crucial parameters, it describes the analytical method adopted in deducing pan wall temperatures, fuel temperatures, time-varying mass burn, heat fluxes received by the fuel surface as feedback. It also describes the MATLAB code developed to predict the unsteady burn rate, heat feedback to fuel surface, and effects of different parameters that alter the burn behavior of pool fire. The results and discussion of the experimental work and the predictions, the comparison of experimental data with the predicted data are also set out.

- **Chapter 6** contains an overview and concluding remarks.

Chapter 2

Experimental Techniques and Methodology

This chapter describes various experimental tools and techniques used in the study of the unsteady pool fire burning process to obtain the mass loss, pan wall temperatures, condensed phase temperatures, and gas-phase temperatures. Details of fuels, pans used and their thermal properties are also presented.

2.1 Experimental Tools

2.1.1 Weighing Balance

Electronic digital balances are used in this experimental work to obtain the varying mass loss with time. Three different balances of different capacities were used which were connected to data acquisition systems to convert the analog data into digital form and store it. The balances that were used in the experiment were calibrated with a standard range of weight for the full-scale range of operation before the conduct of the experiments. The specifications of the balances used are as follows.

Digital electronic balance, ESSAE – DS852
Digital electronic balance, BEST – N369
Digital electronic balance, BEST – A729

2.1.2 Pans

In order to study the effects of different control parameters listed in the objectives, pans of various sizes and materials are used to conduct experiments. Mild steel pans of 0.2, 0.3, 0.4, 0.5, 0.92, and 2 m diameter with depths of 40, 50 and 60, 90 and 145 mm are used to evaluate the freeboard, fuel thickness, and pan diameter effects on the mass burn rate. The freeboard effect is evaluated by using a fixed fuel depth with pans of different depths. Pans 0.2 m diameter, 40 mm deep, and 3 mm thick made of aluminum alloy, stainless steel, mild steel, and glass are used to elucidate material property effects on mass burn rate. Figure 2.1 shows pans used in this work. The specific notation used is as follows: C50060MS3 means a circular pan of 500 mm diameter, with 60 mm depth made of mild steel with 3 mm wall thickness. C2K145MS3 means a 2000 mm diameter pan with other notations as described here.

2.2 Fuels used and their properties

The fuels used in this study are n-heptane, diesel, kerosene, methanol, and ethanol to cover a range of fuels. Table 2.1 shows the thermodynamic and transport properties, thermal diffusivity of the liquids is an order of magnitude lower than the pan material and hence the heat transfer process through the liquids has to account for the unsteady process.

2.3 Thermal Properties of Wall Material

Table 2.2 presents the data on the pan wall materials considered. While several thermal properties of the pan were obtained from data sheets, thermal conductivity which is a more sensitive property of the composition was experimentally obtained by measuring a one-dimensional temperature profile and extracting thermal conductivity from the data. The data matched with information from

(a)

(b)

(c)

Figure 2.1: (a) Pans of 0.2 m dia, 40 mm depth made of stainless steel (SS), mild steel (MS), aluminum alloy (Al) and glass (GL), b) MS pans of 0.2, 0.3, 0.4 and 0.5 m dia, 40, 50 and 60 mm depth and c) MS pan of 2 m dia, 145 mm depth

Table 2.1: Properties of the fuel

Fuel	ρ_{fu} kg/m^3	T_{bfu} K	c_{pfu} kJ/kgK	L_{fu} kJ/kg	k_{fu} W/mK	α_{fu} mm^2/s	μ_{fu} mNs/m^2
n-Heptane	680	369	2.1	322	0.14	0.090	0.409
Diesel	850	660	1.9	300	0.15	0.098	3.35
Kerosene	810	490	2.01	320	0.145	0.089	1.64
Methanol	791	338	2.57	1100	0.202	0.093	0.507
Ethanol	785	351.4	2.57	846	0.16	0.082	0.98

published sources excepting for Al. In this case, it turned out to be an alloy whose precise composition could not be obtained from production sources, and the measured value of k_w = 60 W/mK is very different from published values (120 to 200 W/mK). Nevertheless, it is much higher than MS. If we make a simple estimate of the transient conduction times using $t_{cond} \sim h_{pan}^2/4\alpha_w/2$, we get the values set out in the last column. Except for glass, the transient conduction times are small compared to the burn time. This implies that a steady conduction process along the wall will be a good approximation.

2.3.1 Thermocouples and Data acquisition system (DAQ)

Thermocouples of K type with a bare junction size of 0.4 mm that can measure up to 1530 K are used in this work. They are mounted at the required locations to measure the pan wall temperatures, fuel temperatures and flame temperatures. Figure 2.2 shows the thermocouples mounted on the pan wall by welding the thermocouple by placing it in the small dent created for the purpose of mounting the junction. The data acquisition is carried out with the help of Measurement Computing MC personal DAQ -56 series with acquisition

Table 2.2: Properties of pan ($t_{cond} \sim h_{pan}^2/4\alpha_w/2$)

Material	d_{pan}	t_w	ρ_w	c_{pw}	k_w	α_w	h_{pan}	t_{cond}
	mm	mm	kg/m^3	kJ/kgK	W/mK	mm^2/s	mm	s
Al	200	3	2730	0.91	60	24.1	40	8.5
MS	200	3	7800	0.46	32	8.9	40 - 60	22 - 100
SS	200	3	7800	0.46	16	4.45	40 - 60	44 - 200
SS [19]	200	3	7830	0.48	21	5.6	40	35
Glass	190	3	2230	0.75	1.14	0.68	40	590

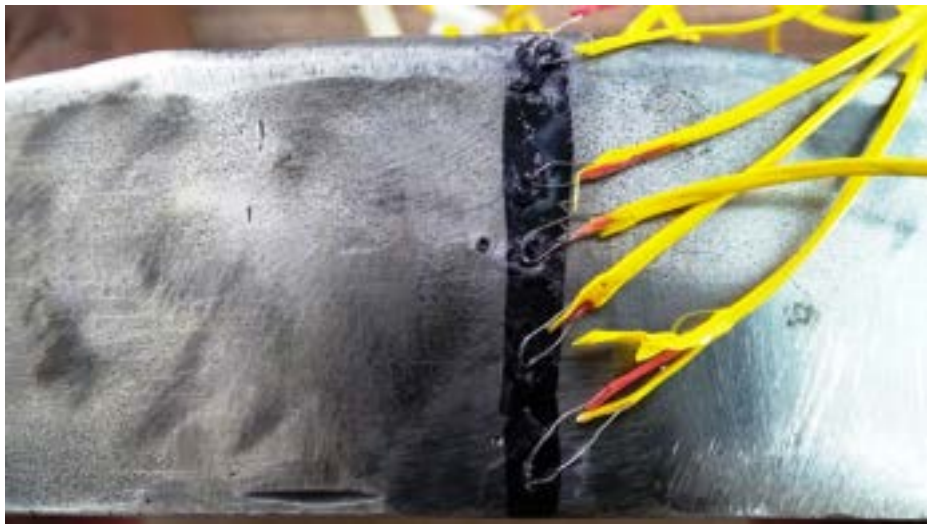

Figure 2.2: Themocouples mounted on side wall of SS pan

rate of 80 Hz. The thermocouple with long enough support rod was introduced into the n-heptane pool fires of 0.2, 0.5, and 2 m diameter pans. Figure 2.3 shows that thermocouple that has about 5 mm of open bare wire with the bead and the rest covered by alumino-silicate insulation inserted into the flame of 0.1 m diameter n-heptane pool fire to measure the flame temperature. It was uncovered that on introducing cold thermocouple into the fire resulted in temperatures of 850 C (1120 K) and on withdrawal, fair amount of sooting on the thermocouple bead and the leading support was observed. Inferring that the cold wire resulted in immediate soot deposition, the thermocouple was heated to flame temperatures in a separate lean high temperature LPG flame and then was quickly introduced. This resulted in temperatures of 950 C (1220 K) for few seconds and after which it started decreasing slowly. Again withdrawal of the thermocouple showed slight sooting. The inference from these trials was that preheated beads would help alleviate the soot related problems. Figure 2.4 shows the flame temperature data for n-heptane, diesel, kerosene, and ethanol fuels. The difference in the measured flame temperatures without and with bead heating is shown in the case of n-heptane. The measured temperatures compared with those of earlier researchers are set out in Table 2.3. The temperature reported by Chen et al (1991) is by using a 0.5 mm wire based thermocouple. The bead would be typically of 1 mm size. It is most likely that soot coating has led to the measurement of lower temperature as discussed above and the true temperature is close to 1200 K. As can be noted, the comparison between the present measurements and those of earlier researchers is excellent considering the fact that high temperature thermocouple measurements are accurate up to $\pm$ 50 K.

2.4 The experimental setup for burn rate measurements

Figure 2.5 shows the arrangements for the measurement of mass loss, wall temperatures and temperatures within the liquid at the centerline, and gas-

Figure 2.3: Themocouple arrangement for flame temperature measurement

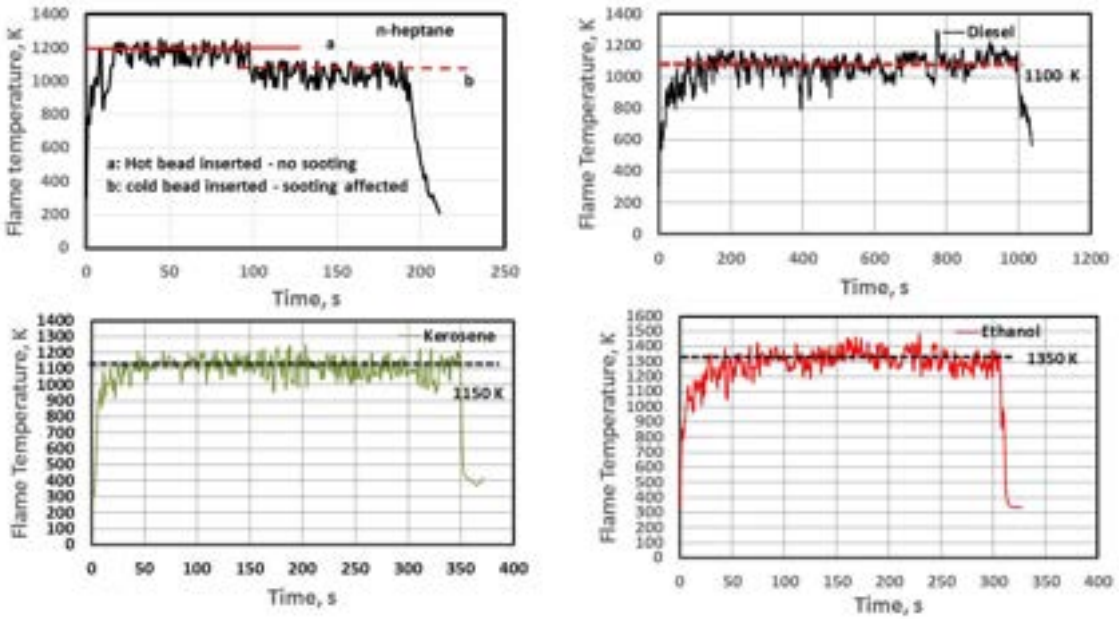

Figure 2.4: Centerline flame temperature at a height of 0.4 d_pan vs time for n-heptane, diesel, kerosene and ethanol fuels

Table 2.3: A comparison of measured flame temperatures

Fuel	Author	d_{pan} (m)	T_f (K)
n-heptane	Chen et al (1991)	0.2	1073
	Koseki (1991)	0.6	1200
	Present	0.2 - 2	1200
Diesel	Present	0.2	1100
Kerosene	Bouhafed et al (1988)	0.15	1100
	Present	0.2	1150
Methanol	Weckman and Strong (1996)	0.3	1440
	Present	0.2	1450
Ethanol	Fischer et al (1987)	0.5	1300
	Present	0.2	1350

phase temperatures. K-type thermocouple of 0.4 mm diameter with a bead size of 0.4 mm is used to obtain the temperature data. To obtain wall temperature data a small dent on the pan wall at the required location was made and the thermocouple was mounted as shown in Fig. 2.2, to obtain the liquid phase temperature data the thermocouples were mounted from the openings made on the bottom surface of the pan. In order to obtain the flame temperature, thermocouples were mounted at the required heights and a wire length of about 5 mm was exposed to fire. The pan itself is placed over an Alumino-silicate blanket of 25 mm thickness that rests over a balance of 5 kg capacity with an accuracy of 100 mg for small pan fire tests and a balance of 60 and 1000 kg capacity with an accuracy of 1 g and 10 g for larger pans is used. For extracting initial fuel temperature effects, the pan and fuel were heated and brought to the desired temperature before starting the experiment. The experiments were restricted to temperatures above the ambient temperature because it was found that moisture condensation affected the experiments at lower temperatures.

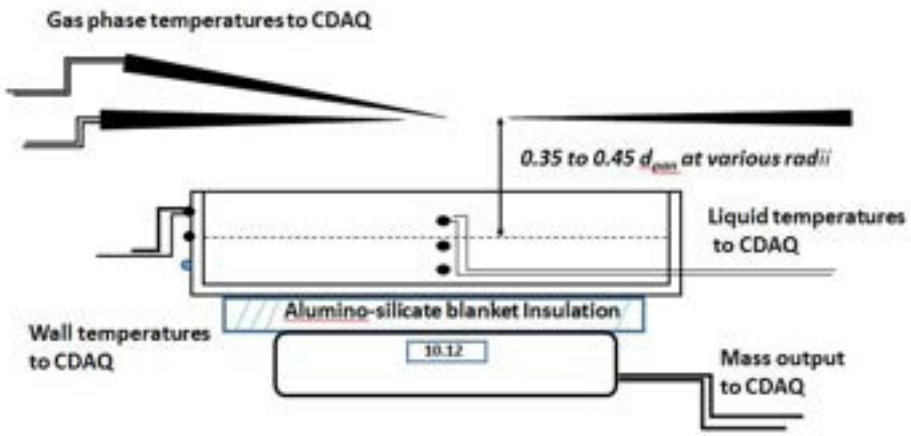

Figure 2.5: Schematic diagram of the experimental arrangement used in the experiments to include mass loss, pan wall temperatures, condensed phases and gas phase temperatures during the burn

The indoor fire test facility of 18 m x 12 m x 12 m as seen from outside and a 2 m pool fire inside the laboratory of staggered perforated walls burning in a quiescent condition is seen in Fig. 2.6. Further, to ensure even smaller wind disturbances for the pool fires of up to 0.5 m diameter, a simple and special construction made using the shade net is shown in the figure 2.7. Measured ambient disturbances were less than 0.2 m/s and visible indication of the flame always showed symmetry expected of quiescent environment.

Figure 2.6: Indoor fire laboratory - On the left is the outside view. On the right is the 2 m circular pan fire burning inside the laboratory.

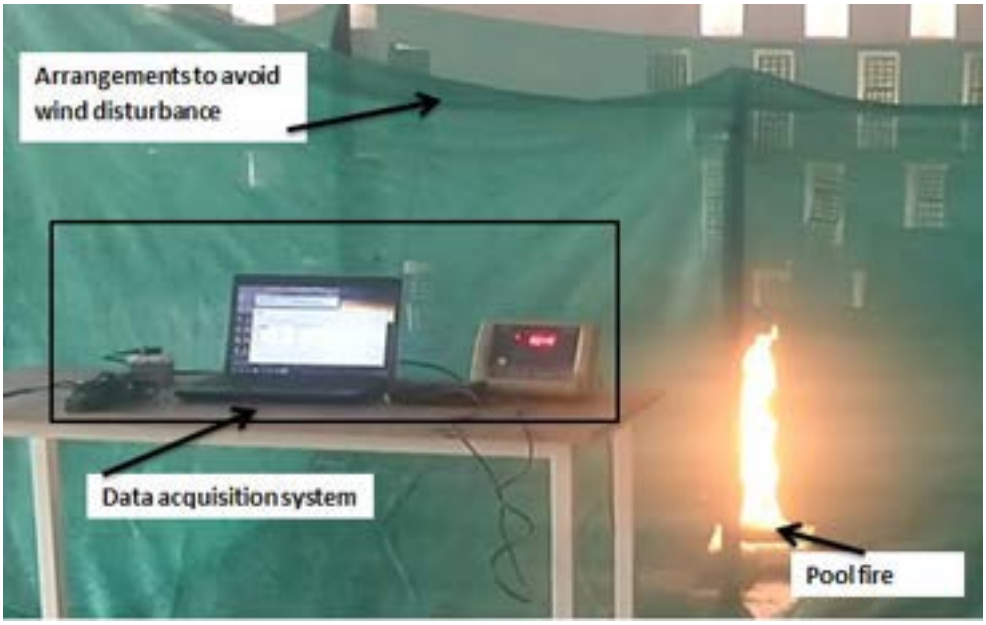

Figure 2.7: The experimental arrangement with a fine outside net to make the environment quiescent for small pool fires

Table 2.4: Measured quantities and equipment used

Measured quantity	Equipment Used
Fuel mass loss with time	Weighing balances of 5, 60 and 1000 kg capacity
All temperatures	K-type thermocouple with 0.4 mm bead
Wind Velocity	Turbine type anemometer, range - 0.1 to 2.4 m/s

2.5 Summary

All the measurement tools used along with the experimental techniques and properties of fuels and the pans are presented in this chapter. Table 2.4 summarizes the quantities measured with their corresponding measurement tool.

Chapter 3

Experiments and the data

The earlier chapter dealt with the experimental tools that have been used to make the required measurements in this thesis. The present chapter describes the specific experiments carried out to elucidate the effects of different control parameters on the mass burn rate of pool fires. Table 3.1 shows the experiments performed along with the purpose - the parameter variation that will provide data. Experiments in 0.2 m to 2 m diameter MS pans, 40, 50, 60, 90, and 145 mm deep with n-heptane fuel are performed to understand the fuel depth and pan diameter effect on the mass burn rate. Experiments in 0.2 m diameter, 40 mm deep pans made of AL, MS, SS, and GL were conducted at n-

Table 3.1: List of Experiments performed to study the effects of various control parameters on the mass burn rate. (a: n-Heptane; b: Methanol; c: Ethanol, d: diesel; e: kerosene; Ma* = Material, Pa* = Parameter, All = AL, MS, SS & GL)

d_{pan} m	Ma*	h_{pan} mm	h_{fu} mm	T_0 K	Fuel	Pa*
0.2-2	MS	40-145	10-30	300	a	h_{fu}, d_{pan}
0.2	All	40	10-20	300	a	k_w
0.2-2	MS	40-145	10-20	300	a	h_w
0.2	SS	40	13	321, 347	a	T_0
0.2	MS, SS	40	10-20	300	b - e	Fuel

heptane fuel depths of 10 and 20 mm to delineate the effect of thermal conductivity on the mass burn rate in small diameter pool fires. Select experiments at different initial temperatures in 0.2 and 0.5 m MS pans were performed to replicate the temperature effects performed earlier by Chen et al (2011) and some experiments were performed with the n-heptane fuel floating on water to understand the effect of water on the burn behavior of pan fires. Finally, experiments in a 0.2 m diameter, 40 mm deep MS and SS pan with methanol, ethanol, kerosene, and diesel were performed to determine the fuel property effects. It must be pointed out that while a few are a replication of earlier studies with the current hardware, most others are new, novel and considered very necessary. They were performed with the aim to uncover the effect of various parameters on the burn behavior so that they can provide input for obtaining a correlation for the mean burn flux and also as an aid in deducing a time-varying model to capture the unsteady pool burn behavior.

Table B.1 in the Appendix presents the data of 72 tests that were conducted in respect of the above. Columns 1 to 7 contain the information on the parameters of the pans and the fuel used in the tests and column 8 contains the experimental data on the mean burn flux. The mass loss vs time data will be set out below.

3.1 Effects of pan material, h_{fu} and h_w

As noted from the Tables A.1 and A.4 in the Appendix, the fuel depth influences the burn flux in both steady and unsteady mode of operations, and to explore this aspect, the experiments were performed. The first set of experiments was done to replicate the work of Chen et al. (2011). The plot of fuel mass vs time of present experiments with stainless steel pan along with those of Chen et al (2011) appears in Fig. 3.1. The experimental data of Chen et al. (2011) is at much lower fuel temperatures, perhaps related to the local ambient temperature. Our attempt to replicate the experiments at the same temperature was

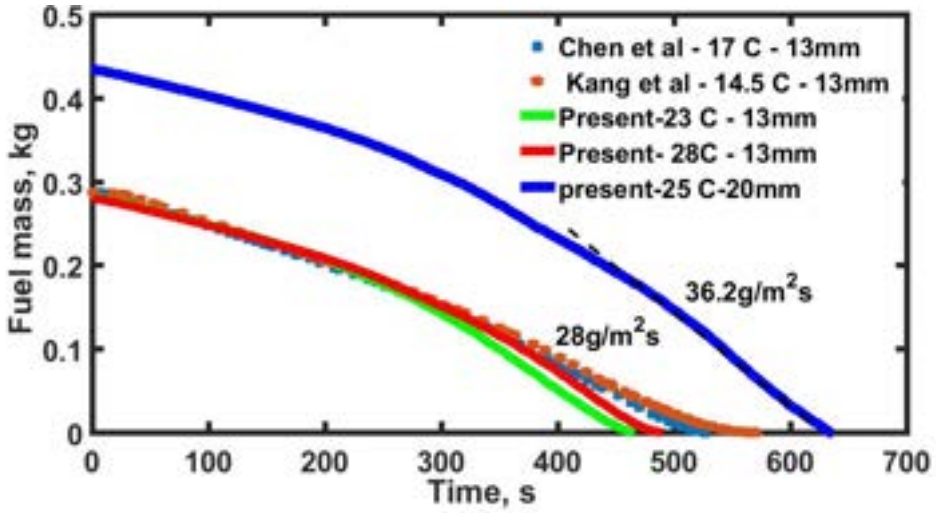

Figure 3.1: Comparison of mass loss with time for 0.2 m SS pans, 40 mm deep with Chen et al. (2011a) for 13 mm n-heptane; also 20 mm heptane, present

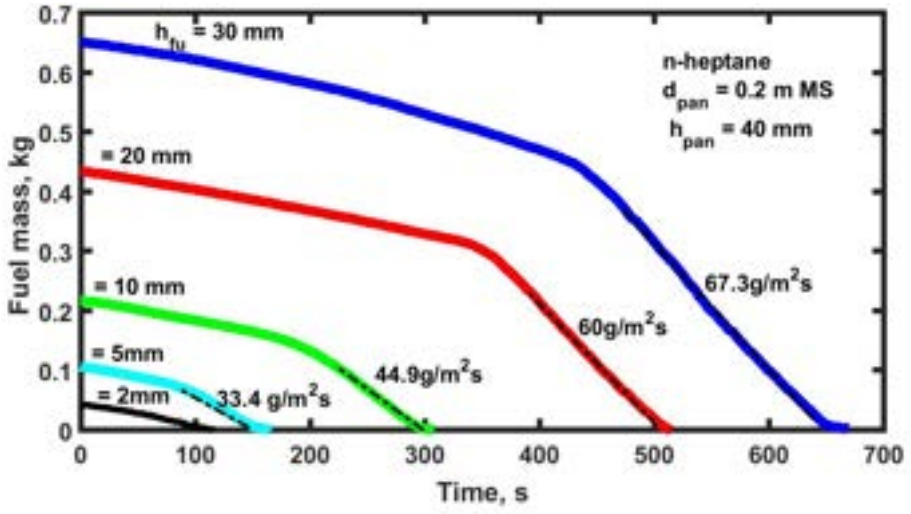

Figure 3.2: Mass loss with time on a 0.2 m dia MS pan, 40 mm deep with 5 - 30 mm n-heptane

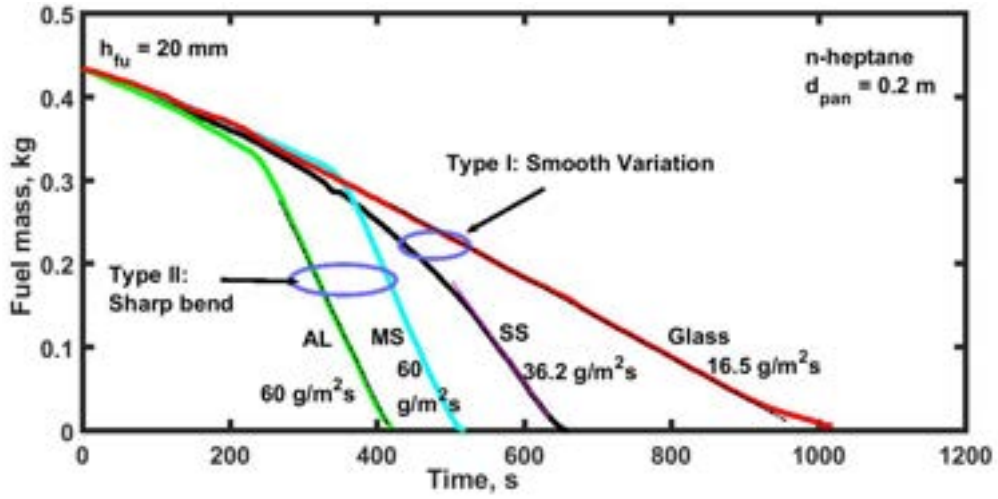

Figure 3.3: Mass loss with time on 0.2 m dia, pans of different materials, 40 mm deep, 20 mm n-heptane

made difficult because of the condensation of moisture and hence, the experiments were limited to the ambient temperature. The initial mass loss matches well and the later mass loss is different due to ambient temperature effects. At h_{fu} = 20 mm, it can be seen that the burn flux ($\dot{m}''_{fu}$) reaches values of 37 g/m^2s.

To further investigate the issue, experiments were carried out on 0.2 m dia MS pan, 40 mm deep with 3 mm wall thickness at fuel depths of 2, 5, 10, 20 and 30 mm. The results are set out in Fig. 3.2. It can be seen that the mass loss curve has two segments - the initial one that seems nearly the same for all the depths and a later one in which the burn rate is significantly larger in slope. The slopes give the $\dot{m}''_{fu}$ when the mass loss is divided by the time over which this mass loss occurs and pan area.

At 5 mm fuel depth, $\dot{m}''_{fu}$ of 24.5 g/m^2s is similar to the value obtained by Chen et al. (2011), but at higher depths, $\dot{m}''_{fu}$ values go up to 60 and 67.3 g/m^2s at 20 and 30 mm depth. It appears that the burn behavior has reached a steady value at this stage. These values are similar to the burn flux values achieved in large pool fires (see Figure 3.15). A quick inference is that this behavior is related to the liquid in the pool having reached boiling, a feature that needs

Figure 3.4: Jacketed pan circulating water at ambient temperature in the jacket

further investigation.

At this stage, it was thought appropriate to examine the burn behavior with pans of different materials to cover a range of thermal conductivity. Figure 3.3 presents mass loss with time with pans of different materials and pan depths of 40 mm and fuel depth of 20 mm. The mass loss rate for the glass pan varies slightly over the burn time, for SS pan increases smoothly over the burn duration, for MS and AL pans, changes very significantly with a sharp change at a time that for AL pan is ahead of MS. If we note that the thermal conductivity of these materials is in increasing order, it can be inferred that the wall heat transfer process must be affecting the behavior directly.

In order to clarify this feature experimentally, another MS pan shown in Fig. 3.4 was fabricated with a 20 mm channel all around the pan side (of 60 mm depth). Two experiments of n-heptane burn with this pan without and with ambient water circulation were performed. The results are set out in Fig. 3.5. As can be noted, for the case without water flow, one has the two segments $\dot{m}''_{fu}$ behavior and with water flow, it is about 12 g/m^2s except for the initial transient. The initial transient is due to the water temperature being slightly higher than the temperature of the fuel. The question of whether the differ-

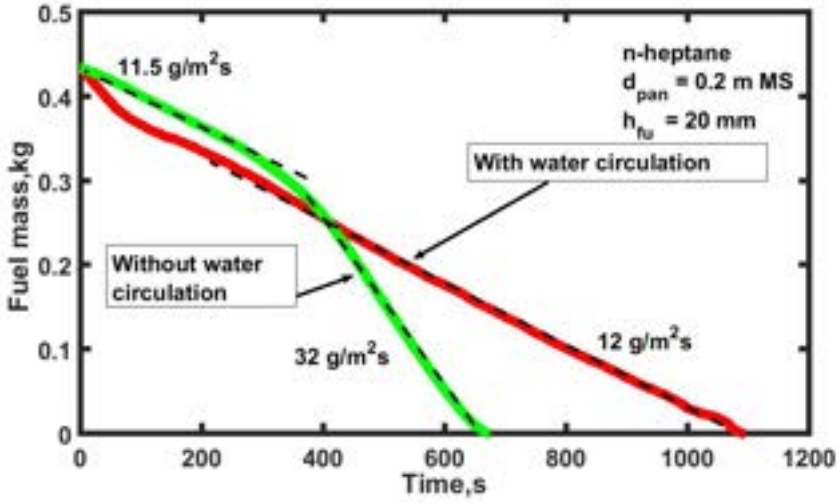

Figure 3.5: Mass loss with time on a 0.2 m dia MS pan with and without water circulation around the side with the uncooled pan bottom resting on ceramic blanket

ence between the results without and with water cooling can be attributed to conduction arises. It was noted that just after the transition to higher burn flux at about 380 s in Fig. 3.5, the fire size grew larger. It was also noted that after this transition, the radiation received at a distance was much higher. Hence, it was inferred that radiation flux would be enhanced to the fuel surface as well. No measurement of the radiation flux received by the surface was performed because the sensitive gauges were unavailable. Instead, it was thought appropriate to elucidate this feature from a composite model aimed at evaluating the magnitudes of all the components of the flux with a satisfactory prediction of the mass loss history for several cases including this case. This is the subject of Chapter 5.

Figure 3.6 shows the comparison of flame during the peak mass burn rate for the experiments performed in 0.2 m diameter GL pan, jacketed MS pan with water circulation, and MS pan with 20 mm fuel depth. It can be observed from the figure that the nature of flame in the Gl pan and jacketed MS pan with water circulation are the same, indicating that wall conduction effects are

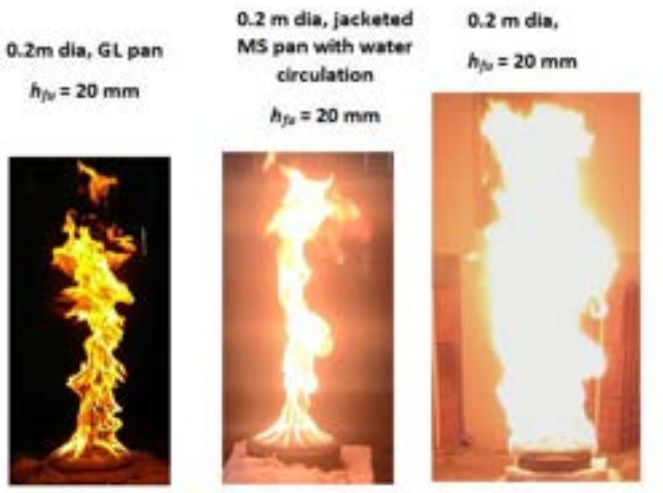

Figure 3.6: Photographs of pool fires at peak burn rate in 0.2 m diameter GL pan, Jacketed MS pan with water circulation and MS pan

suppressed in the jacketed pan and hence the reduced peak flux is obtained. Whereas in the case of normal MS pan the pan wall conduction is high which results in a broad and sporadic flame as shown in the figure and a higher peak burn rate is obtained as indicated in Fig. 3.2.

In order to understand the thermal behavior, each of the pans had thermo-

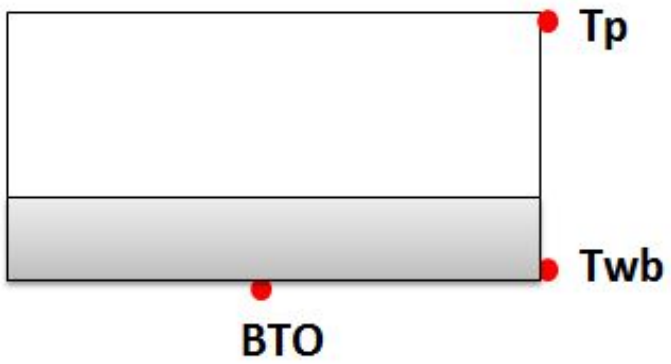

Figure 3.7: Schematic diagram indicating the thermocouple mounting at selected location on pan wall; Tp = Pan tip, Twb = Pan bottom outer edge; BTO = Pan bottom outside

couples mounted at the bottom outer region (T_{wb}) and near the tip of the pan (T_p) as shown in Fig. 3.7. In select experiments, thermocouples were placed at other locations in-between as well. In each of the cases, a 0.4 mm K type thermocouple was welded after creating a small dent at the marked location.

The results of T_{wb} for all the cases on 0.2 m diameter pans of different materials are set out in Fig. 3.8. The left side figure is set with a time coordinate. While the general tendency of faster rise with Al and MS pans is clear when observed carefully, the right side plot of T_{wb} with a fuel regression (reg) rendered dimensionless by the initial fuel thickness, h_{fu}, as z = reg/h_{fu} for these experiments makes the differences in the behavior more clear. The group of plots on the lower end belongs to glass and SS pans - the arrival of heat via the pan wall occurs slowly with these pans. The group with sharper initial rise belongs to MS and Al. Another deduction is that a substantial fuel regression for these pans occurs at higher temperatures, implying that the pool has reached near boiling conditions earlier in these cases.

In order to explicitly extract this feature, the temperature at the center of the pan, 1 mm above the bottom inside the fuel denoted T_{bo} is set out for pans of all materials for a fuel depth of 20 mm in Fig. 3.9. The rise in the liquid temperature is the fastest with pans of AL, MS, SS, and GL in the order of decreasing thermal conductivity. The true origin for this behavior lies in the fact that the gas phase heat flux is much higher in the cases with high thermal conductivity and hence, the heat flux transferred to the liquid is much higher. In each of the cases, the liquid reaches a temperature near the boiling point and levels off, indicating that the burn process during this period occurs with the liquid in bulk boiling mode with AL at first and GL at last. Figure 3.10 show the photographs of the pool fires of 0.2 m MS pan at a stage in which the entire liquid has attained the boiling point. This picture corresponds to Fig. 3.9, curve MS at 400 s. It can be seen that the liquid at the surface is vigorously boiling indicating the possibility of a state between nucleate and

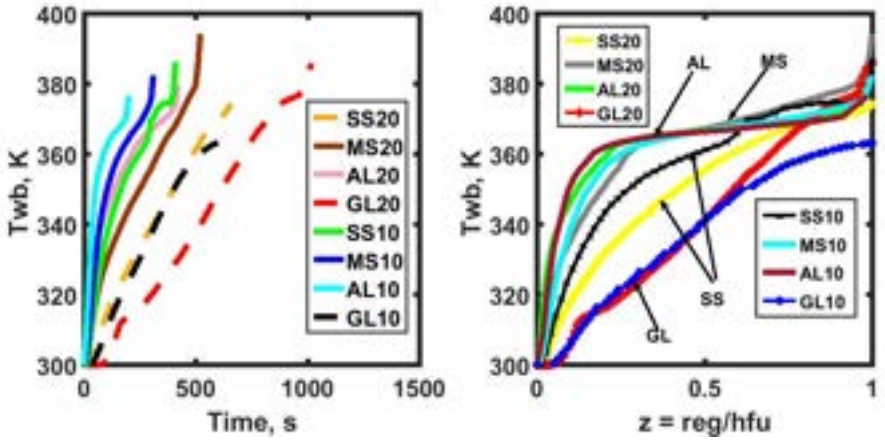

(a) T_{wb} on 200 mm dia 40 mm deep pans of Al, MS, SS and GL materials for 10 & 20 mm heptane

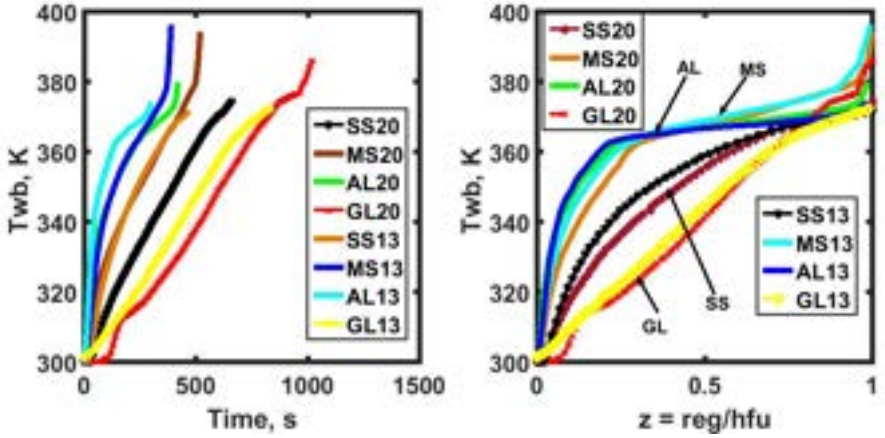

(b) T_{wb} on 0.2 m dia 40 mm deep pans of Al, MS, SS and GL materials for 13 & 20 mm heptane

Figure 3.8: Bottom outer wall temperature, T_{wb} on 200 mm dia 40 mm deep pans of Al, MS, SS and GL materials for 10, 13, & 20 mm heptane

film boiling.

Figure 3.11 shows the variation of the pan tip temperature, T_p, and the bottom outer wall temperature, T_{wb} for pans of different materials. Pan tip temperature is chosen as an important candidate for describing the burn behavior as the pan tip receives the heat from the flame just above it and transfers it along the pan to the bottom region. Pans with lower thermal conductivity

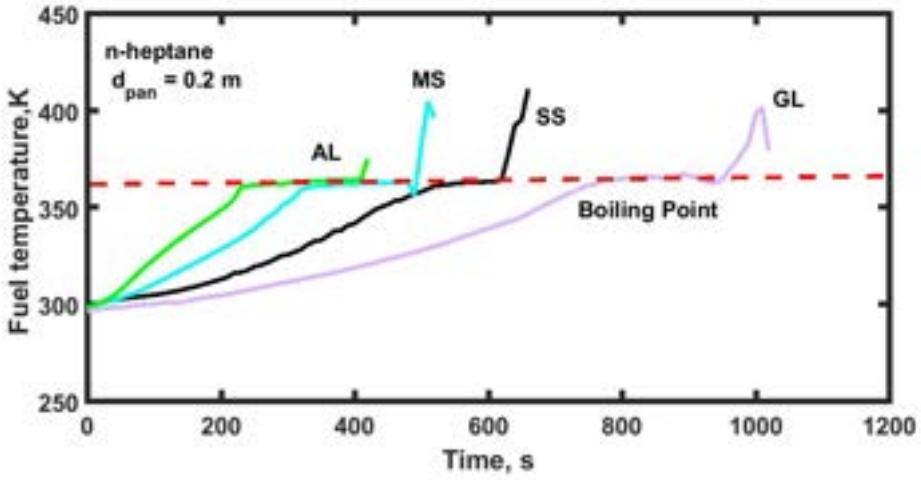

Figure 3.9: Liquid temperature one mm above the pan wall on the centreline, T_{bo} on 0.2 m dia 40 mm deep pans of Al, MS, SS and GL materials at three n-heptane fuel depth of 20 mm

Figure 3.10: The 0.2 m MS pan with n-heptane undergoing vigorous pool boiling. The right side photograph is an expanded version of the left side photograph

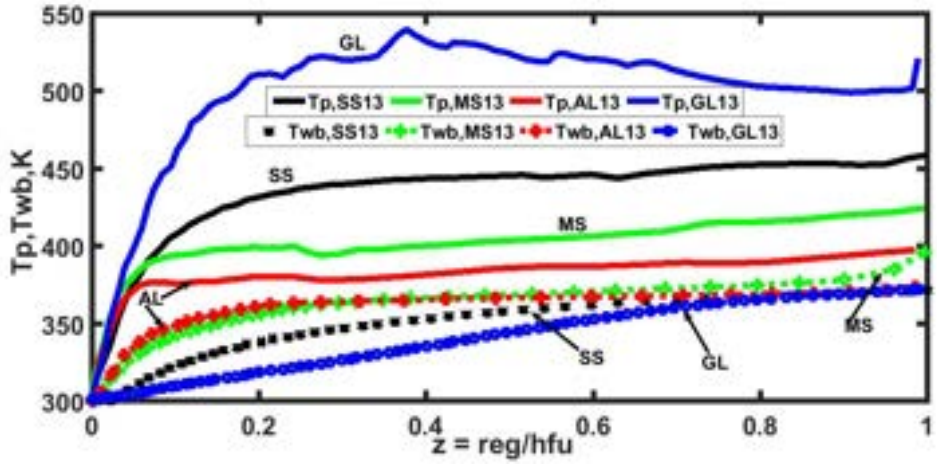

Figure 3.11: The pan tip temperature, T_p and the bottom outer wall temperature, T_{wb} for 0.2 m dia pans of different materials at a fuel depth of 13 mm

reach higher tip temperatures and lower bottom wall temperatures (see the variation for GL pan, in particular). The pan tip temperatures seem to level off for a reasonable time before they begin to increase later. The actual values of T_p during the "steady" regime are about 370 K for Al - just above the boiling point of n-heptane, 390 to 400 K for MS, 430 - 440 K for SS, and 530 to 540 K for GL. These features are important and are expected to aid the development of the mathematical model for predicting the burn behavior.

The measured wall temperatures at specific points on the wall (T_{wall}) are set out in Fig. 3.12 for MS and SS pans. It appears that to a first order, the behavior of T_{wall} with distance along the wall can be considered linear. This trend is similar to the one observed by Chen et al (2011).

In order to understand the effect of water depth on the burn rate of fuel that floats over water, experiments were conducted with 0.2 m and 0.5 m diameter MS pans. The choice of fuel and water depths were made such that the freeboard was kept constant and so, the effect of water could be extracted separately. For instance, in the 0.2 m diameter pan, experiments were performed in 40 mm deep pan at fuel depth of 10 mm n-heptane without water and it is com-

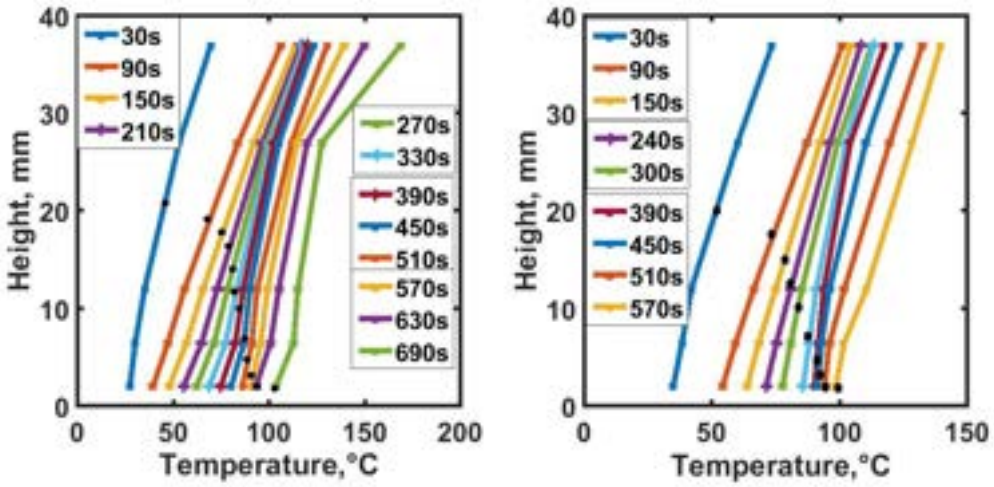

Figure 3.12: The wall temperature, T_{wall} for 0.2 m diameter pans of SS (left) and MS (right) for h_{fu} = 20 mm as a function of distance from tip to bottom at 60 s time intervals. The dotted lines show the position of liquid surface during the burn

Table 3.2: List of experiments on extracting the effect of water on the burn behavior

d_{pan}	h_{pan}	h_{fu}	h_w	h_{fb}
m	mm	mm	mm	mm
0.2	40	10	0	30
0.2	60	10	20	30
0.2	40	20	0	20
0.2	60	20	20	20
0.5	40	10	0	30
0.5	60	10	20	30
0.5	50	20	0	30
0.5	60	20	10	30

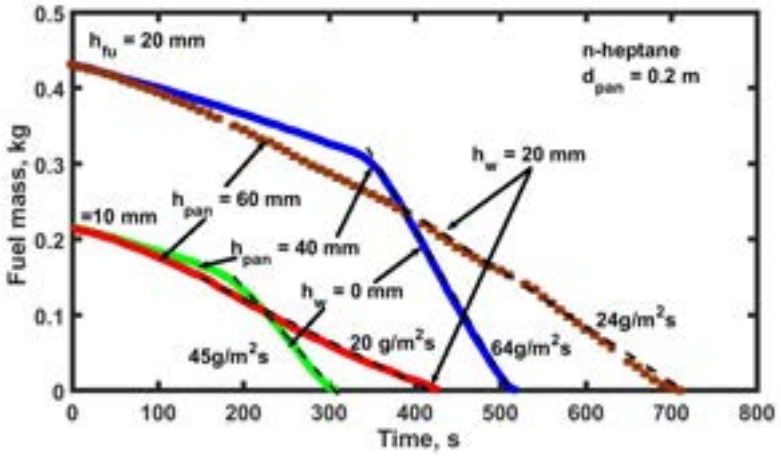

Figure 3.13: Mass loss vs time of 0.2 m MS pan for n-heptane fuel without and with water; C20040-10H-20W implies 0.2 m diameter pan with 10 mm heptane and 20 mm water

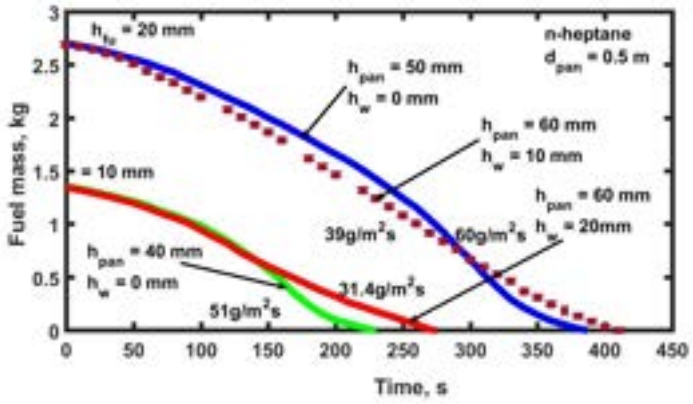

Figure 3.14: Mass loss vs time of 0.5 m MS pan for n-heptane fuel without and with water; C50040-10H-20W implies 0.5 m diameter pan with 10 mm heptane and 20 mm water

pared with the experiment done in a 60 mm deep pan with 10 mm n-heptane floated on 20 mm water, so that the freeboard and fuel depth in both the cases are same and one can extract the water effect separately.

The list of experiments carried out is set out in Table 3.2. Figures 3.13 and 3.14 show the mass loss variation of experiments with fuel only and fuel floating on water for the cases outlined in Table 3.2. It can be observed that at the initial

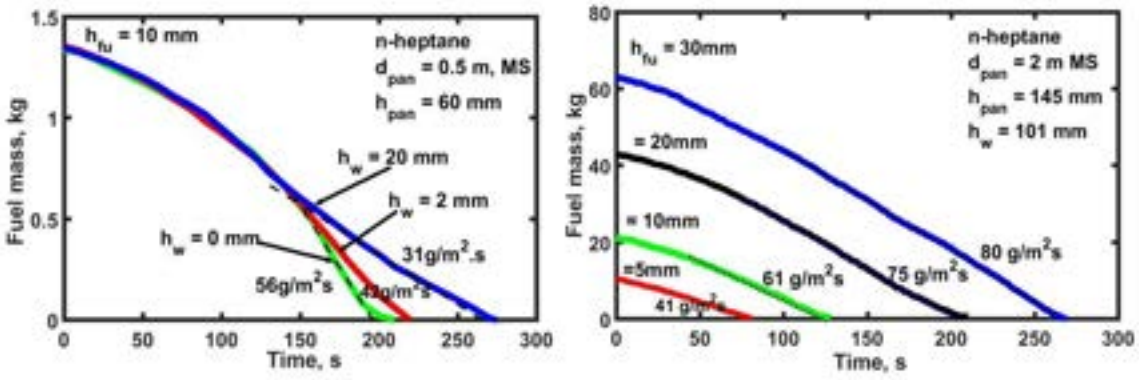

Figure 3.15: Mass loss with time of a 0.5 m diameter mild steel pan, 60 mm deep with 10 mm fuel without water and those floating on 2 and 20 mm water and 2 m dia mild steel pan, 145 mm deep with 5 - 30 mm fuel thickness with water depth of 101 mm

stage burn rate remains same and the deviations occur later. Figure 3.15 shows the variation of the burn rate of 0.5 and 2 m MS pans with different fuel and water thicknesses. In the case of a 0.5 m diameter pan, with 10 mm fuel floated on the different thicknesses of water, it is evident that even though the initial burn rate does not vary for a significant amount of time the maximum and mean burn rate decrease with increasing thickness of water. In this particular plot, the freeboard changes because the sum of the depths of fuel and water increases. The results of the experiments on 2 m diameter, 145 mm deep MS pan conducted with n-heptane fuel thicknesses of 5 to 30 mm floated on 101 mm water show that both the mean and the peak burn flux increase with fuel thickness.

A calculation of the changes in the mean burn flux due to water shows that up to 0.5 m dia pan, the decrease can be estimated at 1 % per mm water thickness up to 20 mm water thickness. For larger diameter pans, the difference is within the error band of the fuel burn mass flux ($\sim$ 5 %) largely because the heat transfer across the interface between the fuel and water constitutes a small

fraction of the heat flux values involved.

The data from various experiments for n-heptane fuel are summarized in Table 3.3. The mean burn flux ($\bar{\dot{m}}''_{fu}$) shown in this table is obtained as the ratio of the fuel mass divided by the burn time and pan cross-sectional area. Also shown is the peak flux obtained from the increased burn rate after a couple of hundred seconds during which the liquid heats up towards boiling with heat flux from the gas phase as well as wall conduction. What is clear from the table is that at each pan diameter, both the mean and peak flux increase with the depth with a tendency to reach asymptotic values. Also, the material of the pan - MS or SS here matters significantly in terms of the burn behavior. This feature that affects the wall-to-liquid heat transfer has been known earlier [Kang et al. 2010].

Further confirmation of wall conduction effects was seen in the videos taken of these fires shows that after some burn time, the fires become broad with the sporadic spewing of the vapors from the side. The flames occasionally turn around and lick the outer regions of the pan indicating direct heating of the pan. This behavior is not uniform all around and occurs sporadically. Since it is already known that the liquid reaches boiling (shown in Fig. 3.9), the wall heat transfer process must be reaching regimes of nucleate boiling (as also pointed out in Chen et al. 2011) with very significant unsteady heat transfer into the fuel. Any approach to modeling the burn process must include these phenomena.

Such sporadic behavior of flame cannot be observed in the steady state pool fires where a constant fuel depth is maintained throughout the experiment and the pan wall heat conduction heat transfer is minimized either by reducing the pan thickness at the upper region of the pan (Ditch et al. 2013) or by cooling the pan bottom by circulating the water (Hamins et al. 1994). Figure 3.16 shows the flame structure for 0.2 m diameter pool fire experiments performed in unsteady and steady mode. As can be noticed from the figure for

Table 3.3: Mean and peak burn rate fluxes (g/m^2s) for various pan fires; burn flux accurate to $\pm$ 5 %; M* =Pan material

				Flux for h_{fu}, mm				
	M*	d_{pan}	h_{pan}	2	5	10	20	30
		m	mm	g/m^2s				
Mean	SS	0.2	40	11.5	16.2	17.8	25.0	28.9
Peak				14.0	20.1	25.7	34.4	41.0
Mean	MS	0.2	40	13.1	22.3	26.6	29.8	34.0
Peak				14.6	33.0	42.5	58.1	67.2
Mean	MS	0.2	60	-	-	-	34.0	37.3
Peak				-	-	-	58.7	64.0
Mean	MS	0.5	60	-	19.9	34.0	40.2	-
Peak				-	22.8	56.4	66.0	-
Mean	MS	0.5	50	15.3	22.6	32.0	40.9	-
Peak				16.3	29.6	57.8	72.9	-
Mean	MS	0.5	40	15.9	23.5	37.0	44.6	-
Peak				18.9	32.4	54.2	74.0	-
Mean	MS	2.0	60	-	-	-	56.2	-
Peak				-	-	-	73.2	-
Mean	MS	2.0	90	-	-	-	58.5	-
Peak				-	-	-	72.4	-

unsteady pool fire experiments during peak burn rate the flame becomes broad and sporadic compared to the flame structure of steady state pool fire, which results in higher mass burn rates. Figure 3.17 shows the flame structure for the experiments performed in 0.2, 0.5 and 2 m diameter MS pans at a fuel depth of 20 mm. In 0.2 m pan the role of pan wall conduction heat feedback to fuel will be high as explained earlier compared to the other two modes of heat

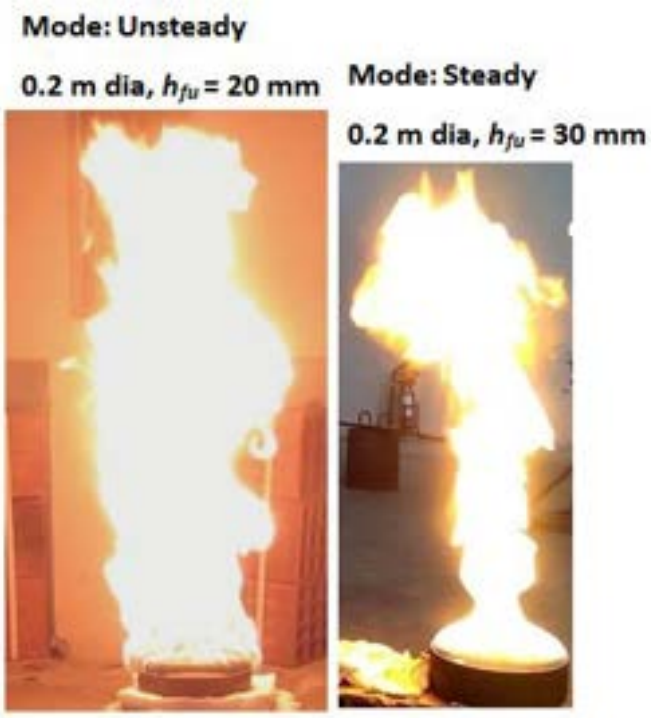

Figure 3.16: Photographs of pool fires in unsteady and steady mode.

transfer whereas in the case of 2 m pan the radiation is the dominant heat transfer mode.

3.1.1 Steady and unsteady pool fires with n-heptane

The pool fire experiment in the steady state arrangement for n-heptane at a fuel thickness of 30 mm was performed in a 0.2 m diameter MS pan and the burn behavior is compared with the unsteady state experiment at the same fuel depth. Figure 3.18 shows the mass burn rate of steady and unsteady state pool fires. As it can be noticed that the initial mass burn rate in both the experiments remains the same since the initial burn rate is largely controlled by the convection in pans of the chosen size. The peak burn flux in the steady state experiment is about 28 g/m^2s and is always lower compared to unsteady pool fires for the reasons explained earlier in chapter 1. Essentially, the heat

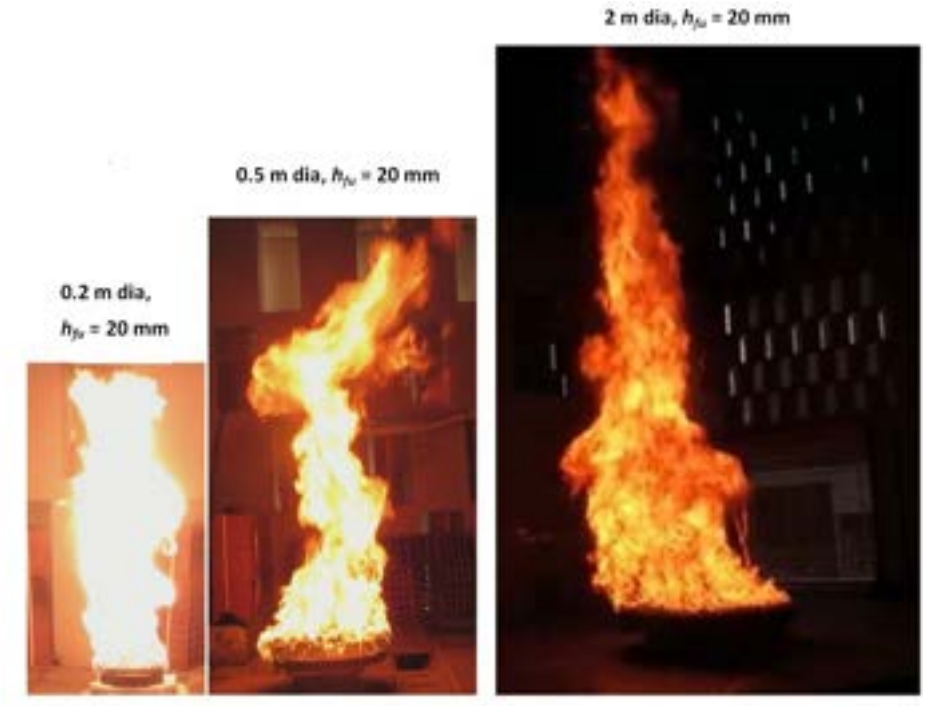

Figure 3.17: Photographs of pool fires in 0.2, 0.5 and 2 m diameter MS pan at a fuel depth of 20 mm

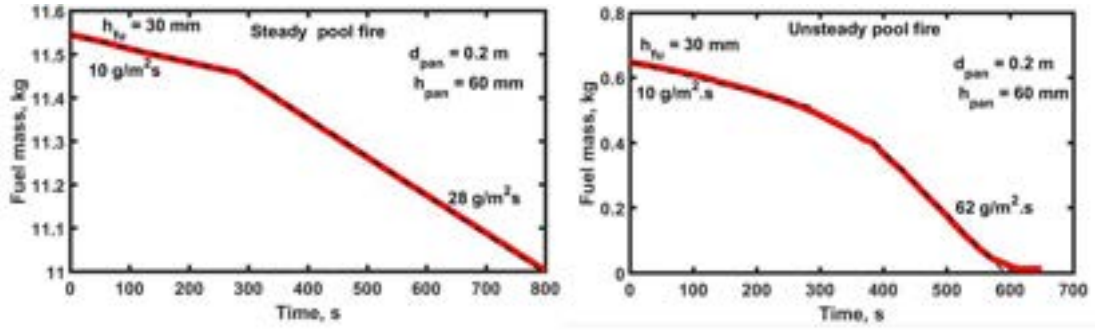

Figure 3.18: Steady (left) and unsteady (right) mode -Mass loss with time on 0.2 m, 60 mm deep pan with 30 mm depth of n-heptane

transfer along the conduction path is drawn away into the incoming fluid which is maintained at a constant temperature. The net heat transfer between the wall and the fuel is small and can be in either direction because while the wall is hotter towards the top, the fuel can be warmer below, and hence, the net heat flux received by the fuel is much lower than in the unsteady mode. Consequently, the behavior of the burn flux is also likewise.

3.1.2 Pool fires on other fuels

Experiments were performed using kerosene, diesel, and alcohol fuels in 0.2 m diameter pans. The comparison of the mass loss vs time of stainless steel pan and mild steel pan experiments with kerosene and diesel fuel at fuel depths of 10 mm and 20 mm are set out in Fig. 3.19. The initial mass loss for kerosene is about 10 g/m^2s in both SS and MS pans, and at later times the higher wall heat transfer in the case of MS pan leads to higher burn flux compared to SS pan. With increasing fuel depth from 10 mm to 20 mm the mass flux varies from 16 to 22 g/m^2s and 27 to 50 g/m^2s in SS and MS pan respectively. This behavior of kerosene is similar to that of n-heptane. The right side of Fig. 3.19 shows the mass loss with the time of 0.2 m SS and MS pan with 10 and 20 mm diesel fuel. It can be seen that the burn flux is nearly constant at a low level of 8 to 9 g/m^2s for both the pans and fuel depths. This means that the heat received from conduction has little influence. Convection alone dominates the heat transfer process because radiation makes a very little contribution at this pan size. The reason for the difference in behavior between diesel and kerosene is that diesel has components with a much higher boiling range compared to kerosene and the heat transferred by conduction is unable to raise the temperature to levels allowing for higher vaporization rates.

Figure 3.20 shows the mass loss with the time of 0.2 m MS pan with 5, 10, and 20 mm depths of ethanol and methanol fuels. The results are nearly identical and fuel depth has little effect. The higher flux of 17 g/m^2s is reached

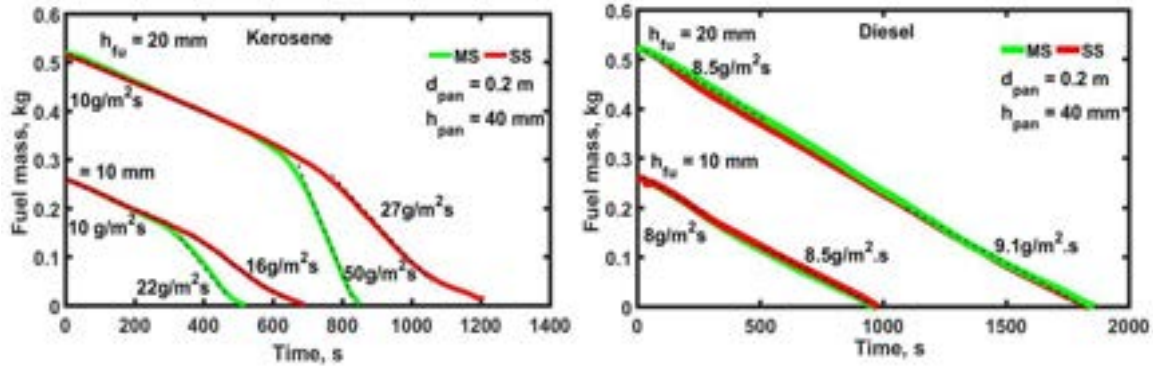

Figure 3.19: Comparison of mass loss with time for 0.2 m SS and MS pans, 40 mm deep with the fuel depths of 10 and 20 mm of kerosene(left) and diesel (right)

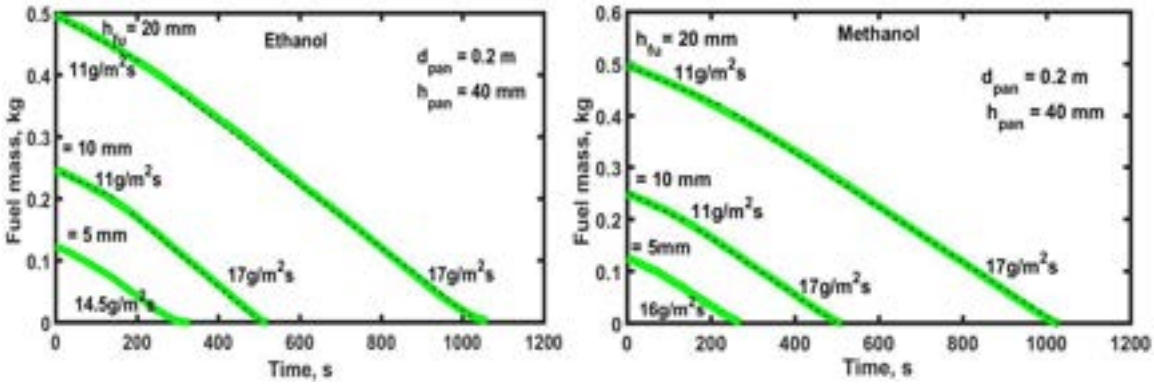

Figure 3.20: Mass loss vs time of ethanol and methanol in 0.2 m dia MS pan with 5, 10, and 20 mm fuel depths

much earlier (as a fraction of total burn time) than in the case of kerosene and n-heptane indicating that convection appears enhanced to larger values and conduction plays a very minor role (because the slope does not change during most of the time).

In order to explore the behavior of the fuels within the liquid phase, the temperatures of the liquid at 1 mm from the bottom are plotted against time in Fig. 3.21. For, n-heptane, ethanol, and methanol which are pure fuels, the temperature reaches their respective boiling points and stays at that temperature

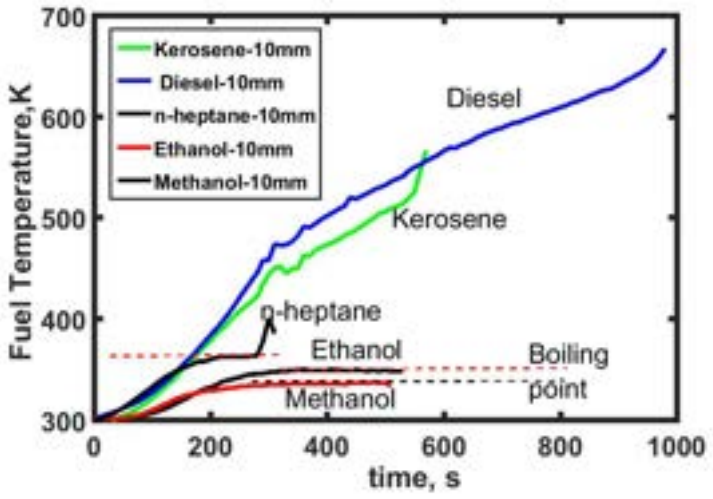

Figure 3.21: Centerline fuel temperature at $1mm$ from bottom of pan vs time for kerosene, diesel, ethanol, methanol and n-heptane fuel in 0.2 m MS pan

till complete burnout occurs. This period of burn when the temperature has reached the boiling point is the bulk boiling condition discussed earlier. This duration is much large for methanol and ethanol because their boiling points are lower than of n-heptane and their high latent heat of vaporization reduces the burn flux. In the case of kerosene and diesel, the temperature keeps on increasing with time till the end of the experiment, since they are fuels composed of various petroleum fractions. In the case of diesel, the temperatures go beyond 650 K indicating to evaporation of some heavy fragments in the fuel.

The comparison of the mass loss vs time of MS pan experiments with n-heptane, kerosene, diesel, ethanol, and methanol with 10 mm fuel thickness is set out in Fig 3.22. Even though the fuel thickness (10 mm) and the pan used are the same, n-heptane has the highest burn flux of about 45 g/m^2s followed by kerosene with burn flux of about 27 g/m^2s essentially due to the differences in the heat feedback to fuel surface and the thermo-chemical properties of the fuels prominent of which are the boiling point, the heat of vaporization and effective flame temperature.

The data from various experiments conducted in 0.2 m diameter MS and SS

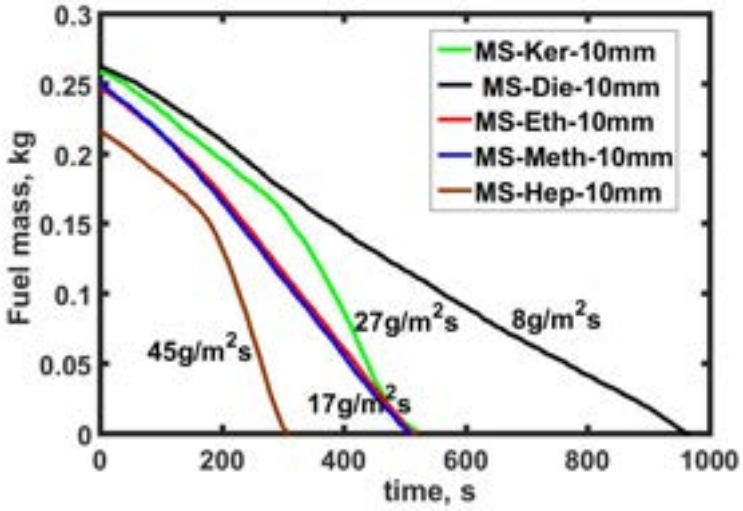

Figure 3.22: Comparison of mass vs time for 0.2 m, 40 mm deep MS pan with n-heptane, kerosene, diesel, ethanol and methanol fuels

pans for methanol, ethanol, n-heptane, kerosene, and diesel are set out in Table 3.4. As it can be noticed from the table that both the mean and peak flux increase with the depth with a tendency to reach asymptotic values for n-heptane. For kerosene, the mass flux increases with fuel depth but for diesel, ethanol, and methanol the increase of flux is not significant even though the depth of fuel is increased. Also, the material of the pan - MS or SS here matters significantly in terms of the burn behavior only for n-heptane and kerosene fuel.

3.2 Summary

In this chapter, apart from the classical pan diameter effect on the burn flux, the effect of various control parameters such as fuel depth, pan material, initial temperature, and thermochemical properties of the fuel are delineated. With respect to fuel depth, it was found that in the pans of smaller diameter (0.2 m) the higher burn fluxes of about 67 g/m^2s, that are generally observed in the large diameter pans are also obtained. The reason for such behavior in the

Table 3.4: Mean and peak burn fluxes (g/m^2s) for 0.2 m dia pan

Flux for h_{fu} (mm) =		5	10	20
Kerosene, SS	Mean	-	11.8	13.6
	Peak	-	16.0	22.0
Kerosene, MS	Mean	-	15.6	19.4
	Peak	-	27.0	50.0
Diesel, SS	Mean	-	8.5	9.0
	Peak	-	8.1	9.1
Diesel, MS	Mean	-	8.7	8.9
	Peak	-	8.0	9.5
Ethanol, MS	Mean	12.0	15.2	15.0
	Peak	14.5	17.2	17.0
Methanol, MS	Mean	14.6	15.6	15.3
	Peak	16.0	17.0	17.0

small pan diameters is due to the enhanced pan wall conduction heat transfer which leads to bulk boiling phenomena resulting in higher mass burn flux. With respect to the pan material effect, the experiments performed with n-heptane fuel in pans made of AL, MS, SS, and GL showed differences directly attributable to the thermal conductivity of the pans. The experiments that in small and moderate diameter pans the decrease in the burn rate is about 1 % per mm water thickness up to 20 mm water thickness. For larger diameter pans the difference is negligible largely because the heat transfer across the interface between the fuel and water constitutes a small fraction of the heat flux values involved. Experiments that were conducted in 0.2 m dia, 40 mm deep, MS pan for methanol, ethanol, kerosene, and diesel fuels, and a few other experiments on diesel and kerosene in 0.2 m dia SS pan at fuel depths of 10 and 20 mm showed that the differences in the burn fluxes are attributed to the difference in their properties and flame temperature that provides the heat

feedback to the fuel surface.

Chapter 4

Correlation for mean burn flux

4.1 Introduction

As explained in chapter 1, models available in the literature for estimating the burn flux of pan fires do not consider all the parameters that control the mean burn behavior of the pool fires. This chapter describes the evolution of a correlation that can be used to obtain the mean burn flux of the pool fires based on a non-dimensional number denoted by M_{pc} that takes into account all the parameters controlling the burn flux. It also explains the approach chosen to evolve the model.

4.2 M_{pc}- Dimensionless pan number

The following behavior must be accounted for in the evolution of M_{pc} so that its increase must imply an increase in burn flux.

- Increase in wall material thermal conductivity (k_w) should increase the heat transfer into the pan and hence increase M_{pc}.
- Increase in freeboard (h_{fb}) and pan depth (h_{pan}) should reduce the heat transfer and hence M_{pc}. The effect of freeboard is not always monotonic as seen from the data.
- Increase in fuel thickness (h_{fu}) increases the burn rate and hence M_{pc}.

- Increase in pan diameter increases the burn rate and must be so reflected in M_{pc}.
- Decrease in pan wall thickness should result in reduced conductive flux and should be reflected in reduced M_{pc}.
- Increase in initial fuel temperature increases the burn rate and hence M_{pc}.
- Increase in water depth over which fuel floats causes a reduction in burn rate and the effect asymptotes beyond some depth.

Rendering conductive heat transfer coefficient, k_w/h_{pan} dimensionless is performed using the convective heat transfer coefficient, $h_{g,conv}$ that is obtained by expecting that the burn flux is controlled by convection in the early stages in a small diameter pan in which the radiation flux is minimal. This gives a value of 0.0045 kW/m^2K. Subsequent burn rate simulations using an unsteady code have confirmed this result. With regard to other dimensions - fuel thickness, freeboard, pan diameter, and pan wall thickness, several possible dimensionless constructions are possible. The candidate for rendering the pan diameter dimensionless should arise from free convective length scale, $[\nu_g^2/g]^{(1/3)}$, where $\nu_g = \mu_g/\rho_g$ is the dynamic viscosity of the hot gases. With μ_g = 1.8 $\times 10^{-5}$ kg/ms, g = acceleration due to gravity, 9.8 m/s^2, this length scale is 0.21 m.

Much effort went into trying to find combinations of these quantities so that a parameter that can characterize the burn rate flux can be found. These parameters include most of the relevant fundamental parameters indicated in objectives and two parameters, namely, ρ_w and $c_{p,w}$ have been treated as fixed constants since it is taken that the pans are made of either stainless steel or mild steel for which the product $\rho_w c_{p,w}$ is the same. There are three dimensionless parameters, P_1, P_2 and P_3 which are defined below.

The parameter P_1 is defined by

$$P_1 = \left[\frac{k_w}{h_{pan} h_{g,conv}} \frac{h_{fu}}{h_{fb}}\right]^{1/4} \tag{4.1}$$

The parameter P_1 is chosen to account for conductive flux in addition to fuel depth effects. The first term in the bracket is discussed in the earlier paragraph. The role of h_{fb} vis-a-vis h_{fu} was deduced after trying out some options. The exponent was varied and the present choice of (1/4) provided a minimal deviation from the observed experimental dependence.

Parameter P_2 is defined by

$$P_2 = \left[1 - \exp(-0.25(d_{pan}/0.21)^{1.5}/P_1)(1 + 0.1(h_{wr}/h_{pan})^{2.3})\right] \tag{4.2}$$

In the above expression, the influence of the pan diameter is such that as it increases, one obtains an asymptotic value controlled by radiation through the exponential term. The exponent 1.5 on the pan diameter scaled by the convective length scale is chosen to provide the variation with the diameter observed in the experimental data. It turns out that Ditch et al (2013) have an exponent on pan diameter that is the same as here. The above expression also accounts for water depth, h_{wr} and it is scaled with pan depth, and when h_{wr} is 0, the associate term becomes 1.

Parameter P_3 is defined by

$$P_3 = \left[\frac{(T_{bfu} - T_0)}{(T_{bfu} - 300)} \frac{300}{T_{bfu}}\right]^{-0.35} \tag{4.3}$$

This parameter accounts for the initial fuel temperature. It increases as the fuel temperature approaches the boiling point. The choice of the expression is such that when T_{bfu} is large, The burn flux increases, and the exponent is chosen using a good fit with data from the present work as well as from Chen et al (2011).

These are now combined to obtain a parameter, M_{pc} as

$$M_{pc} = P_1 P_3 [1.5 + 8.5 P_2] \tag{4.4}$$

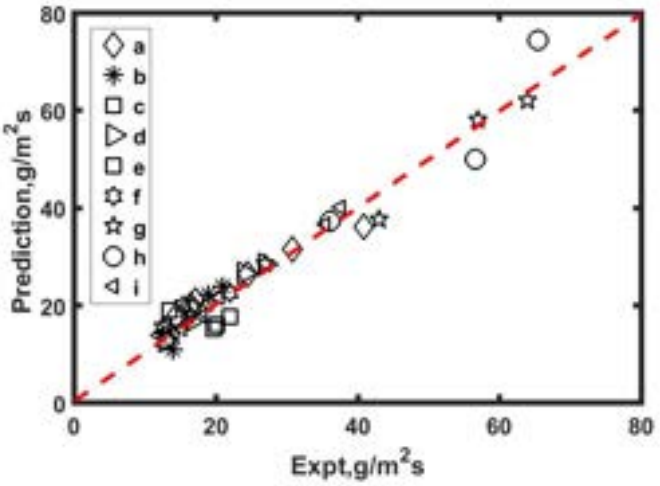

Figure 4.1: Predicted vs experimental burn flux of authors from a to i

Now, the mean mass burn flux can be set out as

$$\bar{m}''_{fu}(g/m^2 s) = [(h_{g,conv}(T_f - T_{bfu})/4L) * M_{pc} \tag{4.5}$$

As can be noted the first part on the right-hand side is the convective burn flux (without the constant - 4)

The authorship and details of data in Fig, 4.1: a: GL-0.338-0.677D-Gasoline-Zhao et al. 2017; b: SS-0.25-2D-Methanol-Ditch et al. 2013; c: SS-MS-0.3-0.6D-Klassen et al.1994; d: SS-0.25-2D-Ethanol-Ditch et al. 2013; e: MS-0.27-0.372D-Ethanol-Fang et al. 2011; f: Gl-0.11-0.29D-Heptane-Hu et al. 2013; g: SS-0.25-2D-Heptane-Ditch et al. 2013; h: MS-SS-0.3-1D-Heptane-Klassen et al. 1994; i: SS-0.1-0.3D-Heptane-Chen et al. 2011.

Details of data Fig, 4.2: j: SS-0.1D-Heptane, k: GL-0.2D-Heptane, l: MS-SS-0.2D-Heptane, m: MS-0.3D-Heptane, n: MS-0.4D-Heptane, o: MS-0.5D-n-H, p: MS-0.92D-n-H, q: MS-2D-n-H, r: MS-0.2D-n-H with water, s: MS-0.5D-n-H with water, t: MS-2D-n-H with water-Shiva kumar et al. 2020, u: MS-SS-0.2D-Diesel, v: MS-SS-0.2D-Kerosene, w: MS-0.2D-Methanol, x: MS-0.2D-Ethanol-Shiva kumar et al. 2022, (n-H = n-Heptane).

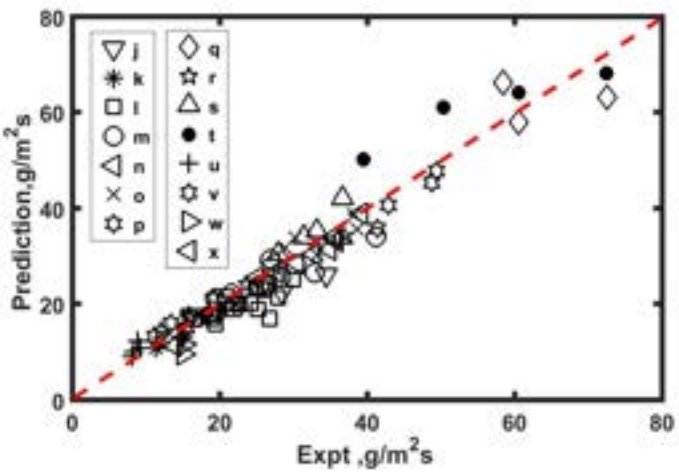

Figure 4.2: Predicted vs. Experimental burn flux of present data

4.3 Predictions and comparison of mean burn flux

The predictions of the correlation 4.5 are set out for the experimental data of the present study in Table B.1. The first seven columns are the parameters of the experiment, the eighth column is the experimental burn flux, and the ninth column titled $Pred1$ is the result from 4.5. Figures 4.2 and 4.1 show a comparison of predictions against experimental mean burn flux for various fuels from present studies and the experiments from literature respectively. As can be noted, the comparison is very good indeed. The root mean square deviation over all the data is less than 5 %. The prediction is termed a correlation and not a curve-fit because the validity of the prediction covers the entire range of useful parameters - d_{pan} from 0.1 to 2 m or beyond, h_{pan} over a wide range that covers 40 to 200 mm, h_{fb} beyond about 5 mm, h_{fu} = h_{pan} - h_{fb}, a range of materials including glass, SS, MS and AL. The correlation does not include the pan wall thickness, t_w in the present format. In the experiments and the parameters used in standard fire tests, t_w is between 3 to 6 mm and for these applications, the predictions are satisfactory. The sensitivities of the predicted burn flux to the parameters controlling it are set out in Table 4.1. It can be seen that the most sensitive parameter is the initial temperature of the fuel.

Table 4.1: Sensitivity of burn flux, $\bar{\dot{m}}''_{fu}$ to various parameter changes each by 10 %

Parameter	%
Pan diameter at 0.2 m	4
Pan diameter at 0.5 m	7
Pan diameter at 2.0 m	1
Wall thermal conductivity	2
Fuel depth	2.5
Pan height	3.5
Freeboard	3.5
Fuel initial temperature at 300 K	22.0
Water depth at 10 mm	0.2

The least sensitive parameter is the depth of water. Pan diameter around 2 m has little sensitivity because the most dominant heat flux - due to radiation does not change around and beyond this diameter.

Chapter 5

Modeling of Unsteady Pool Fires

This chapter explains the physics based model that is developed to capture the transient behavior of an unsteady pool fire by using appropriate models for conduction, convection, and radiation heat transfer rates to the fuel pool. It also describes the computational procedure adopted using the MATLAB code to obtain the mass loss, heat flux feedback to the fuel surface, mass burn rate, and the fuel and pan wall temperatures. The comparison between predictions and the experimental results of mass loss, pan tip temperatures, and the condensed phase temperatures for the experiments performed are discussed. Finally, the contribution of the various heat fluxes to vaporize the fuel and their variation with different control parameters is also discussed.

5.1 Elements of New Model

It has been known that the heat flux balance is the basis of burn rate prediction. It is set out as:

Heat flux for vaporization = Heat flux from gas phase due to convection and radiation + Heat flux received by the liquid from the bounding wall

The first term is given by $\rho_{fu}\dot{r}[L+c_{p,fu}(T_s-T_{bot})]$ where ρ_{fu} and $c_{p,fu}$ and L are the density, specific heat, and latent heat of vaporization of the fuel, $\dot{r}$ is the linear regression rate, T_s and T_{bot} are the surface and the bottom layer temperature of the fuel. Fuel surface temperature can be set as ambient temperature or of heated fuel as in the case of Chen et al (2011). The bottom layer temperature is

also the initial set temperature but changes with time because of heat transfer from the surface and heat transfer to the bottom of the wall by conduction.

5.1.1 Convection term

The second term with respect to heat flux from gas phase has two components - convection and radiation. The convective flux, is given by

$$\dot{q}''_{conv} = h_{g,conv}(T_f - T_s) \tag{5.1}$$

With regard to the gas phase heat transfer coefficient, $h_{g,conv}$, it was determined from the experimental data across all diameters and wall materials, that there is an initial phase of mass loss vs time that can be predicted well with a value of 0.0045 kW/m^2K. This inference was obtained by examining the experimental data of n-heptane over all the cases. More particularly when glass is considered as the pan material and with small fuel thickness, the largest contribution to heat transfer was by convection. Thus, it can be taken that it is a result hinted at by the initial examination of the experimental data and confirmed by simulation (See Mukunda et al. 2020). This was found satisfactory for all experiments at ambient pressure of 1 atm. Experiments by Li et al (2009) and Fang et al (2011) at very different altitudes showed a pressure dependence of the pan fires and has been a subject of studies (deRis et al. 1973, Alpert. 1976, Wieser et al. 1997). The pressure dependence drawn from the work of deRis et al (1973) is taken to give

$$h_{g,conv} = 0.0045p^{2/3} \tag{5.2}$$

5.1.2 Gas Phase Radiation

The radiation model deployed here is different in its elements compared to those used in literature and is a consequence of the results of the experiments that have shown that the mass flux from smaller diameter pans ($\sim$ 0.2 m) can become as large as larger pans when larger depths of fuel are involved. The

fact that the flux can increase significantly due to fuel vaporization processes controlled by wall conduction (discussed below) has to be accounted for to explain much higher burn rates in smaller diameter pans. The increase in the burn flux is so large with values comparable to large pool fires that conduction alone was found inadequate to explain the results. Also, when the pan diameter increases from about 0.2 m considered small, through larger values up to 2 m and at different fuel thicknesses, it was found imperative to invoke a dependence due to enhanced burn flux at small diameters. To introduce a dimensionless approach, a Reynolds number based on fuel mass flux and pan diameter are invoked. The diameter dependence is also brought into account for flame emissivity coupled with changes in view factor. Further, accounting for pressure dependence is performed based on the work of deRis et al (1973). Therefore, radiation flux is expressed as

$$\dot{q}''_{rad} = p^{2/3} evf \sigma T_f^4 \text{ with} \tag{5.3}$$

$$evf = 0.02\left[1 - e^{-0.00045 ff \frac{\dot{m}''_{fu} d_{pan}}{\mu_g}}\right] \text{ and} \tag{5.4}$$

$$ff = 1 - e^{[-0.4 g d_{pan}^3/\nu_g^2]} \tag{5.5}$$

where evf is the product of the constant part of emissivity and view factor and ff is a further correction to pan size effects on radiation, determined after comparing with radiation effects at fixed fuel thickness over a range of pan diameters. In the expression for evf, the increase in radiant flux is expected due to enhanced flame height because of the need to account for larger fuel depths. The value of 0.02 in the expression for evf is a constant that has been determined to get a good comparison of the mass vs time for 0.2 and 2 m diameter pans and remains unchanged. In ff, the term within the exponentiation is essentially, the Grashof number. It can also be interpreted that the pan diameter d_{pan}, is rendered dimensionless by the free convective length scale $[\nu_g^2/g]^{1/3}$ (this value is 0.21 m for the choice of the temperature for evaluating the kinematic viscosity). Thus the radiation flux is based on both on Reynolds number and Grashof number. The above correlation was shown to give a mean error of less

than 5 % over a wide range of parameters.

5.1.3 Wall Conduction to Fuel

The third term related to wall conduction is modeled using the heat flux balance at the pan edge. Several models were attempted before arriving at the following approach. It is conceived that the top region (constituting a region of the order of the thickness of the pan) has a temperature, T_p and the heat transfer occurs from the flame with temperature T_f that moves down the pan wall by conduction. The difference in the heat flow will raise T_p over a time. The heat balance equation is

$$m_w c_{pw} t_w \frac{dT_p}{dt} = h_{g,ft}(T_f - T_p)A_1 - h_m(T_p - T_0)A_1 \tag{5.6}$$

where m_w, c_{pw}, t_w and A_1 refer to mass, specific heat, and wall thickness and the cross section - $\pi d_{pan} t_w$, $h_{g,ft}$ is the gas phase heat transfer coefficient near the wall tip (of a zone of t_w) and h_m, the wall heat transfer coefficient. It is defined by the ratio of $k_w/(h_{fb}$ + fuel regression). Fuel regression, reg is obtained as $\int_0^t \dot{r} dt$ with $\dot{r}$ being the linear regression rate of the fuel. We can recast the eqn. 5.6 as

$$\frac{dT_p}{dt} = \frac{h_{g,ft}}{\rho_w t_w c_{p,w}} \left[(T_f - T_p) - \frac{h_m}{h_{g,ft}}(T_p - T_0) \right] \tag{5.7}$$

At t = 0, since T_p = T_0, we get

$$\left[\frac{dT_p}{dt} \right]_{t=0} = \frac{h_{g,ft}}{\rho_w t_w c_{p,w}}(T_f - T_0) \tag{5.8}$$

We denote $dT_p/dt]_{t=0}$ by G. From the experimental data on T_p vs time shows that $dT_p/dt]_{t=0} = G$ is around 2.8 K/s. We express h_m by $k_w/(h_{fb} + reg)$ and write

$$\frac{dT_p}{dt} = G \left[\frac{T_f - T_p}{T_f - T_0} - \frac{k_w}{h_{pan} h_{g,ft}} \frac{h_{pan}}{h_{fb} + reg} \frac{T_p - T_0}{T_f - T_0} \right] \tag{5.9}$$

The quantity $k_w/(h_{pan} h_{g,ft})$ is denoted by cTp and is a constant whose parametric dependence of various quantities must be determined yet. Thus the final form of the equation for T_p is

$$\frac{dT_p}{dt} = G \left[\frac{T_f - T_p}{T_f - T_0} - cTp \frac{h_{pan}}{h_{fb} + reg} \frac{T_p - T_0}{T_f - T_0} \right] \tag{5.10}$$

The distribution of the wall temperature from the tip to the bottom wall center needs to be described. The wall temperature variation was described in Fig. 3.12 and the inference from there was that to the first order the temperature variation can be taken to be linear. The temperature distribution along the radius of the circular pan bottom must be a constant value if it is steady (because the steady solution in a cylindrical geometry leads to this result). However, a thermocouple mounted at the bottom wall center shows an increase in temperature, in fact close to the liquid temperature next to the wall. In view of this finding, it is taken that the linear heat transfer drop to the central region defined as a circular part of radius = $d_{pan}/4$ will heat up this region with time. This assumption leads to

$$\rho_w c_{pw} \pi (d_{pan}/4)^2 t_w \frac{T_{wbc}}{dt} = \frac{k_w}{(h_{pan} + d_{pan}/4)} (T_p - T_{wbc}) \pi d_{pan} t_w \tag{5.11}$$

where T_{wbc} is the temperature in the bottom central zone of a diameter = $d_{pan}/2$. This equation can be recast as

$$\frac{T_{wbc}}{dt} = \frac{k_w}{(h_{pan} + d_{pan}/4)} \frac{16}{\rho_w c_{pw} d_{pan}} (T_p - T_{wbc}) \tag{5.12}$$

This equation is solved numerically along with other equations since T_p is also a function of time. The heat transferred to the liquid is computed using two temperatures, T_{w1} and T_{wb}, the values at the position of the liquid layer during the burn and at the bottom of the edge of the pan, essentially to obtain a better estimate of the heat transfer.

Using linear temperature drop along the wall discussed above we can set

$$T_{w1} = T_p - (T_p - T_{wbc}) \frac{h_{fb} + reg}{h_{pan} + d_{pan}/4} \tag{5.13}$$

$$T_{wb} = T_p - (T_p - T_{wbc}) \frac{h_{pan}}{h_{pan} + d_{pan}/4} \tag{5.14}$$

We need to device a method to determine cTp and C_3 to complete the predictive scheme. For this purpose, it is intended to seek the connection between the steady maximum value of T_p, identified as T_{pm} and various parameters for the experiments conducted. The T_{pm} values are the lowest for Aluminum

(just above the boiling point of n-heptane) and very high for glass and moderate for small pan diameters and very high for large diameters (see the discussion on Fig. 3.11). Plots of T_{pm} with M_{pc} showed that the variation is not monotonic. Hence a new dimensionless parameter was conceived so that this behavior would be monotonic. The parameter, W defined as

$$W = \left[\frac{d_{pan}h_{gcv0}}{k_w}\right]^{0.5} d_{pan}^{0.25} \left[\frac{h_{fu}h_{fb}}{h_{pan}^2}\right]^{0.1} \left[\frac{T_{bfu}}{T_0}\right]^{0.5} \tag{5.15}$$

The choice of the various terms needs description. The first term on the right-hand side of the equation accounts for conductive and convective flux using d_{pan} as the characteristic dimension instead of h_{pan} as is the case with M_{pc}, the last term accounts for fuel initial temperature effects as in the case of M_{pc}. The third term with a small exponent was introduced to take into account the effect of freeboard in conjunction with fuel depth and the parameter d_{pan} in $d_{pan}^{0.25}$ should be understood to be rendered dimensionless by a constant $[\nu_g^2/g]^{(1/3)}$. Since this is not introduced into the equation, expressing d_{pan} in SI units would be appropriate. It must be understood that the development of the parameter W took place in stages after determining the strongest influences first and moving towards smaller influences trying to preserve the monotonicity of the behavior as set out in Fig. 5.1. Though several points at small W showed deviations, these did not reflect in the overall behavior of the mass loss vs. time predictions. The expression for T_{pm} vs W becomes

$$T_{pm} = 320 + 410W \tag{5.16}$$

Having calculated T_{pm}, we can get cTp from

$$cTp = \frac{T_f - T_{pm}}{T_{pm} - T_0} \tag{5.17}$$

The conductive heat transferred to the liquid is taken as

$$\dot{q}''_{cond} = h_{g-w,fu}\left[(T_{wb} - T_{bot}) + 4\frac{(h_{fu} - reg)}{d_{pan}}[(T_{w1} + T_{wb})/2 - (T_s + T_{bot})/2]\right] \tag{5.18}$$

where $h_{g-w,fu}$ is the heat transfer coefficient from the wall to the liquid, T_{bot} is the liquid bottom temperature and T_s is the liquid surface temperature, both

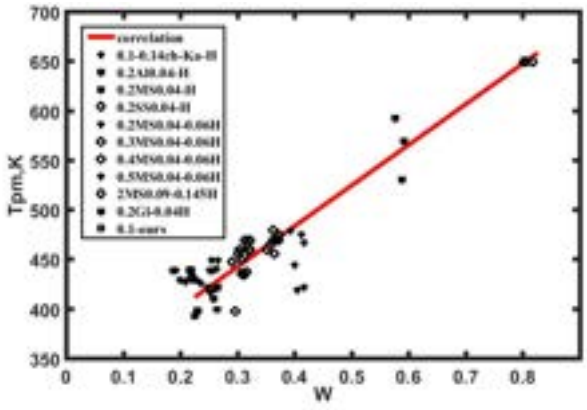

Figure 5.1: Variation of steady maximum wall tip temperature, T_{pm} with a dimensionless parameter, W (*0.2MS0.04-0.06H, implies 0.2 m diameter mild steel pans of 0.04 to 0.06 m depth with n-heptane fuel*)

treated uniform over the diameter and are determined from the liquid phase conduction analysis to be discussed below. In the above equation, the first term in the parenthesis on the right hand side corresponds to heat transfer from the pan bottom to the liquid and the second term to the heat transfer from the sides to the liquid. In the latter, an average of temperatures is taken. While there are several equivalent ways of accounting for heat transfer, it may be taken that this approach is satisfactory.

It is necessary to describe the approach to determine the pan wall heat transfer coefficient $h_{g-w,fu}$. As explained in chapter 3, aluminum and mild steel pans exhibit a sharp change in slope (identified as type II) unlike stainless steel and glass that shows a smooth behavior (identified as type I). The experiments at fuel temperature close to the boiling point also exhibited such behavior while all other experiments showed smooth variation (type I), even in the large diameter MS pans. To account this for behavior and obtain predictive procedure over a wide range of geometric and thermochemical parameters, it was thought necessary to classify them using dimensionless quantities. After a detailed examination, it was found that it would be necessary to invoke a non-dimensional

number $Mpc1$ as follows.

$$Mpc1 = \left[\frac{k_w}{h_{pan}h_{gcv0}}\right]\left[\frac{4t_w}{d_{pan}}\right]\left[\frac{h_{fu}}{h_{pan}}\frac{L_{fu}}{c_{pfu}(T_{bfu}-T_0)}\right]^{0.25}\left[1-0.3(h_{pan}/d_{pan})^{0.125}\right] \tag{5.19}$$

The first term on the right-hand side of the equation accounts for the conductive flux scaled with the convective flux, again as in the case of M_{pc}, second and fourth terms account for the pan wall thickness and pan depth effects and the third term accounts for the fuel depth and fuel properties effect. With this parameter, the wall heat transfer coefficient is set out as

$$h_{g-w,fu} = h_{g,conv}, for\ Mpc1 < 1 \tag{5.20}$$

$$h_{g-w,fu} = S_l, for\ Mpc1 > 6.5\ \&\ m_{fu}/m_0 < C_2 \tag{5.21}$$

$$h_{g-w,fu} = h_{g,conv}\left[1 + C_3\frac{reg}{h_{fu}}\right],\ \ for\ \ Mpc1 > 1\ \&\ \ Mpc1 \leq 6.5 \tag{5.22}$$

The constants C_2 and S_l are chosen for best fits to a few cases of the simulation and seeking good comparison with experimental data. For cases with sharp variation in mass vs time behavior (type II),

$$S_l = 0.1Mpc1 - 0.26 - 0.0017(Mpc1)^2 \ \text{ for } \ 6.5 < \text{Mpc1} < 10 \tag{5.23}$$

$$S_l = 0.45 \ \text{ for} Mpc1 > 10 \tag{5.24}$$

The specific values in the above expressions were determined after testing the code with changes in the values noted above to get a good fit for the variation with time on a few cases. The value of constant C_2 is obtained as

$$C_2 = 0.6 + 0.0575(Mpc1 - 6) \ \text{ for } \ 6.5 < \text{Mpc1} < 10 \tag{5.25}$$

$$C_2 = 0.83 - 0.3(Mpc1^{0.25} - 1.78)/Mpc1^{0.25} \ \text{ for } \ \text{Mpc1} > 10 \tag{5.26}$$

In order to determine C_3, calculations were made on several cases using the pan burn code (to be described below) to determine its value that gives the best fit of mass loss vs time data. The variation of C_3 with different parameters and

possible dimensionless quantities that could be conceived from these parameters to seek a consistent and smooth behavior was attempted. These needed the evolution of a new parameter, W_1 defined below.

$$W_1 = \frac{1}{222}\left[\frac{k_w}{h_{fb}h_{gcv0}}\right]^{0.5}\left[\frac{h_{pan}}{d_{pan}}\right]^{0.5}\left[\frac{T_{bfu}}{T_0}-1\right]^{0.25} \tag{5.27}$$

Here again, the choice of the variables in the terms within the brackets followed the same procedure for W and M_{pc1}. With this parameter, C_3 is obtained from

$$C_3 = 2200(W_1 - 0.026) \tag{5.28}$$

Thus, conduction modeling that is very important for small and medium sized pans ($<$ 1 m diameter) and the constants needed to get good comparisons with experimental data are T_{pm}, C_2, S_l and C_3. These are related to dimensionless quantities W, $Mpc1$ and W_1. The choice of the properties of fuel and pan wall materials, and conditions of operation (like the fuel temperature) control these parameters. There are *no adjustable constants* in the model.

5.1.4 Liquid Phase Conduction

The heat transfer process inside the liquid is taken to be conduction only. As explained in chapter 1 this inference is arrived at by first noting that since the liquid in-depth is always at a lower temperature, there will be no upward natural convection and then the results of the experiments by Ditch et al (2013) where it was shown that the presence or absence of glass beads below the surface has little influence on the burn rate of the steady combustion process. Further, Chen et al (2011) have performed their unsteady analysis taking only the conduction process as relevant.

There are two aspects to the liquid phase conduction process. The increase of surface temperature with time and the conduction process through the fuel or fuel-on water. We consider the conduction process first. Transient conduction process is governed by the dimensionless quantity $y/\sqrt{\alpha_{fu}t}$ where $\alpha_{fu} =$

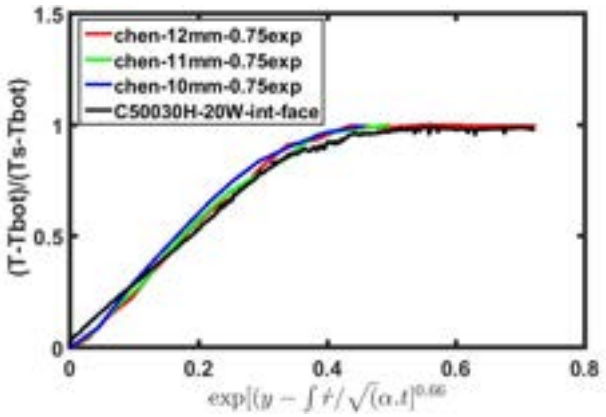

Figure 5.2: Centre line temperatures inside the liquid for heptane pool fire in 200 mm dia pan (Chen et al, 2011) and the heptane-water interface temperature for 30 mm heptane and 20 mm water (present) on dimensionless coordinates

$k_{fu}/(\rho_{fu}c_{p,fu})$ is the thermal diffusivity of the fuel. Since the fuel is regressing, y distance into the liquid is replaced by $y - \int \dot{r}dt$. The temperature at any location inside the fuel is given by $(T - T_{bot})/(T_s - T_{bot})$ being a function of a dimensionless coordinate $(y - \int \dot{r}dt)/\sqrt{\alpha_{fu}t}$. It has been taken as

$$\frac{T - T_{bot}}{T_s - T_{bot}} = exp[-C_4\eta_{fu}^m] \text{ where } \eta_{fu} = \frac{(y - \int \dot{r}dt)}{\sqrt{\alpha_{fu}t}} \tag{5.29}$$

Temperatures measured inside n-heptane fuel in the experiments of Chen et al. (2011) and one experiment from this laboratory were chosen for exploring the validity of the above expression. Among various choices, it turned out that m = 0.66 gave a fit with a linear behavior up to a point when the temperature reached the near-boiling point. Data on liquid temperatures at various depths from Chen et al. (2011, 2012) and fuel-water interface temperature from an experiment on 500 mm pan with 30 mm heptane and 20 mm water is shown in Figure 5.2. In the plot α_{fu}, the thermal diffusivity of heptane is taken as 0.09 mm^2/s. As can be noted all of the data collapses on a single line for the chosen coordinate. The temperature profile can therefore be summarized as

$$(T - T_{bot}) = 3(T_s - T_{bot})exp[-\eta_{fu}^{0.66}] \quad \text{for } 0 < \eta_{fu} < 0.33 \tag{5.30}$$

Beyond a value of η_{fu} > 0.33, boiling point is reached. The result for 30 mm heptane and 20 mm water departs from the linear behavior in Figure 5.2 due to the role of water close to the boiling point. We need to consider the variation of the surface temperature to reach the boiling point. Surface temperature increases because the difference between the heat flux from the gas phase and the heat flux due to conduction into the liquid raising the temperature of the liquid layer. While classically, this is treated using Clausius-Clapeyron equation (see Quintiere 2005) assuming *equilibrium at the surface*, in the current approach, it is treated as *a rate process* in which the enthalpy rise rate of the surface layer of thickness, δ_l equals the differences in the fluxes between the gas phase and liquid phase. The flux into the liquid $\dot{q}_l''$ = $k_{fu} dT_s/dy$ at $(y - \int \dot{r} dt)$ = δ_l is obtained as

$$\left[k_{fu}\frac{dT_s}{dy}\right]_{\delta_l} = \dot{q}_l'' = 3k_{fu}(T_s - T_{bot})G_l \tag{5.31}$$

$$G_l = \frac{0.66exp[-\eta_l^{0.66}]}{\delta_l^{0.34}(\sqrt{\alpha_{fu}t})^{0.66}} \tag{5.32}$$

The gradient is taken at a depth of δ_l into the surface to avoid singularity. Here $\eta_l = \delta_l/\sqrt{\alpha_{fu}t}$. The heat balance at the surface becomes

$$\rho_{fu}c_{p,fu}\delta_l\frac{dT_s}{dt} = \dot{q}_{tot}'' - \dot{q}_l'' \tag{5.33}$$

The value of δ_l is chosen to replicate the surface temperature rise in one experiment. The data of Chen et al. (2011) are used for this purpose.

5.2 Computational Procedure

The equations described above are set out in a MATLAB code called *M-Panburn* to obtain mass loss vs time result for a given set of parameters. The geometric and fuel related parameters are those described in Tables 2.1 and 2.2. The gas phase density and viscosity are taken as $c_{p,g}$ = 1.0 kJ/kgK, μ_g = 1.8 x 10^{-5} kg/ms. For specific calculations, fuel initial temperature, T_0, the fuel thickness, h_{fu} are required to be set.

The flame temperature-time behavior that includes the initial ignition transient is the input for the gas phase flux as well as wall conduction. The gas phase temperature with time is simulated through an expression that allows for random fluctuations. It is taken as

$$T_f = T_0 + (T_{fm} - T_0)[1 - exp(-t/5)] + C_4[sin(\pi t/30 + tR(t)] \tag{5.34}$$

where C_4 is a constant taken here as 15 and $R(t)$ is a random function of value between 0 and 1. An increase in C_4 implies a larger fluctuation in gas phase temperature. The gas phase flux fluctuates likewise, with fluctuations in radiation flux being much larger. The condensed phase dynamics controlled by the slow conduction process average the fluctuation. After trials and examination of experimental data, it was thought adequate to take the value as indicated. Then, cTp is calculated from equation 5.17 and the eqn. 5.10 is treated to get dTp/dt. With a time step taken as 1 s here the calculation of T_p is advanced. Then, eqn. 5.11 is solved to get T_{wbc}. Following this, T_{w1} and T_{wb} are calculated from eqns. 5.14. Using the heat transfer coefficients, $h_{g,conv}$ = 0.0045 kW/m^2K and eqn. 5.20, 5.21, & 5.22, $h_{g-w,fu}$ is obtained. These are used then to calculate convective and conductive fluxes from 5.1 and 5.18. Radiation flux is calculated from the eqns. 5.5. These are summed up to get the total flux, $\dot{q}''_{tot}$. Both the surface temperature, T_s, and the bottom liquid temperature, T_{bot} are then calculated using eqns. 5.33. When both surface and in-depth temperatures reach the boiling point they are set at the boiling point. It must be pointed out that even though the radiation flux depends on the burn flux which itself is not known, the calculation is performed in an explicit mode by providing an arbitrary small value to begin with, and proceeding forward at each time with the previous values. Since the changes that occur are slow compared to the chosen time step (1 s) and are controlled by convection in the early part, this approach is considered satisfactory. These are then used in the heat balance equation to get the fuel mass flux as

$$\dot{m}''_{fu} = \frac{\dot{q}''_{tot}}{L_{fu} + c_{p,fu}(T_{bfu} - T_{bot})} \tag{5.35}$$

With the information on the fuel mass flux, the amount consumed in the time step and the amount remaining is obtained. The process is repeated till burnout - the mass remaining goes below a small fraction - say 1 % in the code *M-Panburn*.

5.3 Results of n-heptane fuel

Predictions over 79 different cases covering the range of materials, fuel depth, pan diameter, and various fuels have been obtained. Comparisons of predictions are shown for experiments of refs [Li et al. 2009, Chen et al. 2011, Kang et al. 2010, and Chen et al. 2012]. In so far predictions are concerned, mean burn flux (or total burn time), fuel mass vs time behavior, and the tip wall temperature are in the order of importance. Detailed comparison of predictions and experimental results shows that it is outstanding for 49 cases, moderate for 25, poor for about 5. It is not that comparisons cannot be made better in the small number of cases, but would require specific tuning, something that is not contemplated here because it would not add value if the code has to be used as a predictive tool. The code output has a result on $\bar{m}''_{fu}$ from the dimensionless correlation, from the unsteady code itself, their mean, and the deviation of this value from the experimental result. Since the code has also approximations due to the choice of the constants c_{Tp} and C_3 which depend on the dimensionless parameters, there will also be inaccuracies in the results. The choice of a mean value is intended to average out these inaccuracies. However, in some cases, the experimental value is closer to that from either the correlation or the code and has a larger deviation from the mean.

Figure 5.3 shows the comparison of mass vs time for 0.2 m pans made of Aluminum, MS, SS, and Glass for n-heptane at a fixed fuel depth of 13 mm. The quality of mass vs time prediction seems outstanding for all the cases. As can

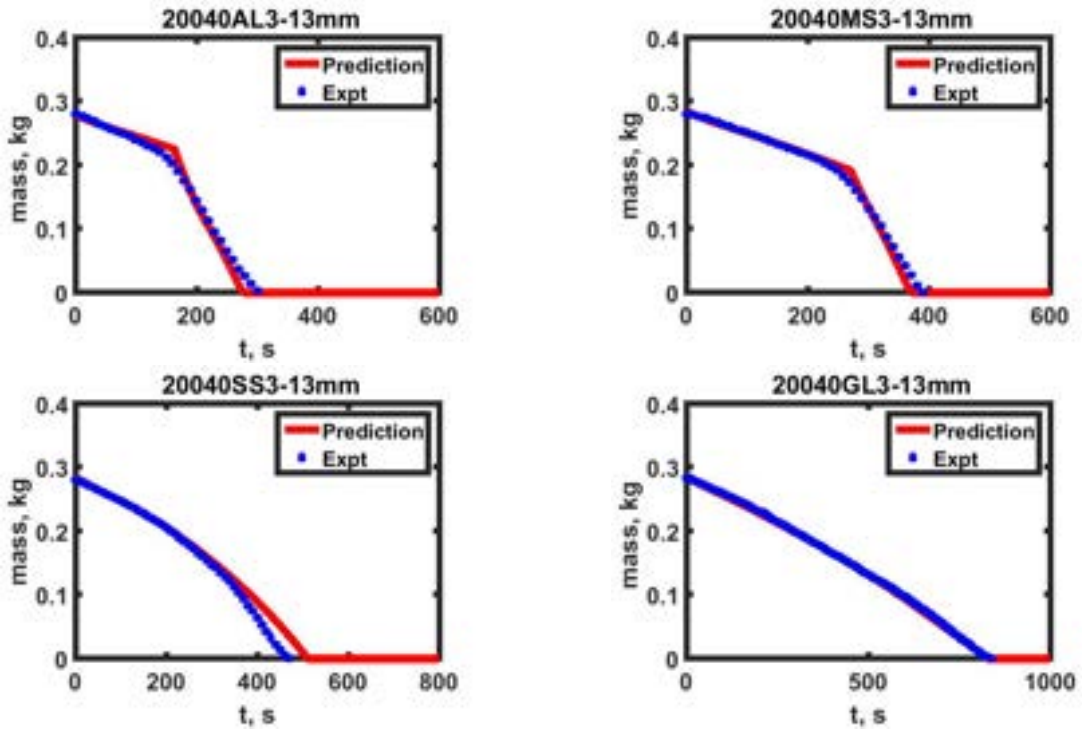

Figure 5.3: Comparison between predictions and experiments on mass vs time for Aluminum (Al), Mild steel (MS), Stainless Steel (SS) (all 200 mm dia) and glass (GL), 190 mm dia at a n-heptane fuel depth of 13 mm

be noted, MS and AL pans belonging to sharp transition (type II) and SS and GL show smooth variation (type I), and the comparison between predictions and experiments is good. In the case of glass, the flux does not deviate much indicating that conduction and radiation are playing little role in the burn process.

Figures 5.4 and 5.5 present the results of mass vs time comparisons between code and experiments for SS pans and MS pans as a function of depth at 10, 13, 20, and 30 mm for n-heptane fuel. The quality of predictions seems reasonable to very good in terms of burn time. In the case of MS pans experiments it is useful to bring out that the break in slope has a relationship with the non-dimensional quantities through relationships 5.22 to 5.27.

Figure 5.6 shows the comparison of mass vs time for the experiments per-

formed at different initial temperatures by Chen et al (2011, 2012) and Kang et al (2010) in a 0.2 m diameter pan for n-heptane fuel. The comparison is impressive considering that the data at 343 K is close to the boiling point (369 K). Differences in the tail-off zone are due to minor wind effects at the end. Comparisons of pressure effects on burn flux for the data from Li et al (2009) shown in Fig. 5.7 appears moderately good. As can be noted that the code is able to capture the effect of pressure on the mass loss rate considering the fact that Ditch et al (2013) had expressed concerns regarding the experimental data in relationship to their correlation.

Figure 5.8 shows the comparison of mass vs time for pan diameters of 0.2, 0.3, 0.5, and 2 m, at a fuel depth of 20 mm for n-heptane fuel. As can be noted the diameter effect is captured very well particularly at large depths where the burn flux attains large values (65 g/m^2s) comparable to large diameter pans.

We turn our attention to predictions of pan tip temperature. Figure 5.9 shows the comparison of experimental and predicted pan tip temperature by the code for AL, MS, SS, and GL pan with 13 mm fuel depth, as the pan tip temperature is one of the important parameter that aids in precise modeling of the wall conductive heat flux into the fuel. The predictions are reasonable-to-good for the cases whose data are set out. In the case of glass, the prediction shows a growing trend and the data shows that it has stabilized at around 530 K much earlier. This is conjectured to be due to the fact that there will be radiant losses and free convective losses due to the flow of air around the pan not accounted for in the model.

The mass burn rate obtained from the code for 0.3, 0.4, 0.5, and 2 m diameter MS pans with 20 mm n-heptane fuel is shown in the figure 5.10. As it can be noted the variation of the mass burn rate with the time and pan diameter is capture well.

The magnitudes of the fluxes for different wall materials for 0.2 m case are set out in Fig. 5.11. Convective flux is about 4 kW/m^2 for all the cases. The

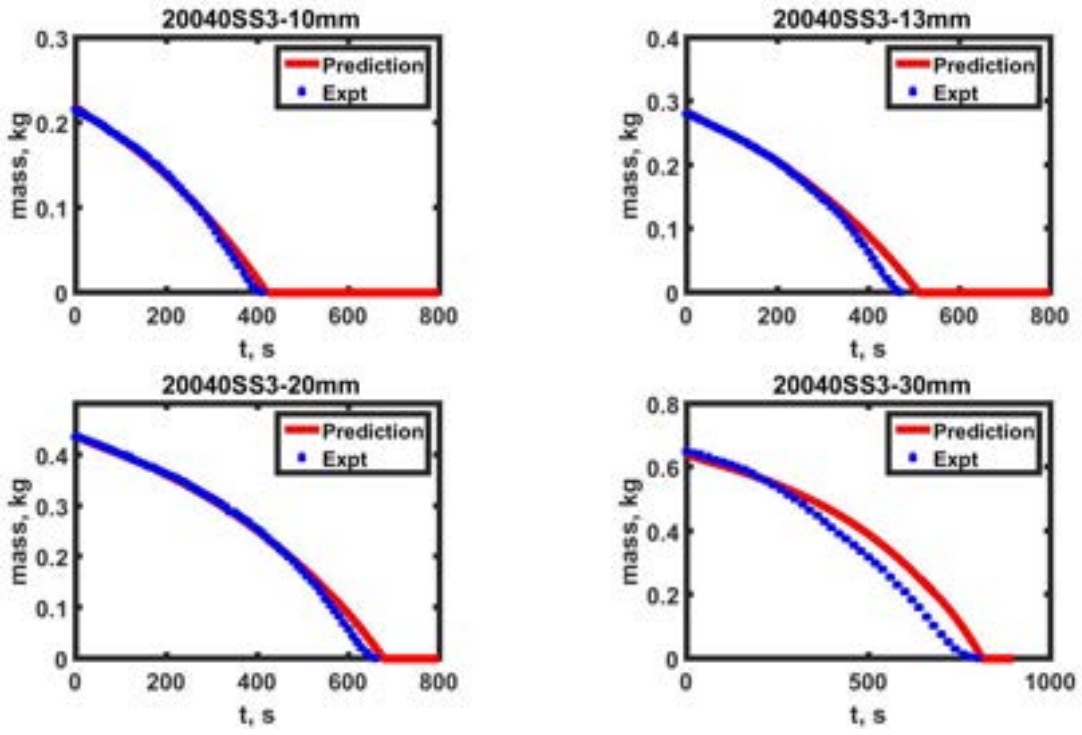

Figure 5.4: Comparison between predictions and experiments on mass vs time for SS pan 0.2 m dia, 40 mm deep for n-heptane fuel depths of 10, 13, 20 and 30 mm

radiative flux increases with burn because the mass flux is increasing and the peak flux values are close to 65 g/m^2s. The conductive flux increases through the burn very significantly for SS, MS, and Al pans. The peak flux values for Al, MS, SS, and GL are 32, 24, 9, and 5 kW/m^2. It is the conductive flux contribution that leads to this behavior. While the fraction of conductive flux is more than 35 % for metals, it is about 10 % for glass. Figure 5.12 presents the flux components for MS pans with increasing diameter. As can be seen, the role of radiation gets enhanced with increasing diameter. While the contribution of conductive flux decreases with increasing diameter.

Table B.1 presents the results of comparisons between predictions and experiments on mean mass flux for over 50 different conditions for methanol, ethanol, n-heptane, kerosene, and diesel fuels with three data from Chen et al (2011), Kang et al (2010) and Li et al (2009). In this table, $Pred_1$ is obtained from

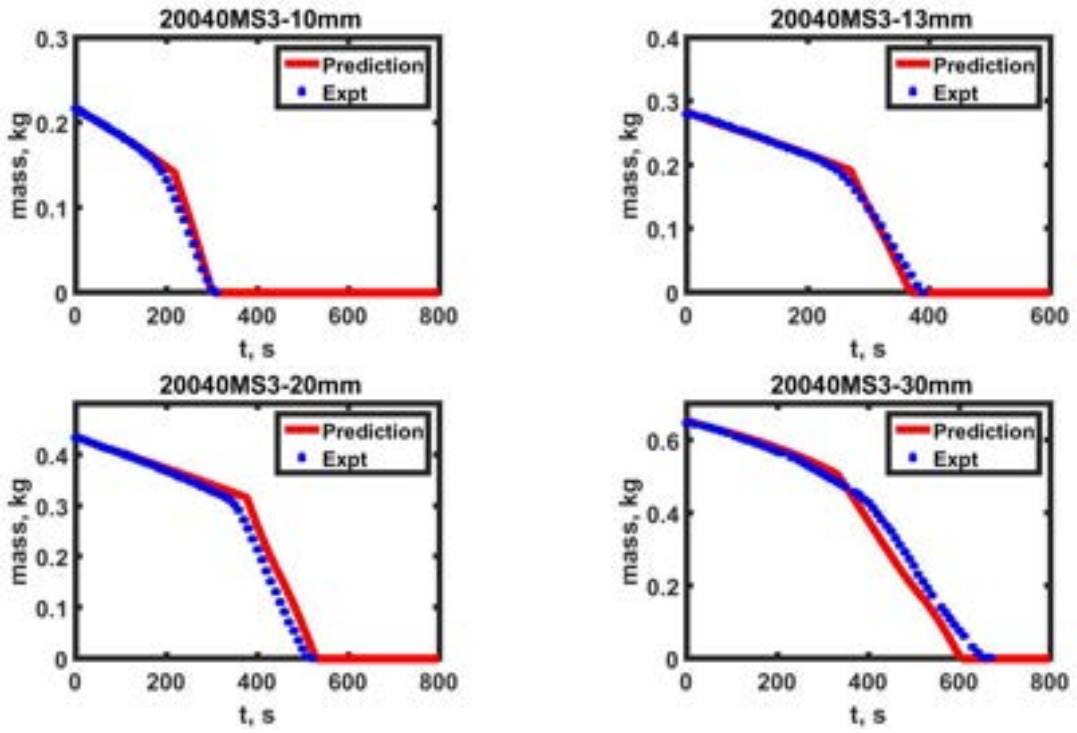

Figure 5.5: Comparison between predictions and experiments on mass vs time for MS pan 0.2 m dia, 40 mm deep for n-heptane fuel depths of 10, 13, 20 and 30 mm

the correlation and $Pred_2$ is obtained from the MATLAB code. As indicated earlier, an average between $Pred_1$ and $Pred_2$ constitutes the prediction and is compared with the experimental result. The experimental accuracy is set at $\pm$ 5 % based on repeated measurements on specific configurations. Where the prediction and experimental value differ by less than 5 %, the difference is considered negligible. There are cases where the error is much larger. In several of these cases, the comparative mass vs time plot shows that the prediction follows the experimental variation quite accurately till late into the burn and deviates only beyond that stage. It is inferred that all the effects namely diameter, wall conductivity, fuel depth, and freeboard are captured reasonably well.

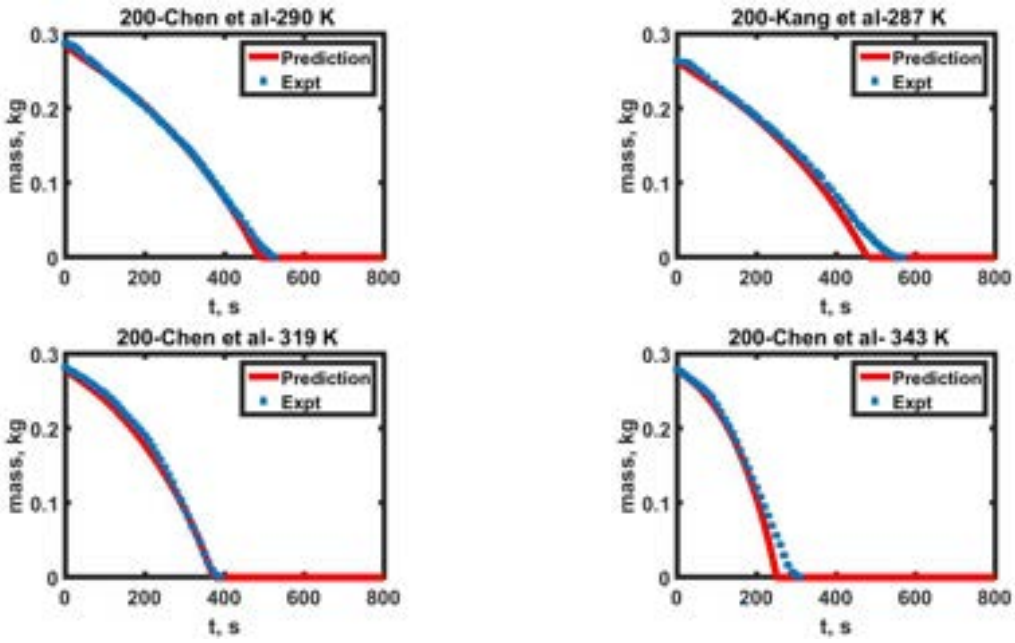

Figure 5.6: Comparison between predictions and experiments on mass vs time for the experiments of Chen et al (2011,2012) and Kang et al (2010) performed in 0.2 m diameter pan at different initial temperatures for n-heptane

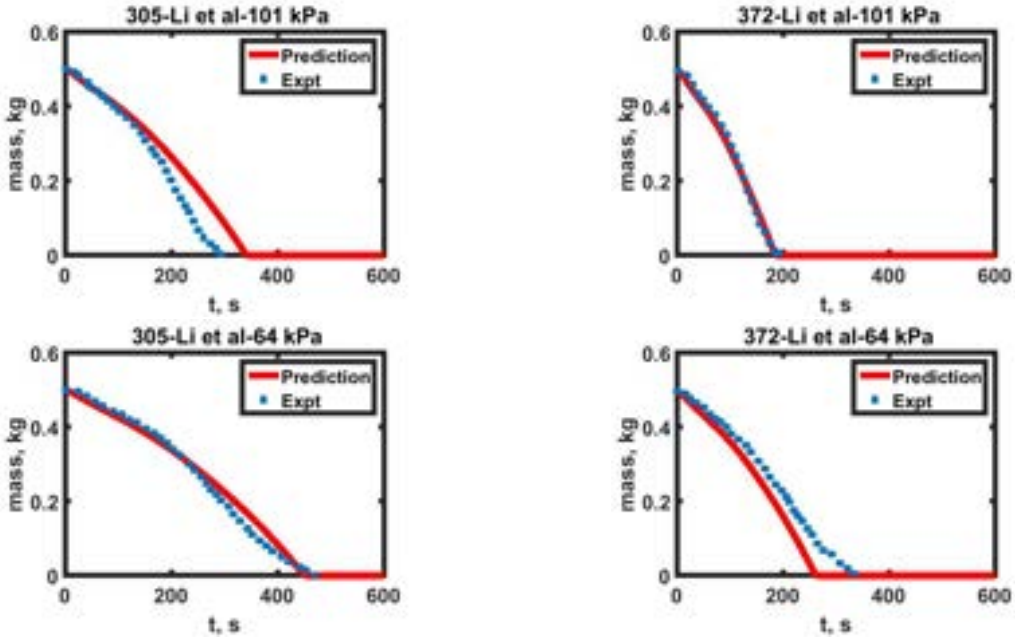

Figure 5.7: Comparison between predictions and experiments on mass vs time for the experiments of Li et al (2009) performed in 0.305 and 0.372 m diameter pans at different atmospheric pressures for n-heptane

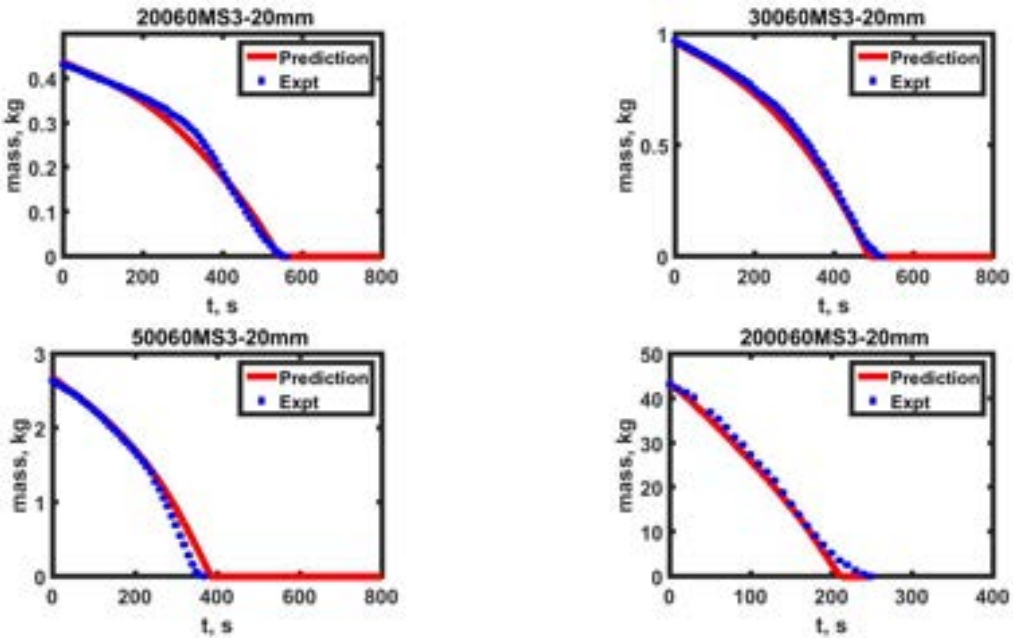

Figure 5.8: Predictions and experiments on mass vs time for MS pans, 60 mm deep for pans of 0.2, 0.3, 0.5 and 2 m diameter with n-heptane fuel depth of 20 mm

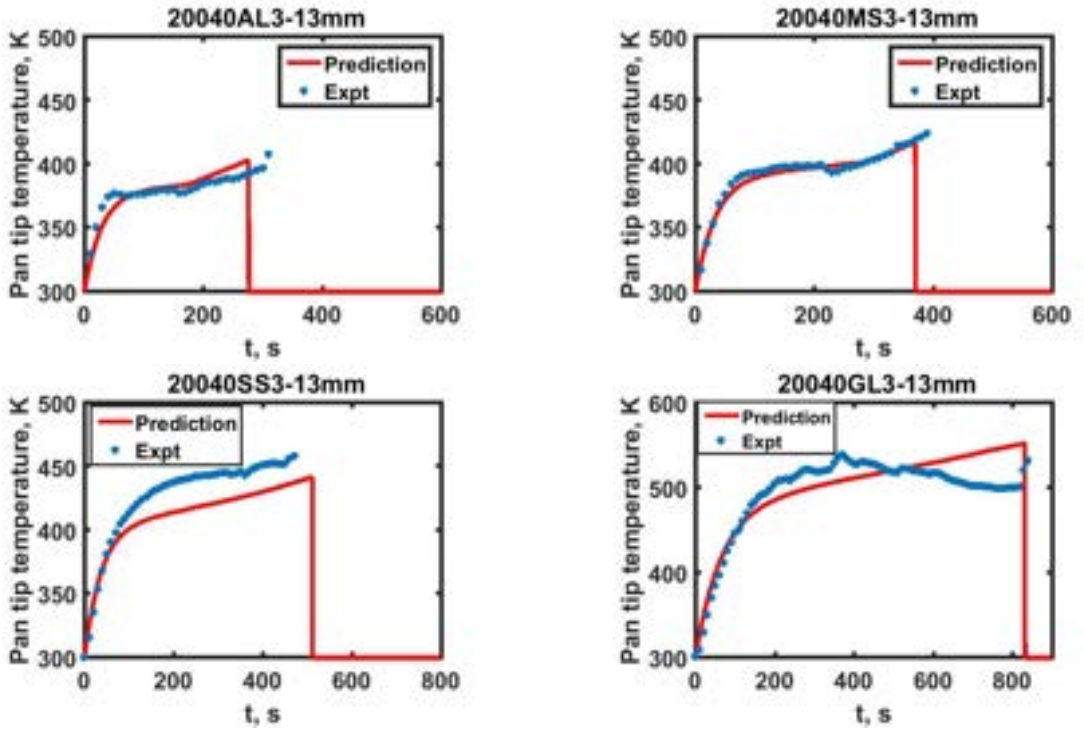

Figure 5.9: Comparison between predictions and experiments on pan tip temperature for AL,MS, SS and GL pan for n-heptane fuel depth of 13 mm

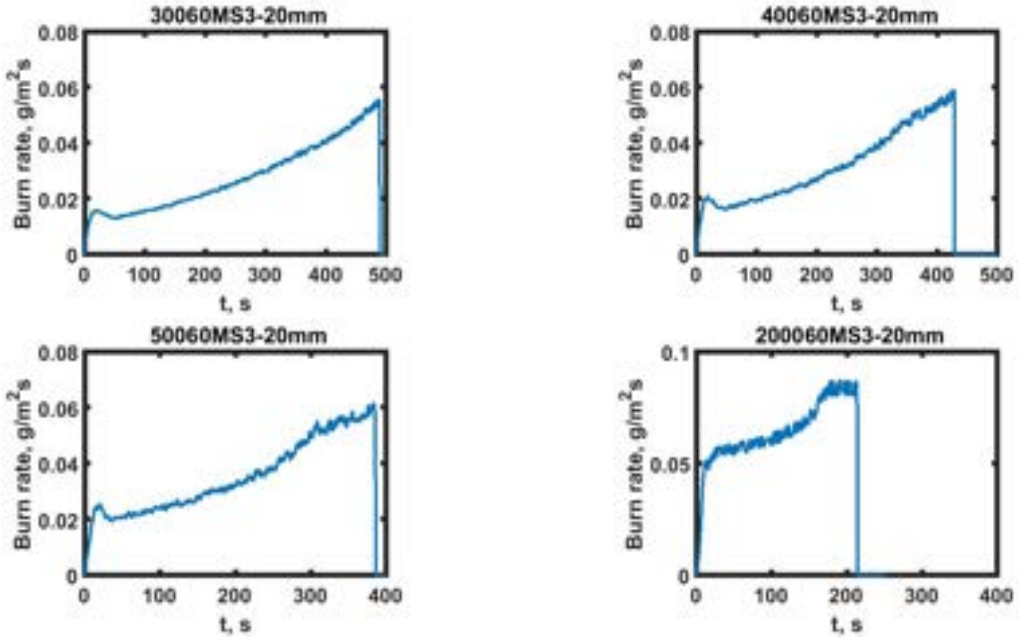

Figure 5.10: Time varying burn flux obtained from the code for 0.3, 0.4, 0.5 and 2 m diameter MS pans with 20 mm n-heptane

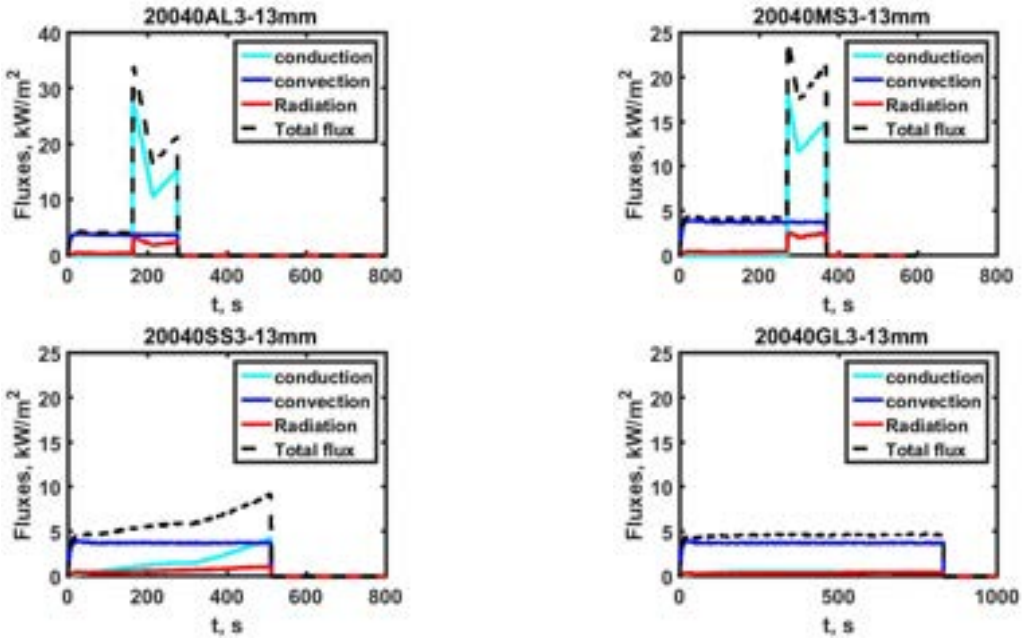

Figure 5.11: The variation of convective, radiative and conductive fluxes for Al, MS, SS and GL pans of 0.2 m dia, 40 mm deep with 20 mm n-heptane

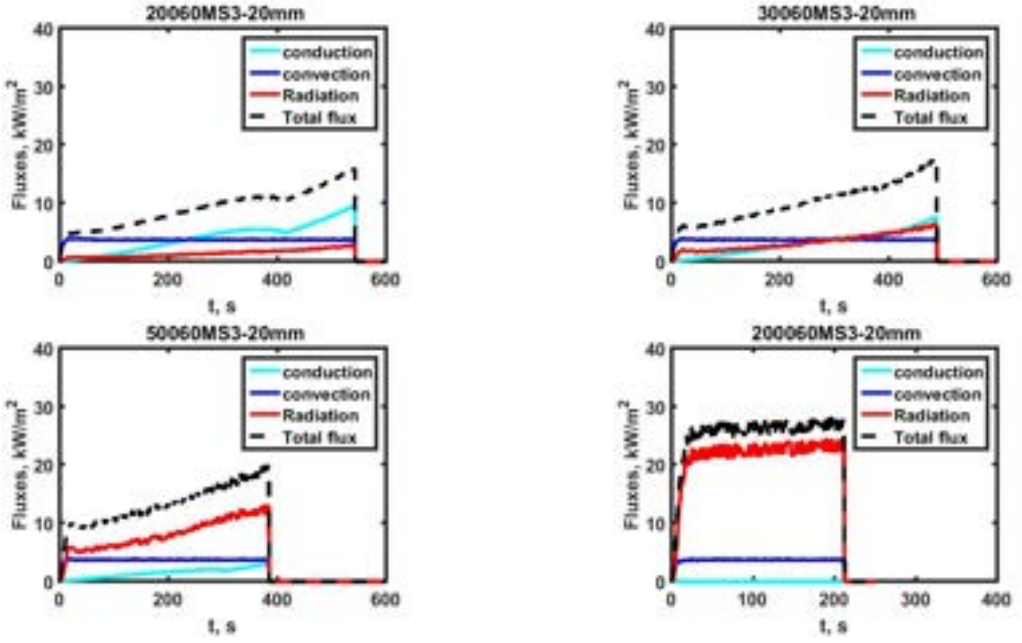

Figure 5.12: The variation of convective, radiative and conductive fluxes for MS pans of 0.2, 0.3, 0.5 and 2 m dia, 60 mm deep with 20 mm n-heptane fuel

5.3.1 Pans of diameter < 0.2m

Hayasaka (1999) and Chen et al (2011,2012) have experimented upon SS pans of 0.05, 0.1 and 0.141 m diameter. Experiments were conducted here for comparison purposes with SS (ours) and glass for 0.1 m diameter. The predictions made using $M - Pan - burn$ are set out in Table 5.1. As can be noted, the predictions even for high fuel temperatures seem reasonable. Here again, the predictions seem not unreasonable if we note that the methodology followed is the same as for larger diameter pans.

Table 5.1: $\bar{m}''_{fu}$ (g/m^2s) for 0.05, 0.1, 0.141 m dia SS (C-K = Chen et al (2011, 2012) and Kang et al (2010) and GL -Glass pans with n-heptane fuel

d_{pan}	h_{pan}	h_{fu}	h_{fb}	T_0	Expt	$Pred_1$	$Pred_2$	Mean	% Error
m	m	m	m	K	g/m^2s	g/m^2s	g/m^2s	g/m^2s	-
0.141	0.04	0.013	0.027	278	14.0	14.5	15.3	14.9	negble
C-K	0.04	0.013	0.027	290	15.2	15.2	15.6	15.4	negble
	0.04	0.013	0.027	319	18.1	18.0	19.0	18.5	negble
	0.04	0.013	0.027	343	31.2	23.0	30.1	26.3	- 30
	0.04	0.013	0.027	365	37.6	40.2	40.3	40.2	negble
0.10	0.04	0.013	0.027	290	12.4	13.9	15.3	13.4	-9
C-K	0.04	0.013	0.027	319	13.4	16.3	15.1	15.7	+ 7
	0.04	0.013	0.027	343	18.4	20.3	22.1	21.2	-8
	0.04	0.013	0.027	365	36.8	36.7	41.0	38.8	-11
0.1	0.04	0.010	0.030	300	15.8	14.2	16.2	15.1	- 14
Present	0.04	0.013	0.027	300	15.8	14.1	12.4	13.2	- 12
SS	0.04	0.020	0.020	300	18.4	16.5	17.1	16.8	negble
	0.04	0.030	0.010	300	17.0	21.0	16.5	18.7	+20

Table (continued)

d_{pan}	h_{pan}	h_{fu}	h_{fb}	T_0	Expt	$Pred_1$	$Pred_2$	Mean	% Error
m	m	m	m	K	g/m^2s	g/m^2s	g/m^2s	g/m^2s	-
0.1	0.04	0.010	0.030	300	10.1	8.2	14.0	11.1	+ 10
Present	0.04	0.020	0.020	300	10.8	9.0	14.7	11.8	+ 10
GL	0.04	0.030	0.010	300	11.9	9.6	13.8	11.7	negble
0.05 (Hayasaka. 1996)	0.11	0.110	0.000	298	16.9	7.9	16.5	12.2	- 28

5.4 Results for other fuels

As indicated in chapter 3, the experiments were performed in 0.2 m diameter MS and SS pan to explore the fuel depth and the pan material effects on the burn behavior of pool fires with methanol, ethanol, kerosene, and diesel fuels. Predictions for these experiments are obtained using the code discussed in chapter 4. The comparisons of predictions with the experiments performed by Zhao et al (2018) for gasoline pool fires in glass pans are also shown. Figures 5.13 and 5.14 show the comparison of mass vs time for 0.2 m pans made of SS and MS for kerosene and diesel at fuel depths of 10 and 20 mm. The quality of prediction in capturing the nature of burn behavior as well as the burn time for both kerosene and diesel taking into account the effect of fuel depth and pan material appears very good.

Figure 5.15 shows the comparison of mass vs time for 0.2 m diameter MS pan with methanol and ethanol at a fuel depth of 10 and 20 mm. As can be noted, the prediction of mass loss is outstanding for all the cases. Comparisons of pan

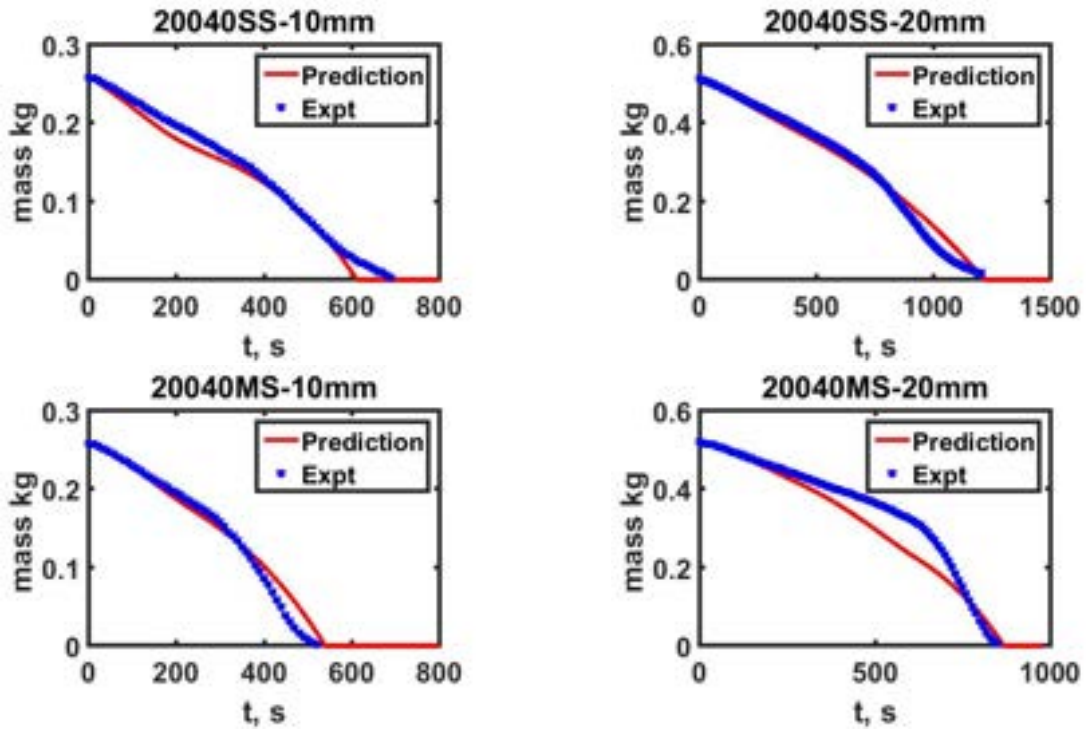

Figure 5.13: Comparison between predictions and experiments on mass vs time for Stainless Steel (SS) and Mild steel (MS) pan of 0.2 m diameter, for kerosene at h_{fu} = 10 and 20 mm

diameter effect on the mass burn rate of gasoline pool fires for the data Zhao et al (2018) shown in figure 5.16 are reasonably good. The code is able to capture the effect of pan diameter on the mass loss rate even for different fuels. Figure 5.17 shows the comparison of the experimental and predicted pan tip temperature for the experiments performed in 0.2 m dia, MS pan with 10 mm fuel depth for methanol, ethanol, kerosene, and diesel fuel. The predictions are reasonable to good for the cases considered. The comparisons between experimental data and the prediction of fuel temperatures at 1 mm height from the inside pan wall surface for methanol, ethanol, kerosene, and diesel fuels are shown in the Fig. 5.18. As can be observed, the predictions are quite good for pure fuels. In the case of kerosene and diesel fuels, the predictions are good till few hundred seconds and deviation occurs afterwards, a feature inferred to be so because of various petroleum fractions vaporizing at different temperatures.

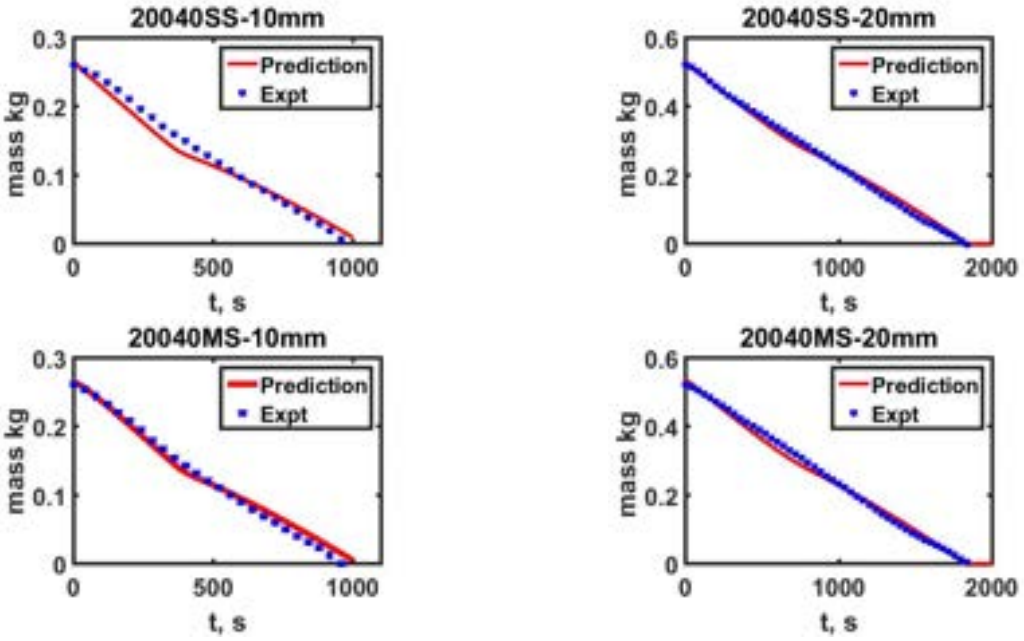

Figure 5.14: Comparison between predictions and experiments on mass vs time for Stainless Steel (SS) and Mild steel (MS) pan of 0.2 m diameter, with diesel at h_{fu} = 10 and 20 mm

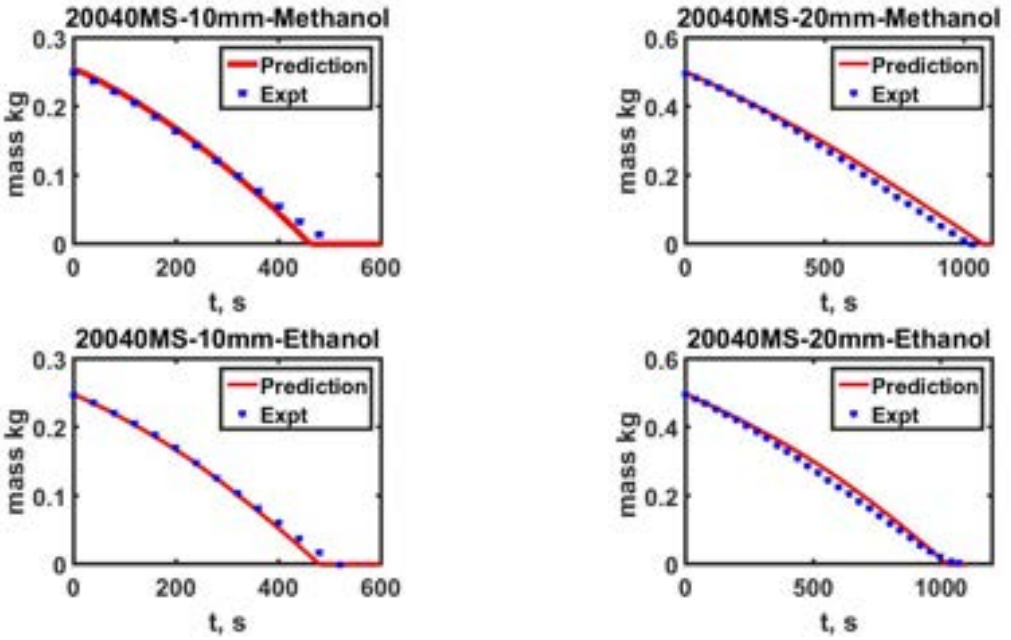

Figure 5.15: Comparison between predictions and experiments on mass vs time for Mild steel (MS) pan of 0.2 m dia, at h_{fu} = 10 and 20 mm for methanol and ethanol

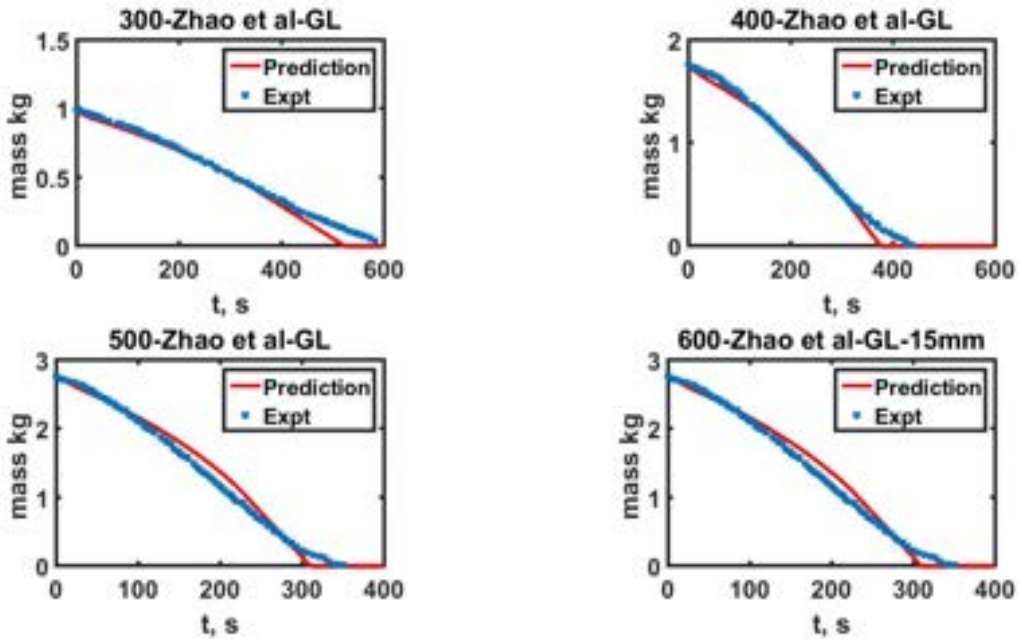

Figure 5.16: Comparison between predictions and experiments on mass vs time for the experiments of Zhao et al (2018) performed in 0.3, 0.4, 0.5 and 0.6 m diameter glass pan with gasoline

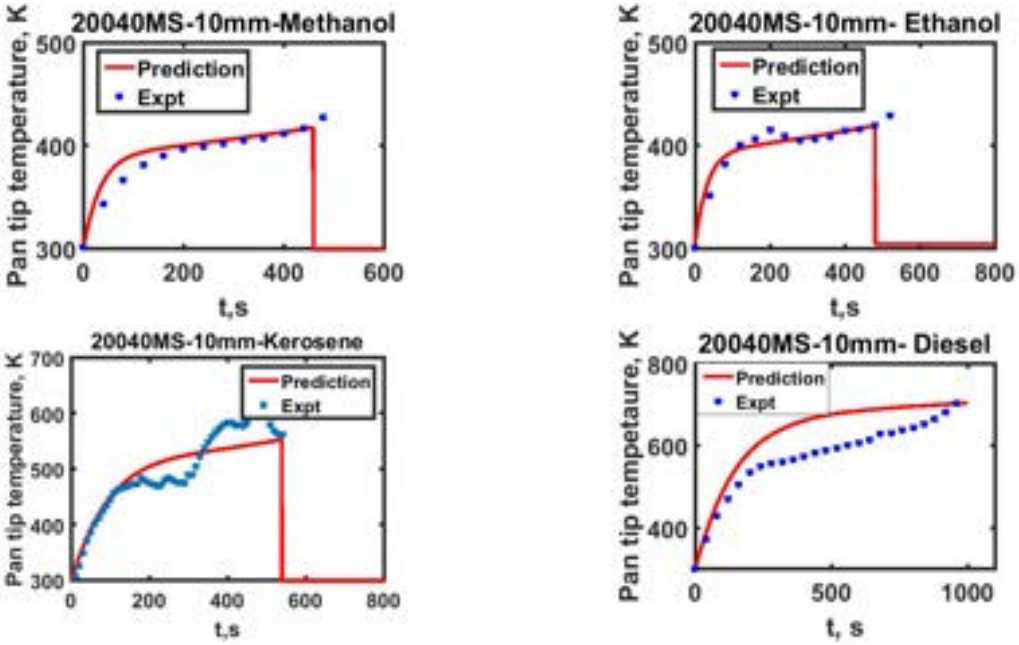

Figure 5.17: Comparison between predictions and experiments on pan tip temperatures for 0.2 dia, MS pan with 10 mm fuel depths of methanol, ethanol, kerosene and diesel

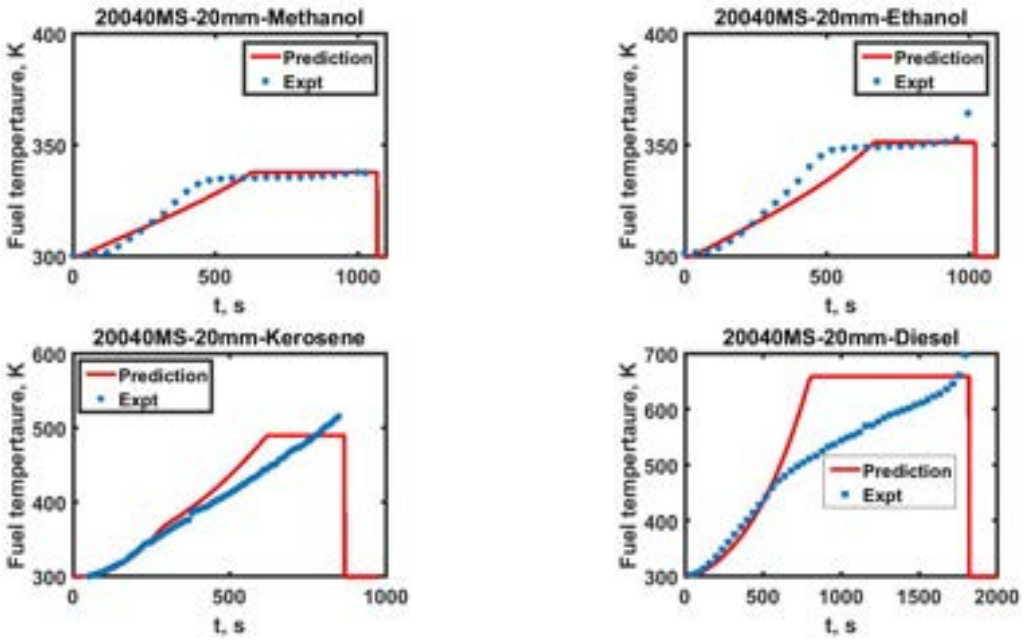

Figure 5.18: Comparison between predictions and experiments on fuel temperatures at 1 mm from the inside bottom surface of pan for 0.2 dia, MS pan with h_{fu}=20 mm of methanol, ethanol, kerosene and diesel

5.5 Summary

Based on the results of burn behavior observed in chapter 3, a physics inspired model is developed to predict the time varying mass burn rates of pool fires. In the convection term, a convective heat transfer coefficient of 0.0045 kW/m^2K is considered sufficient for all pan diameters, fuels, and wall materials to provide an accurate fit for the initial fuel burn flux as it is evident from the comparison of simulations with experimental fuel mass vs time. This may be treated as a new result of significance not uncovered in the literature till now. Further, in this model, the classical expression for the radiation term is altered to overcome the dependence of radiation on the extinction coefficient, since there are inconsistencies in their values as explained in chapter 1. To introduce a dimensionless approach, a Reynolds number based on fuel mass flux and a length scale based on pan diameter, and a constant that invokes the Grashof number are invoked. To explain the higher mass burn rates in the smaller diameter pans for n-heptane pool fires, the wall conduction effects are invoked by considering the experimentally consistent linear variation of temperatures along the pan wall. As observed from the experiments, there are two types of mass loss variations. Type II variation with the sharp bend for AL and MS pans and for the experiments performed at higher initial temperatures and type I variation with the smooth curve for all other data even for the pans of larger diameters. To account for this behavior and to obtain the best fit for the mass vs time, non-dimensional numbers W_1, $Mpc1$, and W are invoked. Based on earlier work as well as in the present study, the convective heat transfer in the condensed phase is considered negligible. Only conduction is considered inside the liquid phase. In order to obtain the liquid temperatures, the enthalpy raise rate of the fuel surface layer is treated as a rate process rather than assuming the equilibrium at the surface (generally done using Clausius-Clapeyron equation) and the temperature of the fuel surface and the bottom of the pan are obtained. The comparison between the experimental data and the predictions

obtained for time varying mass loss, pan tip temperature, and fuel temperatures over a wide range of pan diameters, pan materials, fuel depths, initial temperatures, pressures, and fuels are done and the results show that the code is able to capture the effect of various control parameters on burn behavior of pool fires for nearly all the pool fire experiments of the present author and others. The variation of mass burn rate with the pan diameter and magnitudes of the heat flux feedback to the fuel surface and their variation with the different pan material and pan diameters is also brought out. A particularly important point to note is that the radiative flux varies through burn time because the conductive heat transfer builds up the liquid temperature to pool boiling stage and in this transition, the flame behavior moves from small to large.

Chapter 6

Concluding remarks

This thesis has contributed to understanding the burn behavior of unsteady pool fires through carefully designed experiments and modeling. Its contributions are at both levels of improving the understanding and exploring the effects of various control parameters such as fuel depth, pan material, pan diameter, thermo-chemical properties of fuel, and initial temperature on the mass burn rate of pool fires. The experimental studies was initiated after noting that earlier literature had data but many unresolved issues or conflicts. In order to determine the extent of influences of various controlling geometric and thermodynamic parameters, experiments were conducted over specifically designed pans with different depths and diameters from 0.1 to 2 m with n-heptane fuel without water and n-heptane floated on the water. The experiments were also performed on fuels namely, kerosene and diesel, ethanol and methanol, in 0.2 m diameter MS and SS pan to explore the effects of fuel depth and pan material on the burn flux.

The experiments have captured the data on mass burn vs time, wall tip temperatures, in-depth liquid temperatures to provide data for understanding and validation. These show that for small diameter pans of 0.2 m class with n-heptane fuel,

- The lowest fuel mass flux is 11 ± 2 g/m^2s for all pan materials considered.
- The minimum flux is achieved for the glass pan at 10 mm fuel depth and 2 mm depth in SS pan.

- The minimum flux increases for MS and Al towards larger values at higher fuel depths as also with SS and other metals to as high as 65 g/m^2s beyond about 20 mm fuel depth and this is related to wall conductivity heat inputs into the fuel that leads to bulk boiling and the highest possible burn rates. These kind of burn rate is generally observed in the larger diameter pans.

- With regard to the effect of water (on which the fuels float), the mean burn flux decrease is estimated at 1 % per mm of water depth up to 0.5 m dia pan and 20 mm water depth. For larger diameter pans the effect of water is negligible.

The experiments in 0.2 m diameter MS and SS pan for methanol, ethanol, kerosene, and diesel fuels show that

- The initial mass burn rate of these fuels in 0.2 m dia, pan are not different from n-heptane and its value is about 11 $\pm$ 2 g/m^2s.

- The peak mass burn rate for the kerosene fuel increases with an increase in the fuel depth and thermal conductivity of the pan.

- For diesel, the effect of fuel depth and pan material on the burn flux is insignificant, indicating that the pan wall heat conduction is not able to transfer enough heat into the liquid to contribute to evaporation.

- In the case of experiments on ethanol and methanol, the peak burn rate does not increase with the increase in the fuel depth.

A correlation based on the non-dimensional number Mpc to obtain the mean mass burn rate of pool fires considering the effects of fuel depth, pan wall conductivity, freeboard, water depth, initial fuel temperature, and properties of fuels, apart from the well-known pan diameter effect has been deduced. This

correlation gives a good estimate of the burn rate flux over the range of parameters. It is useful to note that this correlation works well for the experiments performed even under steady state conditions.

After noting the non-availability of a mathematical model that captures the time-varying behavior of pool fire in the literature, the study was initiated and a mathematical model to calculate the burn rate in an unsteady pan fire considering all the controlling geometric, thermodynamic, and transport properties was developed and the calculations were coded into MATLAB software and named as *M-Pan-burn*. This code calculates the instantaneous burn rate flux using the modeled heat flux from the various components of convection, conduction, and radiation. The convective heat transfer coefficient of 0.0045 $p^{2/3}kW/m^2K$ has been found valid over all the pan and fuel parameters discussed in this thesis. The model for radiation is different from what has been in the literature as it had to account for enhanced burn flux due in part due to radiation something not accounted for in earlier models. This model uses fire emissivity and a view factor both of which have diameter dependence captured using the appropriate Reynolds number and Grashof number. The maximum temperature at which radiation occurs is based on a measured mean fire temperature for the specific fuels. This choice is assumed to account for all the chemistry effects influencing the heat release process. Wall conduction modeling invokes experimental features, namely the initial temperature rise rate that appears to be independent of pan material and fuel depth, a near-linear temperature variation along the wall, and the fact that all the heat transfer along the wall appears at the center of the pan after it transfers the heat to the liquid. This heat transferred raises the bottom temperature in time as it cannot achieve a steady state.

Three dimensionless numbers $Mpc1$, W, and $W1$ are brought in to evolve a correlation for the three important constants, $C2$, cTp, and $C3$ in the model with cTp controlling the peak wall tip temperature, $C2$, and $C3$ controlling the heat

transfer by conduction into the liquid. The liquid heat transfer is treated unsteady with dependence on the fuel thermal diffusivity and its behavior based on the classical unsteady heat transfer approach and with the associated constant obtained by comparison with specific experimental data. These features are integrated into the code *M-Pan-burn* that needs the wall and fuel thermal property data as well as initial fuel depth and temperature as inputs to predict the burn behavior. It must be emphasized that there are no free constants in the code to make predictions. The results of this code show that the predicted burn behavior follows the experimental burn profile nearly exactly in several cases and provides the magnitude of various components of heat flux, pan tip temperature, in depth liquid temperatures, and the mass burn rate with time. The conductive flux varies with time something that could have been anticipated but obtained only by using an unsteady code of the kind described here.

The mean burn flux values are obtained as an average between that from the correlation and *M-Pan-burn* code and presented as the final result for the mean burn flux. The comparison with the experimental results is excellent-to-good in most cases. Where there is a departure, it turns out that the predicted burn profile matches with that from the experiment for the early part of the burn, and the deviation occurs later. One of the important uses of the code would be to deploy it for incremental parameter influences since it will be more accurate than predictions for a new set of parameters.

6.1 Future possibilities

As explained in chapter 1, most of the standards use the large diameters unsteady pool fires as the source of fire in the testing of fire fighting products such as foam, dry chemical powder, and CO_2 extinguishers. The experimental work performed in this research work shows that the higher peak burn rates which are found in the larger diameter pool fires can also be reached in the smaller diameter pans at higher fuel depths for fuels like n-heptane (standard

fuel used in the testing). This result can lead one to think in terms of revisiting the standards for the qualification of fire fighting products and revising them to reduce the cost of testing without compromising on the aims of standards and the researchers can make use of the smaller pan fires as a source of fire during the development stage of the new fire extinguishment products before going to full-scale testing.

The extension of the studies presented here can be extended to the conduct of rigorous experiments and predictions of pan fires in flash fire apparatus. Preliminary experiments have shown that the burn fluxes can go up as much as 170 g/m^2s. Speculations involve conductive-radiative influences caused by forced convection heat transfer into the sides of the pan. However, definitive work needs to be performed.

Extension to other fuels like peroxides with a much lower stoichiometric ratio with air than alcohols awaits consideration.

Appendices

Appendix A

Pan fire data from literature

Table A.1: Data on Large steady hydrocarbon pool fires with circular pans from literature; Op - St = Operation Steady, Mat = Pan material - MS or SS = Mild or Stainless steel, B. F = Burn flux

d_{pan} mm	Op	h_{fu} mm	h_{pan} mm	h_{fb} mm	t_w mm	h_w mm	Mat	B. F g/m^2s	Author
					n-Heptane				
1.00	St	87	102	15.0	1.6	0	MS	65.5	Klassen & Gore, 1992
1.00	St	63.5	73.0	9.5	3.2	0	SS	55.0	Ditch et al, 2013
1.20	St	-	-	-	-	-	-	45.0	deRis et al, 2000
2.00	St	-	-	-	-	-	-	60.0	deRis et al, 2000
2.00	St	63.5	73.0	9.5	-	0	SS	61.6	Blanchat et al, 2011
2.00	St	63.5	73.0	9.5	-	0	SS	64.0	Blanchat et al, 2011
					JP8				
1.00	St	63.5	73.0	9.5	3.2	0	SS	40.0	Ditch et al, 2013
2.00	St	63.5	73.0	9.5	-	0	SS	40.4	Blanchat et al, 2011
2.00	St	63.5	73.0	9.5	-	0	SS	37.0	Blanchat et al, 2011
2.00	St	63.5	73.0	9.5	-	0	SS	37.6	Blanchat et al, 2011
2.00	St	63.5	73.0	9.5	-	0	SS	35.7	Blanchat et al, 2011
2.00	St	63.5	73.0	9.5	-	0	SS	37.4	Blanchat et al, 2011
					Toulene				
1.00	St	87	102	15.0	1.6	0	MS	67.1	Klassen & Gore, 1992
1.00	St	63.5	71.0	7.5	3.2	0	SS	47.0	Ditch et al, 2013
					Kerosene				
1.39	St	-	-	-	-	-	-	36.0	Bilnov & Khudiakov, 1961
2.64	St	-	-	-	-	-	-	37.4	Bilnov & Khudiakov, 1961
22.9	St	-	-	-	-	-	-	49.8	Bilnov & Khudiakov, 1961
30.0	St	-	-	-	-	-	-	65.0	Bilnov & Khudiakov, 1961
50.0	St	-	-	-	-	-	-	65.0	Bilnov & Khudiakov, 1961
					Diesel				
0.80	St	-	-	-	-	-	-	38.3	Bilnov & Khudiakov, 1961
1.30	St	-	-	-	-	-	-	46.8	Bilnov & Khudiakov, 1961
2.60	St	-	-	-	-	-	-	49.6	Bilnov & Khudiakov, 1961

To be continued

Table (continued)

d_{pan} m	M	h_{fu} mm	h_{pan} mm	h_{fb} mm	t_w mm	h_w mm	Mat	B.F g/m^2s	Author
1.00	St	100	200	100	3	0		39.0	Sudheer & Prabhu, 2010

Table A.2: Data on Large unsteady hydrocarbon pool fires with circular pans from literature; Op - Un = Operation Unsteady, Mat = Pan material - MS or SS = Mild or Stainless steel, B. F = Burn flux

d_{pan} mm	Op	h_{fu} mm	h_{pan} mm	h_{fb} mm	t_w mm	h_w mm	Mat	B. F g/m^2s	Author
					n-Heptane				
1.22	Un	76	76	0	2.7	0	MS	67.6	Kung & Stavriandis, 1982
1.22	Un	76	76	0	2.7	0	MS	68.6	
1.74	Un	76	76	0	2.7	0	MS	73.0	
2.70	Un	-	-	-	–	-	-	81.0	Koseki et al, 1989
6.00	Un	-	-	-	-	-	-	79.0	
10.0	Un	-	-	-	-	-	-	98.0	
					Gasoline				
3.00	Un	-	-	-	-	-	MS	60.0	Koseki, 1989
10.0	Un	-	-	-	-	-	SS	88.0	Koseki, 1989
					Kerosene				
30.0	Un	-	-	-	-	-	-	61.0	Koseki et al, 1989
50.0	Un	-	-	-	-	-	-	61.0	Koseki et al, 1989
					Diesel				
1.50	Un	5.5	-	-	-	-	Concrete	32.0	Chatris et al, 2001
3.00	Un	6.6	-	-	-	-	Concrete	44.0	Chatris et al, 2001
4.00	Un	8.1	-	-	-	-	Concrete	56.0	Chatris et al, 2001

Table A.3: Data on small steady hydrocarbon pool fires with circular (C) and square (S) pans from literature; Op - St = Operation Steady, Mat = Pan material - MS or SS = Mild or Stainless steel, B. F = Burn flux

d_{pan} m	Op	h_{fu} mm	h_{pan} mm	h_{fb} mm	t_w mm	h_w mm	Mat	C/S	B. F g/m^2s	Author
					n-Heptane					
0.10	St	26	30	4.0	5	0	MS	S	12.0	Hu et al, 2014

To be continued

Table (continued)

d_{pan} mm	M	h_{fu} mm	h_{pan} mm	h_{fb} mm	t_w mm	h_w mm	Mat	C/S	B.F g/m^2s	Author
0.15	St	26	30	4.0	5	0	MS	S	15.0	Hu et al, 2014
0.20	St	26	30	4.0	5	0	MS	S	16.0	Hu et al, 2014
0.20	St	26	30	4.0	5	0	MS	S	22.0	Hu et al, 2014
0.25	St	63.5	73.0	9.5	3.2	0	SS	C	27.0	Ditch et al, 2013
0.30	St	87	152	65.0	1.6	0	SS	C	36.8	Klassen & Gore, 1992
0.50	St							C	39.0	de Ris et al, 2000
0.50	St	63.5	73.0	9.5	3.2	0	SS	C	38.0	Ditch et al, 2013
0.60	St	87	102	15.0	1.6	0	MS	C	56.6	Klassen & Gore, 1992
				JP8						
0.25	St	63.5	73.0	9.5	3.2	0	SS	C	13.0	Ditch et al, 2013
0.50	St	63.5	73.0	9.5	3.2	0	SS	C	29.0	Ditch et al, 2013
				Toulene						
0.25	St	63.5	73.0	9.5	3.2	0	SS	C	35.0	Ditch et al, 2013
0.30	St	87	152	65.0	1.6	0	SS	C	42.3	Klassen & Gore, 1992
0.50	St	63.5	73.0	9.5	3.2	0	SS	C	43.3	Ditch et al, 2013
0.60	St	87	102	15.0	1.6	0	MS	C	77.0	Klassen & Gore, 1992
				Diesel						
0.15	St							C	9.9	Blinov & Khudiakov, 1961
0.50	St							C	25.5	Blinov & Khudiakov, 1961
0.50	St	100	200	100	3	0		C	27.0	Sudheer & Prabhu, 2010
0.70	St	100	200	100	3	0		C	33.0	Sudheer & Prabhu, 2010
				Kerosene						
0.15	St							C	12.5	Blinov & Khudiakov, 1961
0.20	St							C	22.1	Blinov & Khudiakov, 1961
0.30	St							C	24.9	Blinov & Khudiakov, 1961
0.80	St							C	31.8	Blinov & Khudiakov, 1961

Table A.4: Data on small unsteady hydrocarbon pool fires with circular (C) and square (S) pans from literature; Op - Un = Operation Unsteady, Mat = Pan material - MS or SS = Mild or Stainless steel, B. F = Burn flux

d_{pan} mm	Op	h_{fu} mm	h_{pan} mm	h_{fb} mm	t_w mm	h_w mm	Mat	C/S	B. F g/m^2s	Author
					n-Heptane					
0.10	Un	13	40	27.0	3	0	SS	C	18.0	Chen et al, 2011
0.10	Un	13	40	27.0	3	0	SS	C	19.0	Kang et al, 2010
0.10	Un	30	40	10.0	3	0	MS	S	37.5	Fang et al, 2011
0.11	Un	30	40	10.0	3	0	MS	S	44.1	Fang et al, 2011
0.12	Un	30	40	10.0	3	0	MS	S	35.9	Fang et al, 2011
0.13	Un	30	40	10.0	3	0	MS	S	43.3	Fang et al, 2011
0.14	Un	30	40	10.0	3	0	MS	S	47.9	Fang et al, 2011
0.141	Un	13	40	27.0	3	0	SS	C	20.0	Kang et al, 2010

To be continued

Table (continued)

d_{pan} mm	M	h_{fu} mm	h_{pan} mm	h_{fb} mm	t_w mm	h_w mm	Mat	C/S	B.F g/m^2s	Author
0.141	Un	13	40	27.0	3	0	SS	C	22.0	Chen et al, 2011
0.17	Un	30	40	10.0	3	0	MS	S	45.4	Fang et al, 2011
0.20	Un	30	40	10.0	3	0	MS	S	44.6	Fang et al, 2011
0.20	Un	13	40	27.0	3	0	SS	C	24.0	Chen et al, 2011
0.20	Un	13	40	27.0	3	0	SS	C	22.3	Kang et al, 2010
0.20	Un	7.4	15	7.6	3	0	GL	S	14.5	Zhao et al, 2017
0.20	Un	11.2	15	3.8	3	0	GL	S	20.0	Zhao et al, 2017
0.24	Un	30	40	10.0	3	0	MS	S	50.0	Fang et al, 2011
0.27	Un	30	40	10.0	3	0	MS	S	52.6	Fang et al, 2011
0.27	Un	10	50	40	3	0	SS	S	23.0	Li et al, 2009
0.30	Un	4.1	15	10.9	3	0	GL	S	17.0	Zhao et al, 2017
0.30	Un	8.2	15	6.8	3	0	GL	S	21.0	Zhao et al, 2017
0.33	Un	30	40	10.0	3	0	MS	S	65.9	Fang et al, 2011
0.33	Un	8	50	42	3	0	SS	S	25.0	Li et al, 2009

Table A.5: Data on Methanol and ethanol; Op - St/Un = Operation Steady or Unsteady, Mat = Pan material - MS or SS, S = Square, C = Circular, B. F = Burn flux

d_{pan} mm	Op	h_{fu} mm	h_{pan} mm	h_{fb} mm	t_w mm	h_w mm	Mat	S/C	B. F g/m^2s	Author
Ethanol, large pans										
2.00	St	-	-	-	-	0	-	C	27.0	deRis et al, 2000
2.00	St	63.5	73.0	9.5	-	0	SS	C	26.4	Blanchat et al, 2011
2.00	St	63.5	73.0	9.5	-	0	SS	C	27.2	Blanchat et al, 2011
2.00	St	63.5	73.0	9.5	-	0	SS	C	26.4	Blanchat et al, 2011
2.00	St	63.5	73.0	9.5	-	0	SS	C	25.8	Blanchat et al, 2011
2.00	St	63.5	73.0	9.5	-	0	SS	C	26.9	Blanchat et al, 2011
Ethanol, small pans										
0.25	St	64	73.0	10	3.2	0	SS	C	13.0	Ditch et al , 2013
0.50	St					0		C	18.0	deRis et al, 2000
0.50	St	63.5	73.0	9.5	3.2	0	SS	C	17.0	Ditch et al, 2013
0.10	Un	30	40	10	3	0	MS	S	17.5	Fang et al, 2011
0.11	Un	30	40	10	3	0	MS	S	17.9	Fang et al, 2011
0.12	Un	30	40	10	3	0	MS	S	19.3	Fang et al, 2011
0.13	Un	30	40	10	3	0	MS	S	19.6	Fang et al, 2011
0.14	Un	30	40	10	3	0	MS	S	19.8	Fang et al, 2011
0.17	Un	30	40	10	3	0	MS	S	20.4	Fang et al, 2011
0.20	Un	30	40	10	3	0	MS	S	19.6	Fang et al, 2011
0.24	Un	30	40	10	3	0	MS	S	19.9	Fang et al, 2011
0.27	Un	30	40	10	3	0	MS	S	20.2	Fang et al, 2011
0.33	Un	30	40	10	3	0	MS	S	22.2	Fang et al, 2011

To be continued

Table (continued)

d_{pan} mm	Op	h_{fu} mm	h_{pan} mm	h_{fb} mm	t_w mm	h_w mm	Mat	S/C	B. F g/m^2s	Author
					Methanol, large pans					
1.20	St	80	80.0	0				C	20.7	Burgess et al, 1961
1.80	St	80	80.0	0				C	24.3	Burgess et al, 1961
1.00	St	87	102	15	1.6	0	MS	C	14.4	Klassen & Gore, 1992
1.00	St	63.5	73.0	10	3.2	0	SS	C	19.0	Ditch et al, 2013
2.00	St	63.5	73.0	10	-	0	SS	C	20.1	Blanchat et al, 2011
2.00	St	63.5	73.0	10	-	0	SS	C	21.1	Blanchat et al, 2011
2.00	St	63.5	73.0	10	-	0	SS	C	19.8	Blanchat et al, 2011
2.00	St	63.5	73.0	10	-	0	SS	C	19.9	Blanchat et al, 2011
2.00	St	63.5	73.0	10	-	0	SS	C	20.0	Blanchat et al, 2011
2.00	St	63.5	73.0	10	-	0	SS	C	19.8	Blanchat et al, 2011
1.22	Un	76	76	0	2.7	0	MS	C	20.1	Kung & Stavriandis, 1982
2.44	Un	76	76	0	2.7	0	MS	C	21.1	Kung & Stavriandis, 1982
					Methanol, small pans					
0.10	St					0		C	13.2	Akita & Yumoto, 1965
0.10	St	80	80	0		0		C	13.2	Burgress & Grumer, 1961
0.10	St	63.5	73.0	9.5	3.2	0	SS	C	12.0	Ditch et al, 2013
0.10	St	12	12	0	2.5	0	Quartz	C	10.5	Vali et al, 2014
0.10	St	12	12	0	2.5	0	CU	C	9.5	Vali et al, 2014
0.10	St	12	12	0	2.5	0	SS	C	9.1	Vali et al, 2014
0.20	St					0		C	13.5	Akita & Yumoto, 1965
0.20	St	80	80	0.0		0		C	13.2	Burgress & Grumer, 1961
0.25	St	63.5	73.0	9.5	3.2	0	SS	C	13.0	Ditch et al, 2013
0.25	St					0		C	13.0	Babrauskas, 1983
0.30	St	87	152	65	1.6	0	SS	C	13.0	Hamins et al, 1994
0.30	St					0		C	13.5	Akita & Yumoto, 1965
0.30	St	140	150	10	1.3	0	MS	C	13.5	Chan kin et al, 2019
0.32	St					0		C	13.1	Babrauskas, 1983
0.50	St	63.5	73.0	9.5	3.2	0	SS	C	14.0	Ditch et al, 2013
0.50	St					0		C	14.3	Akita & Yumoto, 1965
0.60	St	87	102	15	1.6	0	MS	C	13.4	Klassen & Gore, 1992

Appendix B

Pan fire data from present experiments

Table B.1: $\bar{m}''_{fu}$ $(g/m^2 s)$ for 0.2, 0.3, 0.4, 0.5 and 2 m dia pans with different fuels; Expt, $Pred_1$, $Pred_2$, Mean, % Error; negble = error is less than experimental accuracy $\sim$ 5 %, CK refers to Chen et al (2011) and Kang et al (2010), Li-1 to Li et al (2009) at 64 kPa, and Li-2 of Li et al (2009) at 101 kPa,

d_{pan} m	h_{pan} mm	h_{fu} mm	h_w mm	h_{fb} mm	T_0 K	Mat	Expt $g/m^2 s$	$Pred_1$ $g/m^2 s$	$Pred_2$ $g/m^2 s$	Mean $g/m^2 s$	% Error -
						n-heptane					
0.2	40	10	0	30	300	AL	30.0	23.0	25	24.0	-8
	40	13	0	27	300	AL	28.5	23.3	28.5	26.0	-15
	40	20	0	20	300	AL	34.1	26.3	30.1	28.0	-20
0.2	40	10	0	30	300	MS	21.9	21.1	18.9	19.9	negble
	40	13	0	27	300	MS	22.7	23.3	20.7	21.7	negble
	40	20	0	20	300	MS	26.2	26.6	23.15	24.6	negble
0.2	50	10	0	40	300	MS	19.0	20.6	18.5	19.9	negble
	50	20	0	30	300	MS	24.3	25.1	21.8	21.7	-7
	50	30	0	20	300	MS	25.1	27.0	24.4	24.6	negble
0.2	60	20	0	40	300	MS	25.2	25.1	21.5	22.8	-7
	60	30	0	30	300	MS	26.7	27.4	24.2	25.8	negble
	60	40	0	20	300	MS	27.9	28.5	25.5	27	negble
0.2	40	10	0	30	300	SS-o	16.6	16.7	17.5	17.1	negble
	40	13	0	27	300	SS-o	18.8	17.8	19.1	18.5	negble
	40	13	0	27	319	SS-o	23.9	20.2	20.1	20.0	negble
	40	13	0	27	343	SS-o	30.0	25.1	26.0	25.5	negble
	40	20	0	20	300	SS-o	20.9	21.3	22.3	21.5	negble
	40	13	0	27	288	SS-CK	15.1	17.6	17.2	17.4	negble
	40	13	0	27	319	SS-CK	20.0	21.6	23.8	22.7	+9.2
	40	13	0	27	343	SS-CK	33	29.3	35.2	32.9	+ 18
	40	13	0	27	365	SS-CK	46.0	64.6	43.0	53.8	+ 17
0.19	40	10	0	30	300	GL	11.3	10.8	12.2	11.5	-9
	40	13	0	27	300	GL	12.1	11.7	12.5	12.1	negble
	40	23	0	17	300	GL	15.1	13.3	13.6	13.4	- 13

Table (continued)

d_{pan} m	h_{pan} mm	h_{fu} mm	h_w mm	h_{fb} mm	T_0 K	Mat	Expt g/m^2s	$Pred_1$ g/m^2s	$Pred_2$ g/m^2s	Mean g/m^2s	% Error -
0.3	40	10	0	30	304	MS	25.5	23.9	25.0	24.5	negble
	40	20	0	20	304	MS	30.2	28.5	31	29.7	-8
	40	30	0	10	304	MS	31.1	34.0	32.0	33.0	negble
0.3	50	10	0	40	304	MS	21.9	22.2	25.1	24.3	-12
	50	20	0	30	304	MS	27.2	25.7	29.4	27.4	-12
	50	30	0	20	304	MS	26.5	29.2	29.5	29.4	negble
0.3	60	10	0	50	304	MS	20.0	22.0	23.1	22.5	negble
	60	20	0	40	304	MS	26.2	24.0	27.9	25.6	-13
	60	30	0	30	304	MS	32.7	27.0	31.1	28.8	-15
0.3 (CK)	40	13	0	27	285	SS	21.5	21.7	22.0	21.8	negble
0.372(Li-1)	50	6.7	0	43.3	283	SS	13.6	17.0	17.8	17.4	negble
0.305(Li-2)	50	10	0	40	289	SS	23.0	22.3	19.6	21.0	+12
0.372(Li-2)	50	6.7	0	43.3	289	SS	24.0	23.9	23.1	23.5	negble
0.4	40	10	0	30	301	MS	27.2	28.6	30.4	29.0	negble
	40	20	0	20	301	MS	36.8	33.6	36.0	36.8	-8
	40	30	0	10	301	MS	40.8	39.0	41.1	40.0	negble
0.4	50	10	0	40	301	MS	27.8	26.9	29.1	27.9	-8
	50	20	0	30	301	MS	32.8	31.1	32.4	31.7	negble
	50	30	0	20	301	MS	35.7	34.7	38.4	40.0	+ 11
0.4	60	10	0	50	301	MS	25.2	25.5	28.3	26.8	-9
	60	20	0	40	301	MS	30.6	28.6	31.8	30.2	-10
	60	30	0	30	301	MS	34.9	31.4	35.5	33.4	-12
0.5	40	10	0	30	301	MS	30.2	33.9	33.2	33.5	negble
	40	20	0	20	301	MS	38.8	35.7	37.1	36.4	negble
0.5	50	10	0	40	301	MS	28.9	31.7	33.0	32.3	negble
	50	20	0	30	301	MS	38.6	35.7	37.4	36.4	negble
0.5	60	10	0	50	301	MS	32.4	31.2	32.5	31.8	negble
	60	20	0	40	301	MS	30.6	33.9	32.0	32.9	negble
0.92	150	10	0	140	301	MS	40.4	25.9	53.4	39.6	negble
	150	20	0	130	301	MS	43.6	33.7	53.5	43.6	negble
	150	36	0	114	301	MS	48.5	45.6	53.1	49.4	negble
	150	47	0	103	301	MS	49.7	46.5	53.4	50	negble
2.0	60	20	0	40	300	MS	57.7	67.9	68.3	68.1	negble
	90	20	0	70	300	MS	61.0	66.0	67.1	66.3	negble
	145	30	30	85	300	MS	62.0	64.3	65	64.6	negble
	145	40	30	75	300	MS	73	69	65	66	+9
						Methanol					
0.2	40	10	0	30	300	MS	15.1	17	13	13.8	+13
	40	20	0	20	300	MS	15.1	15.3	12.3	13.7	+13

Table (continued)

d_{pan} m	h_{pan} mm	h_{fu} mm	h_w mm	h_{fb} mm	T_0 K	Mat	Expt g/m^2s	$Pred_1$ g/m^2s	$Pred_2$ g/m^2s	Mean g/m^2s	% Error -
						Ethanol					
0.2	40	10	0	30	300	MS	15.1	16.1	12.2	14.1	negble
	40	20	0	20	300	MS	15.1	15.2	15.8	14.3	negble
						Kerosene					
0.2	40	10	0	30	300	MS	15.6	15.0	18.0	16.5	negble
	40	20	0	20	300	MS	19.8	22.0	19.0	17.0	+14
	40	10	0	30	300	SS	12.0	16.0	13.2	14.6	+17
	40	20	0	20	300	SS	14.0	18.0	13.2	15.6	+11
						Diesel					
0.2	40	10	0	30	300	MS	9.4	9.3	11.8	10.5	+10
	40	20	0	20	300	MS	9.7	9.1	12	10.9	+11
	40	10	0	30	300	SS	8.4	9.3	11.6	10.4	+19
	40	20	0	20	300	SS	8.9	9	11.0	10.0	+11

Bibliography

[1] Akita, K. and Yumoto, T. (1965). Heat transfer in small pools and rates of burning of liquid methanol. Symposium (International) on Combustion, 10(1): 943–948.

[2] Alpert, R. (1977). Pressure modeling of fires controlled by radiation. Symposium (International) on Combustion, 16(1): 1489–1500.

[3] Adiga, K.C., Ramekar, D.E., Tatem, P.A., and Williams, F.W. (1989). Modeling thermal radiation in open liquid pool fires. Fire Safety Science 2: 241-250.

[4] Babrauskas, V. (1983). Estimating large pool fire burning rates. Fire Technol, 19(4): 251–261.

[5] Blinov, V. I., and Khudiakov, G. N. (1961). Diffusion burning of liquids. ReportNo. AD296762, Moscow Academy of Sciences, U S Army Engineering Research and Development Laboratories,Fort Belvoir, Virginia.

[6] Bugress, D. S., Strasser, A., and Grumer, J. (1961). Fire Research Abstracts Revs, 3: 177.

[7] BS, (2009). BS EN 1568-3:2009. Fire extinguishing media. Foam concentrates. Specification for low expansion foam concentrates for surface application to water-immiscible liquids.

[8] Chatris, J. M, Quintela, J., Folch, J., Planas, E., Arnaldos, J., and Casal, J. (2001). Experimental study of burning rate in hydrocarbon pool fires, Combust. Flame 126: 1373-1383.

[9] Chen, B., Lu, S., Li, C., Kang, Q., and Yuan, M. (2011). Unsteady burning of thin layer pool fires, J.Fire Sci., 30: 3-15

[10] Chen, B., Lu, S., Li, C., Kang, Q., and Lecoustre, V. (2011). Initial fuel temperature effects on burning rate of pool fire. J. Hazard Mater., 188: 369-374.

[11] Corlett, R. C. (1970). Gas Fires with Pool-Like Boundary Conditions: Further Results and Interpretation. Comustion and Flame, 14:351–360.

[12] De Ris, J., Murty Kanury, A., and Yuen, M. C. (1973). Pressure modeling of fires. Symposium (International) on Combustion, 14 (1): 1033–1044.

[13] De Ris, J. and Orloff, L. (1972). A dimensionless correlation of pool burning data. Combustion and Flame, 18 (3): 381–388.

[14] De Ris, J. L.,Wu, P. K., and Heskestad, G. (2000). Radiation fire modeling. Proceedings of the Combustion Institute, 28 (2): 2751–2759.

[15] Ditch, B. D., de Ris, J. L., Blanchet, T. K., Chaos, M., Bill Jr., R. G., Dorofeen, S. B. (2013). Pool fires - An empirical correlation. Combust. Flame, 160 (12): 2964-2974.

[16] Dlugogorski, B. Z., and Wilson, M. (2000). Effect of ullage on properties of small-scale pool fires. Dev. Chem. Eng. Mineral Process, 8:149- 166, 2000.

[17] Fang, J., Ran, T., Jin-fu, G., Jin-jun, W., and Yong-ming, Z. (2011). Influence of low air pressure on combustion characteristics and flame pulsation frequency of pool fires.Fuel, 90 (8): 2760–2766.

[18] Fischer, S. J., Hardouin-Duparc, B., and Grosshandler, W. L. (1987). The structure and radiation of an ethanol pool fire. Combustion and Flame, 70 (3): 291–306.

[19] FM, (2007). Approval Standard for Foam Extinguishing Systems. Class Number 5130.

[20] Hamins, A., Fischer, S. J., Kashiwagi, T., Klassen, M. E., and Gore, J. P. (1994). Heat Feedback to the Fuel Surface in Pool Fires. Combustion Science and Technology, 97 (1-3): 37–62.

[21] Hayasaka, H. (1997). Unsteady Burning Rates Of Small Pool Fires. Fire Safety Science, 5: 499–510.

[22] Hottel, H. C. (1958). Certain laws governing diffusive burning of liquids. Fire Res. Abstr. Rev., 1: 41–44.

[23] Hu, L., Liu, S., and Wu, L. (2013). Flame radiation feedback to fuel surface in medium ethanol and heptane pool fires with cross air flow. Combustion and Flame 160: 295–306

[24] ISO 7203-1, (2011). Fire extinguishing media — Foam concentrates. International Organization for Standardization.

[25] Kang, Q., Lu, S., and Chen, B. (2010). Experimental study on burning rate of small scale heptane pool fires. Chinese Science Bulletin, 55 (10): 973–979.

[26] Hasegawa, K., 1989. Experimental study on the mechanism of hot zone formation in open-tank fires. Fire Safety Science 2: 221-230.

[27] Klassen, M. and Gore, J. P. (1992). Structure and Radiation Properties of Pool Fires. Technical Report 60NANB1D1169, School of Mechanical Engineering, Purdue University, West Lafayette, IN.

[28] Koseki, H. (1989). Combustion properties of large liquid pool fires. Fire Technology, 25 (3): 241–255.

[29] Koseki, H. and Mulholland, G. W. (1991). The effect of diameter on the burning of crude oil pool fires. Fire Technology, 27 (1): 54–65.

[30] Koski, J. A., Keltner, N. R., and Sobolik, K. B. (1992). Thermal Test Options. Technical Report SAND92-2324TTC-1236, Sandia National Laboratories, Albuquerque, NM.

[31] Li, Z., He Y, Zhang, H, and Wang J. (2009). Combustion characteristics of n-heptane and wood crib fires at different altitudes, Proc. Comb. Institute, 32: 2481–2488

[32] Modak, A. T. and Croce, P. A. (1977). Plastic pool fires. Combustion and Flame, 30: 251–265.

[33] McCaffery, B.J. (1979). Purely Buoyant Diffusion Flames: Some Experimental Results.Center for Fire Research, NBS.

[34] Mangialavori, G., Rubino, F. (1992). Experimental tests on large-scale hydrocarbon pool fires. Seventh International Symposium on Loss Prevention and Safety Promotion in Process Ind., 83: 1-11

[35] Munoz, M., Arnaldos, J, Casal, J., and Planas, E. (2004). Analysis of the geometric and radiative characteristics of hydrocarbon pool fires. Combustion and Flame, 139: 263–277.

[36] Mukunda. H.S., Shivakumar, A., and Bhaskar Dixit, C. S.(2020). MAT lab code to predict the time varying mass burn rate of pool fires considering the geometric properties of pan and thermo chemical properties of pan and the fuel. FCRC manual - 1903, Fire and Combustion Research Centre, Jain (deemed-to-be university), Bangalore 562 112.

[37] Nakakuki, A. (1994). Heat transfer mechanisms in liquid pool fires. Fire Safety Journal, 23 (4): 339–363.

[38] Ndubizu, C. C., Ramaker, D. E., Tatem, P. A., and Williams, F. W. (1983). A Model of freely burning pool fires. Combustion Science and Technology, 31 (5-6): 233–247.

[39] NFPA 11, (2005). Standard for Low, Medium, and High Expansion Foam. National Fire Protection Association.

[40] Orloff, L. and De Ris, J. (1972). Cellular and turbulent ceiling fires. Combustion and Flame, 18 (3): 389–401.

[41] Orloff, L. and De Ris, J. (1982). Froude modeling of pool fires. Symposium (International) on Combustion, 19 (1): 885–895.

[42] Quintiere, J. G., Fundamentals of Fire Phenomena, John Wiley and Sons, USA 2006, pp.138-154.

[43] Rew, P.J., Hulbert, W.G. and Deaves, D.M. (1997). Modelling of thermal radiation from external hydrocarbon pool fires. Process Safety and Environmental Protection, 75: 81-89.

[44] Raj, V. C. and Prabhu, S. (2018). Measurement of geometric and radiative properties of heptane pool fires. Fire Safety Journal, 96: 13–26.

[45] Shiva Kumar, A., Sowriraajan, A. Ve., Bhaskar Dixit, C. S., and Mukunda, H. S. (2021). Experiments on unsteady pool fires – effects of fuel depth, pan size and wall material, Sadhana, 46.

[46] Shiva Kumar, A., Mukunda, H. S. and Bhaskar Dixit, C. S. (2021). Effects of Fuel Depth and Pan Wall Material for Unsteady Pool Fires with Different Fuels. Fire Technology.

[47] Sudheer, S. and Prabhu, S. V. (2012). Measurement of Flame Emissivity of Hydrocarbon Pool Fires. Fire Technol, 48 (2): 183–217.

[48] Suo-Anttila, J. M. and Blanchat, T. K. (2011). Hydrocarbon characterization experiments in fully turbulent fires : results and data analysis. Technical Report SAND2010-6377, Sandia National Laboratories, Albuquerque, NM.

[49] Sun, H., Wang, C., Liu, H., Li, M., Zhang, A., and Xu, M. (2017). Burning behavior and parameter analysis of biodiesel pool fires. Combustion Science and Technology, 190 (2): 269-285.

[50] UL 162, (2015). Standard for safety foam equipment and liquid concentrates.

[51] Vali, A., Nobes, D. S., and Kostiuk, L. W. (2015). Quantifying the Conduction Pathways in a Laboratory-Scale Methanol Pool Fire. Combustion Science and Technology, 187 (5): 765–779.

[52] Weckman, E. J. and Strong, A. B. (1996). Experimental Investigation of the Turbulence Structure of Medium-Scale Methanol Pool Fires. Combustion and Flame, (105): 245–266.

[53] Wieser, D., Jauch, P., and Willi, U. (1997). The influence of high altitude on fire detector test fires. Fire Safe J. 29: 195–204.

[54] Zhao, J., Huang, H., Wang, H., Zhao, J., Liu, Q., and Li, Y. (2017). Experimental study on burning behaviors and thermal radiative penetration of thin-layer burning. J Therm Anal Calorim, 130: 1153–1162.

[55] Zhao, J., Huang, H., Jomaas, G., Zhong, M., and Yang, R. (2018). Experimental study of the burning behaviors of thin-layer pool fires. Combustion and Flame, 193: 327–334.